

Contents of issue 4 vol. LVI

- 311 W. OSIPIUK, K. ŁUKASZEWICZ, *Strain hardening under non-proportional loading in polycrystalline aluminum alloys*
- 325 M. M. ABDELKHALEK, *Heat and mass transfer in MHD flow by natural convection from a permeable surface with heat generation effects*
- 345 M. S. WĘGŁOWSKI, Y. HUANG, Y. M. ZHANG, *An investigation of metal transfer process in GMAW*
- 363 A. ZBICIAK, *Constitutive modelling and numerical simulation of dynamic behaviour of asphalt-concrete pavement*
- 377 Z. S. OLESIAK, *Włodzimierz Stanisław Trzywdar Burzyński*
- 383 R. B. PECHERSKI, *Burzyński yield condition vis-à-vis the related studies reported in the literature*

STRAIN HARDENING UNDER NON-PROPORTIONAL LOADING IN POLYCRYSTALLINE ALUMINUM ALLOYS

W. O s i p i u k, K. Ł u k a s z e w i c z

Białystok Technical University

Wiejska 45 C, 15-351 Białystok, Poland

In the paper it is postulated that the so-called common slip domains influence the character of the strain hardening phenomena for complex loading paths. The slip domains were evaluated on the basis of the Batdorf–Budiansky slip theory of plasticity. Evolution of a yield surface for different non-proportional tension-torsion loading paths was determined for PA4 aluminum alloy and the hypothesis that the strain hardening depends on the development of the common slip domains was shown to be justified.

1. INTRODUCTION

Investigations of material behavior under non-proportional loading are of fundamental importance for verification and improvement of the theories of non-elastic deformation and creep. Such investigations can provide a deeper insight into the material deformation mechanisms and thus contribute to improvement of the constitutive equations and the related principal theorems concerning solution uniqueness. One of the most significant phenomena occurring during loading of the common structural materials is strain hardening. Unfortunately, the mechanisms underlying the strain hardening lack a complete understanding, and an adequate and practical theoretical model linking the evolution of the microstructures with the parameters at the macro-scale still remains a challenge.

To approach the strain hardening, various phenomenological models have been introduced and the literature does not provide any consistent view on the hardening phenomena. While some references state that the strain hardening is basically of anisotropic (directional) character [1–4], other maintain that in some cases it can be considered isotropic [5]. References [6, 7] indicate the influence of two effects, that is isotropic when depends on the effective strain and anisotropic when it depends on the principal direction of the strain tensor, the isotropic effect being dominant. The reasons behind the different material behavior under different loading conditions have not been satisfactorily explained. The models of strain hardening are, as a rule, of purely phenomenological character and

generally do not consider the underlying phenomena on the micro-structural level.

The goal of the present paper is to try to explain the differences in material behavior observed experimentally on the basis of the concepts of the slip theory of plasticity. The basic ideas of the slip theory have been presented, among others, by [8–13].

It can be observed that researchers of deformable bodies develop theories based on the microstructure of material [14–17] on the one hand, and theories based on models of an ideally homogeneous body representing means of the properties of a polycrystal on the other hand. The theory presented in this paper belongs to the second category.

It is commonly approved that the plastic deformation of a single crystal can be explained by considering the development of crystallographic slips within certain characteristic planes. A polycrystal body consists of a multitude of crystals and grains with different orientations. In a continuum formulation, the total strain can be regarded as a result of an infinite number of slips along all possible slip planes. This is the basic hypothesis of the Batdorf–Budiansky slip theory of plasticity [8]. It is assumed that the non-elastic deformation leads to an increase of the defect density in a material structure within slip bands [18–22]. The defects constitute barriers to further deformation and the resolved shear stress necessary for continued slip becomes greater. The overall effect is an increase of the macroscopic yield stress and is referred to as strain hardening. Therefore it seems to be justified to formulate a hypothesis that the strain hardening can be described in terms of the slip theory.

Analysis of evolution of the yield surfaces under non-proportional loading is of particular importance for understanding of the basic features of material hardening. Here it is postulated that for complex loading paths, the character of strain hardening is influenced by the so-called common slip domains. The main objective of the present work has been to verify the above hypothesis experimentally. To this aim, yield surfaces for different non-proportional loading paths have been determined. The experiments have been carried out using thin-walled tubular samples of PA4 aluminum alloy subjected to tension and torsion. The slip domains have been evaluated on the basis of the modified Batdorf–Budiansky slip theory [23, 24].

It should be emphasized that a number of researchers [9, 25] propose models which are set in the micromechanics of non-elastic deformation to a much larger degree than the model presented in this work. Such models are very complicated mathematically. The model presented in this work is phenomenological to a large extent and relatively simple, as far as the mathematical side is concerned.

2. THEORETICAL CONSIDERATIONS

The Batdorf–Budiansky slip theory assumes that the material is initially isotropic, i.e. that the spatial arrangement of crystals is disordered and that no direction appears to be privileged. A material body is presumed to be composed of an infinite number of crystals (continuum approach). Possible slip planes within an infinitesimal material volume can be visualized as planes tangent to a half-sphere of a unit radius, any such plane being defined by a normal n given by two angles α and β (Fig. 1).

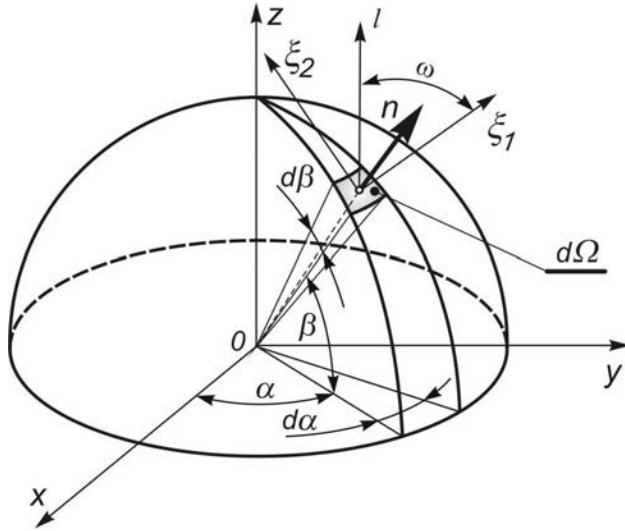


FIG. 1. Half-sphere of unit radius with angles α , β and ω defining the slip planes and slip directions.

The slip direction l within a given slip plane is defined by an angle ω measured from the parallel of latitude axis ξ_1 in the local orthogonal coordinate system (n, ξ_1, ξ_2) (Fig. 1). For all possible slips defined in the n, l system there should be:

$$0 \leq \alpha \leq 2\pi, \quad 0 \leq \beta \leq \pi/2, \quad 0 \leq \omega \leq 2\pi.$$

Among all possible slip systems at a given material point under a given stress state, only some (but possibly infinitely many) will be active. The region on the unit half-sphere corresponding to all slip planes with active slip systems will be here referred to as a slip domain.

By using the tensor transformation rules, the tangent stresses τ in the local coordinates (n, l) can be expressed as follows:

$$(2.1) \quad \tau = \sigma_{ij} l_i n_j \quad (i, j = x, y, z),$$

where σ_{ij} are the stress components in the Cartesian coordinates and n_j and l_i are direction cosines of n and l with respect to the Cartesian coordinates defined as it follows:

$$\begin{aligned}
 l_x &= -\sin \alpha \cos \omega - \cos \alpha \sin \beta \sin \omega, \\
 l_y &= \cos \alpha \cos \omega - \sin \alpha \sin \beta \sin \omega, \\
 l_z &= \cos \beta \sin \omega, \\
 n_x &= \cos \alpha \cos \beta, \quad n_y = \sin \alpha \cos \beta, \quad n_z = \sin \beta.
 \end{aligned}
 \tag{2.2}$$

The total deformation can be calculated by summing up the effects of all active slip systems, namely:

$$\gamma_{ij} = \iint_{\Omega} \int_{\omega_1}^{\omega_2} (n_i l_j + n_j l_i) \varphi d\omega d\Omega \quad (i, j = x, y, z),
 \tag{2.3}$$

where Ω is the surface area of the half-sphere corresponding to active slip systems, $d\Omega = \cos \beta d\alpha d\beta$, ω_1 and ω_2 are angles bounding the slip directions within the slip planes and φ is the slip intensity function [8].

Here some modifications to the slip theory will be introduced and the slip intensity function φ as proposed by BATDORF and BUDIANSKY [8] will not be used. A function of resistance to plastic deformation S is introduced as follows:

$$S = \tau_0 (1 + r\varphi),
 \tag{2.4}$$

where τ_0 denotes the yield stress under pure shear, i.e. the initial resistance to plastic deformation (for $\varphi = 0$) and r is a material constant.

It is assumed that the slip system defined by n and l that develops at a given point of a polycrystal body, results in strain hardening mainly in the same system. It also influences hardening in other slip systems. The slip intensity function φ defined with indexes in the system determined by n and l satisfies the condition $\varphi_{n-l} = \varphi_{nl}$. When the sign of external loading is changed, there is an additional term with the minus sign in the function of resistance to plastic deformation S (2.4) (the value of the function S will decrease). Such an approach makes it possible to describe the Bauschinger's effect [23] among other things. The function of resistance to plastic deformation S applied according to the procedure presented below makes it possible to describe the strain-stress curve of the material, e.g. subject to tension.

Function (2.4) being essentially a phenomenological description of a homogeneous model, accounts for the above fundamental feature of strain hardening observed in experimental investigations of elementary slip processes.

A constitutive law for the plastic resistance of an actual material body could be possibly formulated on the basis of the solid-state physics and mathematical statistics. However, the problem is very complicated and thus a simplified description based on function (2.4) is used here.

For material points within regions where slipping occurs one can write:

$$(2.5) \quad \tau = S,$$

while outside of the above regions (i.e. at material points where there is no slipping):

$$(2.6) \quad \tau < S.$$

The variant of the slip theory used in the present work is based on the relations (2.2)–(2.6). The above relations will be now used to evaluate the characteristics of the strain-hardening phenomena with a particular application to such materials as PA4 aluminum alloy. It can be stated that strain hardening develops in material regions where slipping occurs. The above assumption leads to the following hypothesis: Plastic deformation resulting under a certain load state will influence the deformation under subsequently applied other load state, provided that the slip systems generated under the later load state are influenced by the slip systems developed under the former load state. Whether or not, the case can be judged by inspecting the existence of common slip domains on the unit half-sphere for both loading states.

Let us evaluate the slip domains, first in the case of a specimen subjected to the tensile stress σ_z above the yield point, and then in the case of a specimen subjected to the shear stress τ_{xz} resulting from the torsional moment.

On the basis of Eqs. (2.1) and (2.2), the shear stress τ defined in the system n, l on the half-sphere and resulting from σ_z will have the form:

$$(2.7) \quad \tau(\sigma_z) = \frac{1}{2} \sigma_z \sin 2\beta \sin \omega.$$

In order to evaluate the slip intensity function φ , in the system n, l we need to use Eqs. (2.4), (2.5) and (2.7). Then we will obtain:

$$(2.8) \quad r\varphi(\sigma_z) = \frac{\sigma_z}{2\tau_0} \sin 2\beta \sin \omega - 1.$$

As at the slip boundary $\varphi = 0$, the slip domain can be determined by requiring the expression on the right-hand side of Eq. (2.8) to be zero. It can be easily done using numerical methods.

The plastic deformation ε_z is assigned from Eq. (2.3) after replacing the slip intensity function φ by Eq. (2.8).

In the case of the shear stress τ_{xz} resulting from torsional moment, a procedure of evaluating of the slip domain is similar. On the basis of Eqs. (2.1) and (2.2) the shear stress in the system n, l will be expressed by the form:

$$(2.9) \quad \tau(\tau_{xz}) = \tau_{xz} (\cos \alpha \cos 2\beta \sin \omega - \sin \alpha \sin \beta \cos \omega).$$

After using Eqs. (2.4), (2.5) and (2.9), the slip intensity function will take the form:

$$(2.10) \quad r\varphi(\tau_{xz}) = \frac{\tau_{xz}}{\tau_0} (\cos \alpha \cos 2\beta \sin \omega - \sin \alpha \sin \beta \cos \omega) - 1.$$

The plastic deformation γ_{xz} is assigned from Eq. (2.3) after replacing the slip intensity function φ by Eq. (2.10).

In the case of the concurrent action of tensile force and torsional moment on the basis of Eqs. (2.1) and (2.2), the shear stress in the system n, l will be expressed by the form:

$$(2.11) \quad \tau(\sigma_z, \tau_{xz}) = \frac{1}{2} \sigma_z \sin 2\beta \sin \omega + \tau_{xz} (\cos \alpha \cos 2\beta \sin \omega - \sin \alpha \sin \beta \cos \omega).$$

The slip intensity function φ in the system n, l is assigned on the basis of Eqs. (2.4), (2.5) and (2.11), namely:

$$(2.12) \quad r\varphi(\sigma_z, \tau_{xz}) = \frac{1}{\tau_0} \left[\frac{1}{2} \sigma_z \sin 2\beta \sin \omega + \tau_{xz} (\cos \alpha \cos 2\beta \sin \omega - \sin \alpha \sin \beta \cos \omega) \right] - 1.$$

Equation (2.12), after placing it in Eq. (2.3), is used to determine the plastic deformation resulting from the action of a complex load (tension with torsion).

Rigorous analytical calculation of plastic deformation in the case of complex loading is difficult. This concerns the determination of the boundaries of the slip domains and the evaluation of the function (2.3). The above problem can, however, be easily solved by numerical methods. To this aim the half-sphere of unit radius is divided into a great number h of sufficiently small elementary regions denoted by index k

$$(2.13) \quad \Delta\Omega_k = \cos \beta_k \Delta\beta \Delta\alpha,$$

where $\Delta\beta \Delta\alpha$ are the finite intervals of the angles β and α .

The integrals in Eq. (2.3) are approximated by a sum. The plastic deformation conditioned by slips occurring on the elementary k -th region $\Delta\Omega_k$, will be expressed by the forms:

$$(2.14) \quad (\varepsilon_z)_k = \frac{1}{2} \sin 2\beta_k \cos \beta_k \Delta\beta \Delta\alpha \left[\sum_{p=1}^g \sin \omega_p (\varphi_k)_p \Delta\omega \right]_k,$$

$$(2.15) \quad (\gamma_{xz})_k = \cos \alpha_k \cos \beta_k \cos 2\beta_k \Delta\beta \Delta\alpha \left[\sum_{p=1}^g \sin \omega_p (\varphi_k)_p \Delta\omega \right]_k - \frac{1}{2} \sin \alpha_k \sin 2\beta_k \Delta\beta \Delta\alpha \left[\sum_{p=1}^g \cos \omega_p (\varphi_k)_p \Delta\omega \right]_k,$$

where index $p = 1, 2, 3 \dots g$ at ω denotes successive slip directions within the plane n bounded by the angles ω_1 and ω_2 ; $\Delta\omega$ is the value of the finite interval of the angle ω .

According to Eqs. (2.14) and (2.15), the calculations are performed for all elementary regions $\Delta\Omega_k$ forming the surface of the half-sphere. The results are summed, i.e.:

$$(2.16) \quad \varepsilon_z = \sum_{k=1}^h (\varepsilon_z)_k,$$

$$(2.17) \quad \gamma_{xz} = \sum_{k=1}^h (\gamma_{xz})_k,$$

where h denotes the number of elementary regions $\Delta\Omega_k$ occurring within the slips, i.e. $\varphi_k > 0$. If for a given elementary k -th region of the half-sphere the relation $\varphi_k \leq 0$ holds, no slips occur and then in numerical calculation it is assumed that $\varphi_k = 0$. Values of φ_k for next points of the half-sphere are determined on the basis of Eqs. (2.8), (2.9) or (2.12).

The slip domains corresponding to two stress states σ_z and τ_{xz} applied consecutively can either partially overlap or be completely separated. If overlapping occurs then within certain slip planes defined by their normal n , the slipping under shear stresses τ_{xz} will depend on the slips generated under the previously applied normal stresses σ_z . Thus in such a case the strain hardening caused by tensile loading influences the hardening, resulting from a subsequent torsion loading.

Figure 2 and Fig. 3 illustrate the slip domains corresponding to certain values of the stresses σ_z and τ_{xz} . All calculations are performed for $r = 9.3 \cdot 10^3$, $\tau_0 = 105$ MPa, $\Delta\beta = \Delta\alpha = \Delta\omega = 1^\circ$.

If σ_z and τ_{xz} are just above the yield limit, then the slip domains are relatively small and do not overlap, i.e. there is no interaction between the strain hardening caused by the tensile and torsional loads (Fig. 2).

The slip domains for tension and torsion will partially overlap as in Fig. 3, provided the applied stresses are sufficiently large. Those overlapping parts of the slip domains are defined as common slip regions. In that case, predeformation resulting from tension influences the subsequent torsion.

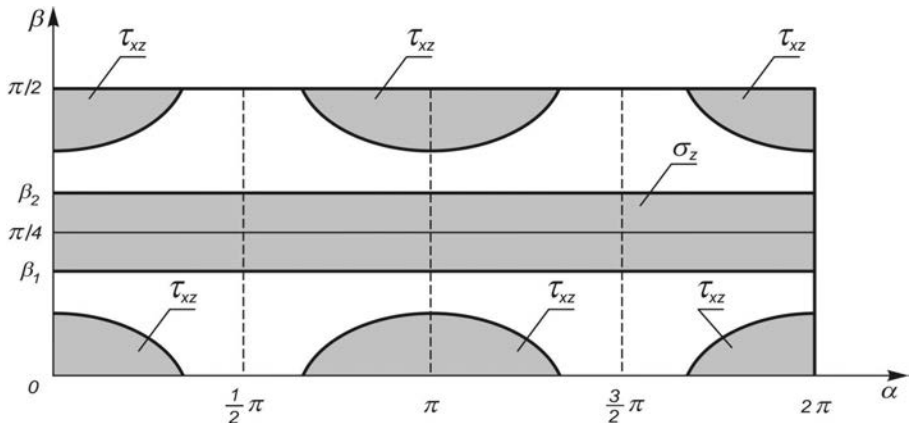


FIG. 2. The slip domains calculated for PA4 aluminum alloy under uni-axial tensile stress state $\sigma_z = 235$ MPa and pure shear stress state $\tau_{xz} = 110$ MPa.

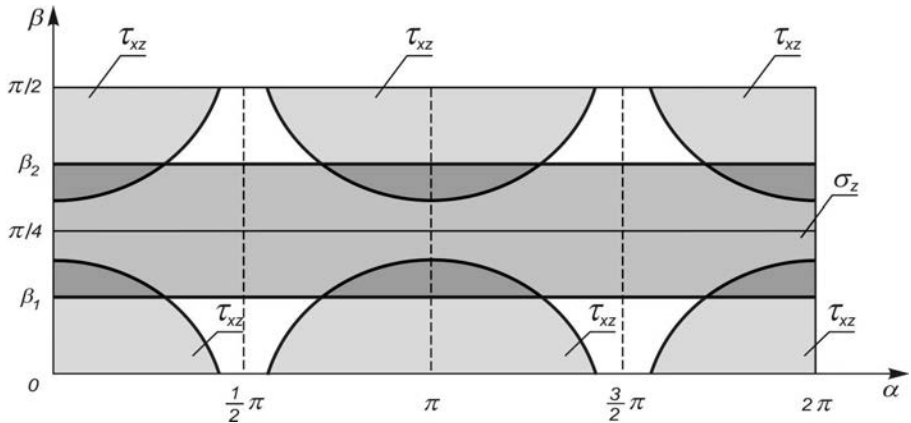


FIG. 3. The slip domains calculated for PA4 aluminum alloy under uni-axial tensile stress state $\sigma_z = 260$ MPa and pure shear stress state $\tau_{xz} = 148$ MPa.

3. EXPERIMENTAL INVESTIGATION

In order to verify the above theoretical considerations, a number of experiments using thin-walled cylindrical samples were carried out on the tension-torsion machine Instron 8502 Plus. The samples were made of aluminum alloy PA4 (containing 0.7–1.2% Mg, 0.6–1.0% Mn, 0.7–1.2% Si, below 0.5% Fe, and impurities of 0.1% Cu and 0.2% Zn). The dimensions of the samples were as follows: the external diameter 17.5 mm, the wall thickness 0.75 mm and the measurement length 75 mm. The samples were subjected to a preliminary homogenizing treatment at a temperature of 438 K for 6 hours. The method de-

scribed in Ref. [26] was used to test for material anisotropy and following the thermal treatment, the mechanical properties were found to be isotropic. The stress-strain curve obtained for tensile loading is shown in Fig. 4. The apparent yield stress under tension was found to be $R_{0.1} = 220.2$ MPa while the elastic modulus was $E = 72319$ MPa. On the basis of the strain-stress curve the initial yield stress has been evaluated $\sigma_0 = 210$ MPa. In that case the initial shear stress is $\tau_0 = 105$ MPa (τ_0 is initial resistance to plastic deformation).

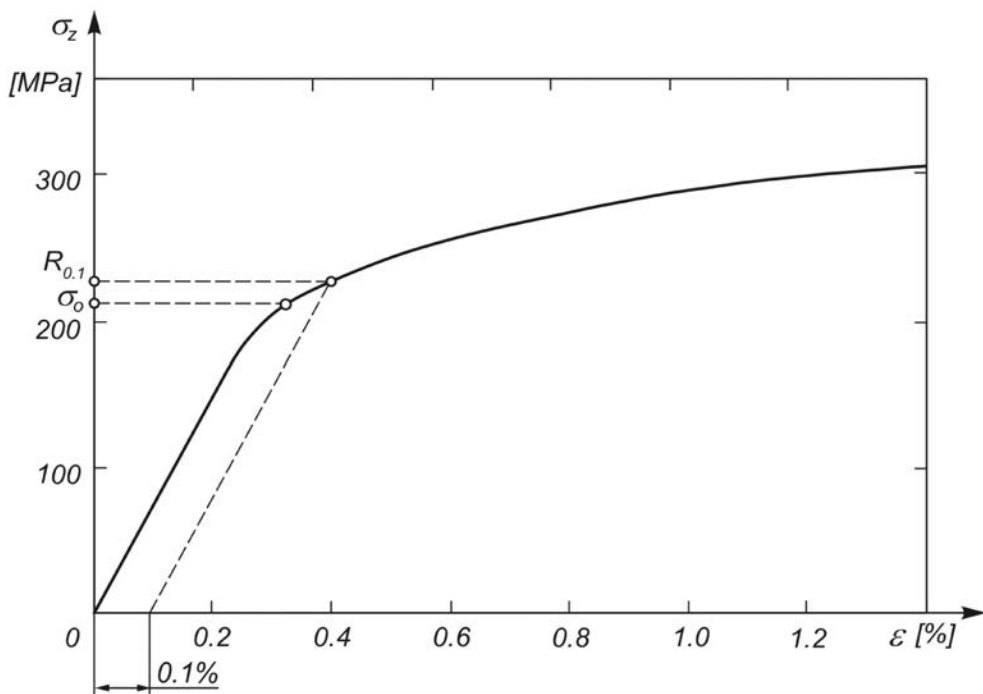


FIG. 4. Stress-strain curve for aluminum alloy: apparent yield stress $R_{0.1} = 220.2$ MPa, initial resistance to plastic deformation $\tau_0 = 105$ MPa.

Two series of experiments were carried out. The samples in the first group were subjected to a tensile force (causing some initial plastic deformation) followed by unloading (partial or complete and different for different samples). Subsequently, a torsional moment was applied and its value was increased from zero up to the point resulting with deformation intensity of 0.1%. The above method based on the apparent yield point (assumed in the present work to represent the yield criterion) proved to be more effective than the Lode extrapolation method, due to a straightforward implementation in the computer program controlling the testing machine. Each loading path was repeated for two samples.

Figure 5 shows the exemplary loading path of the sample that was first subjected to the tensile stress σ_z^B , then unloaded by diminishing stress to the

value σ_z^C , and after that subjected to the shear stress τ_{xz} of the value causing deformation intensity of 0.1%.

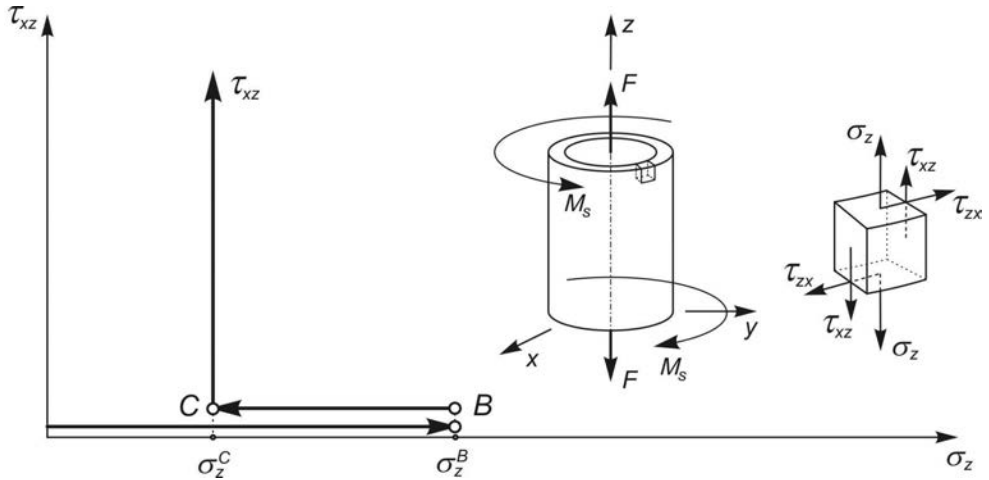


FIG. 5. The exemplary loading path of the sample subjected first to a tensile force and then (after partial unloading) to a torsional moment.

It is observed that as a result of the tensile stresses σ_z^B at the point B , the material slips by $\varphi^B(\sigma_z)$. The value of the slip can be determined on the basis of Eq. (2.8), i.e.:

$$(3.1) \quad r\varphi^B(\sigma_z) = \frac{\sigma_z^B}{2\tau_0} \sin 2\beta \sin \omega - 1.$$

After unloading the sample to the point C and applying a torsional moment resulting with the shear stress τ_{xz} , the plastic resistance function (2.4) will take the form:

$$(3.2) \quad S = \tau_0 [1 + r(\varphi^B + \varphi)],$$

where φ^B denotes the value of the slip intensity function at the point B determined according to (3.1).

It is assumed that plastic deformations do not decay after unloading, i.e. the value of the slip intensity function does not get lower after diminishing tensile stress (strain hardening of a material does not decrease). This being so, on the basis of Eqs. (2.5) and (3.2) the slips condition after partial unloading and subsequent applying the shear stress τ_{xz} will take the following form:

$$(3.3) \quad \tau_0 [1 + r(\varphi^B + \varphi)] = \tau(\sigma_z^C, \tau_{xz}),$$

where the shear stress function $\tau(\sigma_z^C, \tau_{xz})$ in the system n, l is expressed by the relation (2.11) with $\sigma_z^C = \sigma_z^B - \Delta\sigma_z$.

On the basis of the condition (3.3) one will obtain:

$$(3.4) \quad r\varphi = \frac{1}{\tau_0} \tau(\sigma_z^C, \tau_{xz}) - r\varphi^B - 1.$$

The Eq. (3.4) makes it possible to calculate the value of the shear stress τ_{xz} causing the definite plastic deformation in the case when there was a predeformation caused by the tensile stress σ_z^B . The above calculations can be performed using Eqs. (2.11), (2.13)–(2.17), and their results are presented in Fig. 6 as lines a, b, c .

Figure 6 presents graphically the experimental results of strain hardening depending on the loading path. The strain hardening is the cause of the expansion and shift of the plasticity surface, in relation to the initial surface determined for $\varepsilon_i = 0.1\%$.

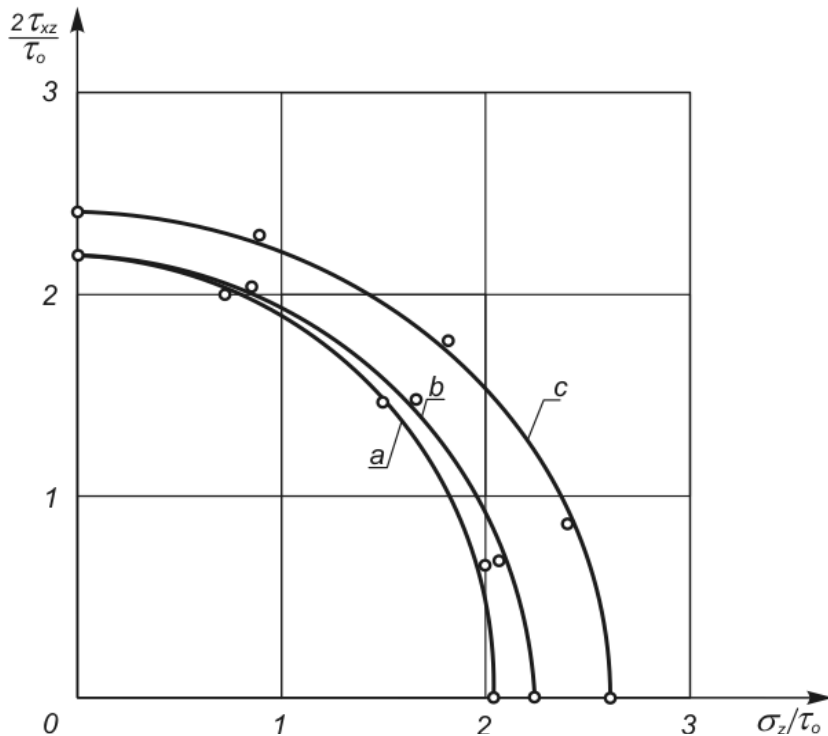


FIG. 6. Evolution of the yield surface for PA4 aluminum alloy determined using thin-walled tubular samples under combined tension and torsion, with initial plastic deformation induced by preliminary tensile loading (a – initial surface; b, c – evolving surfaces for increasing plastic deformation).

4. CONCLUDING REMARKS

Analysis of the experimental results presented in Fig. 6, taking into account the slip domains illustrated in Fig. 2 and Fig. 3, confirms the hypothesis formulated in Sec. 2 of the present paper. The plastic properties of a given material are determined by interaction of the slip systems that develop during loading. At a given material point, the strain hardening corresponding to the plastic deformation under tensile loading influences the subsequent plastic deformation under torsion loading, provided there are common slip domains. The existence of the common slip domains can be verified using the relations presented above.

The case shown in Fig. 2 corresponds to a situation when there is no interaction between the slip systems developed under two consecutively applied stress states. The case is represented by the curves *a* and *b* in Fig. 6. The curve *c* in Fig. 6 corresponds to the location of slip domains as shown in Fig. 3. It can be observed that the slip domains overlap.

The hardening model is found to be a good approximation in cases when plastic deformation is small.

Increasing of plastic deformation causes the common slip domains to grow and thus the yield surface changes not only due to the transformation of its center in the direction of loading but also due to an increase of its size in the transverse directions.

ACKNOWLEDGEMENTS

The research was carried out under the project S/WM/1/07 realized in the Białystok Technical University.

REFERENCES

1. Z. L. KOWALEWSKI, *Creep of metals: experiment and modeling* [in Polish], IPPT PAN, Warszawa 2005.
2. J. LIN, Z. L. KOWALEWSKI, J. CAO, *Creep rupture of copper and aluminium alloy under combined loadings-experiments and their various descriptions*, Int. J. of Mechanical Sciences, **47**, 1038–1058, 2005.
3. F. BARLAT, J. M. FERREIRA DUARTE, J. J. GRACIO, A. B. LOPES, E. F. RAUCH, *Plastic flow for non-monotonic loading conditions of an aluminum alloy sheet sample*, Int. J. of Plasticity, **19**, 1215–1244, 2003.
4. H. P. FEIGENBAUM, Y. F. DAFALIAS, *Directional distortional hardening in metal plasticity within thermodynamics*, Int. J. of Solids and Structures, **44**, 7526–7542, 2007.
5. W. M. MAIR, H. L. D. PUGH, *Effect of prestrain on yield surfaces in copper*, J. Mech. Eng. Sci., **6**, 150–163, 1964.

6. Z. MRÓZ, W. TRĄPCZYŃSKI, D. R. HAYHURST, *Anisotropic creep hardening rule for metals and its application to cyclic loading*, Int. J. of Plasticity, **4**, 279–299, 1988.
7. Z. MRÓZ, W. TRĄPCZYŃSKI, *On the creep hardening rule for metals with memory of maximal prestress*, Int. J. Solids Structures, **20**, 467–486, 1984.
8. S. B. BATDORF, B. BUDIAISKY, *A mathematical theory of plasticity based on the concept of slip*, NACA, TN 1871, 1949.
9. P. DŁUŻEWSKI, *Continual theory of dislocations as a theory of constitutive modeling of finite elastic-plastic deformations* [in Polish], IPPT PAN, **13/96**, Warszawa 1996.
10. T. H. LIN, S. G. RIBEIRO, *Development of a physical theory of plasticity*, Int. J. of Solids and Structures, **17**, 545–551, 1981.
11. Y. F. DAFALIAS, *Orientation distribution function in non-affine rotations*, J. Mech. Phys. Solids, **49**, 2493–2516, 2001.
12. M. V. GLAZOFF, F. BARLAT, H. WEILAND, *Continuum physics of phase and defect microstructures: bridging the gap between physical metallurgy and plasticity of aluminum alloys*, Int. J. of Plasticity, **20**, 363–402, 2004.
13. I. S. NIKITIN, *Constitutive equations of the elastoviscoplastic model and slip theory*, Mechanics of Solids, **42**, 260–270, 2007.
14. A. NEEDLEMAN, M. E. GURTIN, *Boundary conditions in small-deformation, single-crystal plasticity that account for the Burgers vector*, J. of Mechanics and Physics of Solids, **53**, 1–31, 2005.
15. G. WINTHER, D. J. JENSEN, N. HANSEN, *Dense dislocation walls and microbands aligned with slip planes – theoretical considerations*, Acta Mater., **45**, 12, 5059–5068, 1997.
16. N. HANSEN, X. HUANG, D. A. HUGHES, *Microstructural evolution and hardening parameters*, Mater. Sci. Eng., **A317**, 3–11, 2001.
17. M. P. ARIZA, M. ORTIZ, *Discrete Crystal Elasticity and Discrete Dislocations in Crystals*, Arch. Rational Mech. Anal., **178**, 149–226, 2005.
18. D. HULL, D. J. BACON, *Introduction to dislocations*, (Fourth Edition), Pergamon Press, Oxford, 2001.
19. J. ADAMCZYK, *Theory of metals – Part 3. Plastic straining, hardening and fracture* [in Polish], Silesian University of Technology, Gliwice, 1993.
20. H. J. FROST, M. F. ASHBY, *Deformation – mechanism maps. The plasticity and creep of metals and ceramics*, Pergamon Press, Oxford, 1982.
21. K. PRZYBYŁOWICZ, *Metallurgy* [in Polish], WNT, Warszawa 2003.
22. R. J. ASARO, B. ZHU, P. KRYSL, R. BAILEY, *Transition of deformation mechanisms and its connection to grain size distribution in nanocrystalline metals*, Acta Mater., **53**, 4825–4838, 2005.
23. W. OSIPIUK, *Non-elastic deformation and fracture of metals* [in Polish], Białystok Technical University, 1999.
24. K. N. RUSINKO, *Theory of plasticity and non-stationary creep* [in Russian], Lvov, Visca Skola, 1981.

25. F. MOREL, *A critical plane approach for life prediction of high cycle fatigue under multiaxial variable amplitude loading*, Int. J. of Fatigue, **22**, 101–119, 2000.
26. M. ANISIMOWICZ, *Investigation of vibrocreep of metal alloys under plane stress state* [in Polish], IFTR, IFTR Reports, 1978.

Received November 30, 2005; revised version June 16, 2008.

HEAT AND MASS TRANSFER IN MHD FLOW FROM A PERMEABLE SURFACE WITH HEAT GENERATION EFFECTS

M. M. A b d e l k h a l e k

Nuclear Physics Department
Atomic Energy Authority, Nuclear Research Centre
Cairo, Egypt, 13759

The objectives of the present study are to investigate steady two-dimensional laminar flow of a viscous incompressible, electrically conducting and heat-generating fluid, driven by a continuously moving porous plate immersed in a fluid-saturated porous medium, in the presence of a transverse magnetic field. A uniform magnetic field acts perpendicularly to the porous surface which absorbs fluid with a suction velocity. The non-linear partial differential equations governing the problem under consideration have been transformed by a similarity transformation into a system of ordinary differential equations, which is solved numerically by applying a perturbation technique. The effects of material parameters on the velocity and temperature fields across the boundary layer are investigated [28, 29]. A parametric study of all the governing parameters is carried out and representative results are illustrated to reveal a typical tendency of the solutions. Representative results are presented for the velocity temperature distributions as well as the local friction coefficient and the local Nusselt number. Favorable comparisons with the previously published work confirm the correctness of the numerical results.

Key words: heat and mass transfer, magnetohydrodynamics, heat generation, porous media, numerical analysis.

1. INTRODUCTION

The study of the dynamics of conducting fluid finds applications in a variety of engineering problems, the ones related to the cooling processes of nuclear reactors, and those related to the connected flow through a porous medium, since the geothermic region gases are electrically conducting and affected by a magnetic field. Recently many authors has been attracted to magnetohydrodynamic convection problems in non-porous medium, (SPARROW and CESS [1]; RILEY [2]; RAPTIS and SINGH [3]; SACHETI *et al.* [4]; and HUSSEIN [5]. Some works are available in the subject of MHD convection in porous medium (KAFOUSSIAS [6]; GULAB and MISHRA [7]; RAPTIS and KAFOUSIAS [8]; RAPTIS [9]; TAKHAR and RAM [10] and ABDELKHALEK [11–16]). There has been considerable interest in studying flow and heat transfer characteristics of electrically conducting and heat-generating/absorbing fluids (MOALEM [17]; CHAKRABARTI and

GUPTA [18]; VAJRVELU and NAYFEH [19]; CHIAM [20]; CHAMKHA [21]; CHANDRAN *et al.* [22]; HADJINICALAOU [23]; CHAMKHA [24], AL-MUDHAF *et al.* [25] and RAMIREZ-IRAHEA *et al.* [26]).

The main objective of this analysis is the investigation of steady two-dimensional laminar flow of a viscous incompressible, electrically conducting and heat generating fluid, driven by a continuously moving porous plate immersed in a fluid-saturated porous medium, in the presence of a transverse magnetic field. A uniform magnetic field acts perpendicularly to the porous surface which absorbs fluid with a suction velocity. A similarity transformation is used to simplify the numerical effort and a numerical solution for the problem is obtained by the perturbation technique [28, 29]. Numerical results are presented concerning the effects of the Hartmann number, Prandtl number, Darcy number, dimensionless heat generation/absorption coefficient and suction injection parameter. Typical results for the velocity and temperature distributions are presented for various governing parameters. Also, the local skin friction coefficients as well as the heat and mass transfer results are illustrated for representative values of the major parameters.

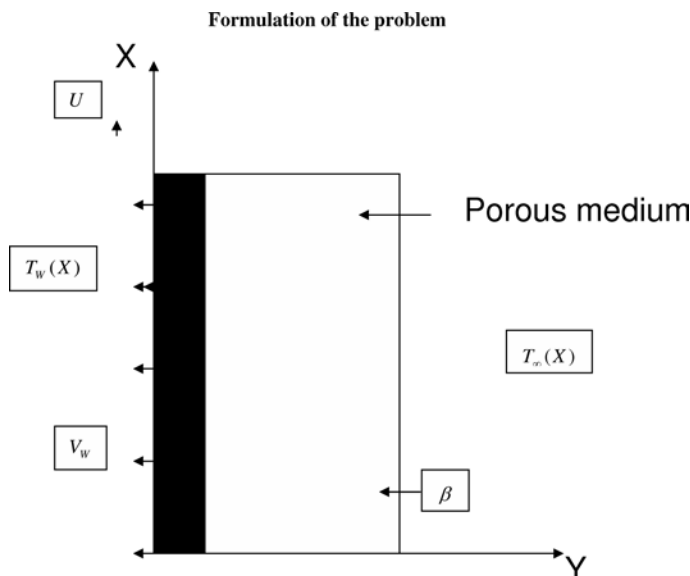


FIG. 1. Physical model and coordinate system.

Consider a two-dimensional steady, laminar, incompressible boundary-layer flow of an electrically conducting and heat-generating fluid, over a porous flat surface embedded in a porous medium, and subjected to a transverse magnetic field (see Fig. 1). It is assumed that there is no applied voltage what implies the absence of an electric field. The transversely applied magnetic field and magnetic

Reynolds number are very small and hence the induced magnetic field is negligible. Viscous and Darcy's resistance terms are taken into account with constant permeability of the porous medium. The MHD term is derived from the order of magnitude analysis of the full Navier–Stokes equations. All thermophysical properties are assumed to be constant. The effects of viscous dissipation, Ohmic heating and Hall currents are neglected. The X -axis is placed along the horizontal plate and Y -axis is perpendicular to it. Let the plate be moving with a constant speed U and at a temperature T_w . Above the plate, the fluid is stationary and is kept at a temperature T_∞ . Under the above assumptions, the boundary layer equations governing the flow and heat transfer over an infinite plate can be written as follows [33].

The continuity equation,

$$(1.1) \quad u_X + v_Y = 0.$$

The momentum equation,

$$(1.2) \quad uu_X + vv_Y = \xi u_{YY} - K^{-1}\xi u - Cu^2 - \sigma \beta^2 \rho^{-1}u.$$

The energy equation,

$$(1.3) \quad uT_X + vT_Y = \rho^{-1}C_P^{-1}(Q(T - T_\infty) + K_e T_{YY}),$$

where X and Y are the dimensional distances along and normal to the surface, respectively; u and v are the components of dimensional velocities along X and Y directions, respectively; T is the temperature, ρ is the fluid density of the medium, ξ is the kinematic viscosity, C_P is the specific heat at constant pressure, K is the permeability of the porous medium, C is the Forcheimer inertia coefficient, K_e is the effective thermal conductivity, β is the magnetic induction, σ is the fluid electrical conductivity and Q is the heat generation/absorption coefficient. The second term on the right-hand side of the momentum Eq. (1.2) denotes the bulk matrix linear resistance, i.e. the Darcy term and the fourth is the MHD term.

The appropriate boundary conditions for the velocity and temperature fields are given by:

$$(1.4) \quad \begin{array}{llll} Y = 0, & u(X) = U, & v(X) = -v_w(X), & T(X) = T_w, \\ Y \rightarrow \infty, & u(X) = 0, & T(X) = T_\infty, & \end{array}$$

where U is a constant, $v_w(X) > 0$ is the fluid suction at the plate surface, and $v_w(X) < 0$ is the fluid blowing or injection at the wall.

In order to make the results more general in their applicability, the equations are solved in non-dimensional form. For this purpose, the following non-dimensional variables are defined:

$$(1.5) \quad \begin{aligned} Y &= \left(\frac{2\xi X}{U} \right)^{0.5} \eta, & u &= U F'(\eta), \\ v &= (\eta F' - F) \left(\frac{\xi U}{2X} \right)^{0.5}, & \theta &= \frac{T - T_\infty}{T_w - T_\infty}. \end{aligned}$$

With a new set of independent and dependent variables, defined by Eq. (1.5), Eq. (1.1) is identically satisfied, and the partial differential equations (1.2)–(1.3) transform into the ordinary differential equations (1.6)–(1.7).

$$(1.6) \quad F''' + FF'' - ((M + D^{-1}) - \alpha_X F') F' = 0,$$

$$(1.7) \quad \theta'' + P_r (F \theta' + \gamma_X \theta) = 0.$$

Primes denote derivatives with respect to η .

The appropriate flat plate, with the free-convection boundary conditions Eq. (1.4), is also transformed into the applicable form, Eq. (1.8):

$$(1.8) \quad \begin{aligned} \eta = 0, & \quad F = F_w, & F' = 1, & \quad \theta = 1, \\ \eta \rightarrow \infty, & \quad F' = 0, & \theta = 0, \end{aligned}$$

where $M = \sqrt{\frac{2\sigma x\beta(x)^2}{\rho U^2}}$ is the Hartmann number, $D^{-1} = \frac{2\xi X}{KU}$ is the inverse Darcy number, $\alpha_X = 2CX$ is the dimensionless inertia coefficient, $P_r = \frac{\rho \xi C_P}{K_e}$ is the Prandtl number, $\gamma_X = \frac{2Q X}{U\rho C_P}$ is the dimensionless heat generation/absorption coefficient, $F_w = -v_w(X)\sqrt{\frac{2X}{\xi U}}$ is the dimensionless suction/blowing coefficient.

The resulting differential equations contain arbitrary parameters, the Prandtl number, the magnetic field strength and the buoyancy force. Solutions for the resulting semi-infinite domain, nonlinear equations are accomplished with a three the part series method. The employed power series, Eq. (1.9), contains term A that satisfies the boundary conditions and differential equations at infinity, the second term that satisfies the boundary conditions at zero and is the solution to the initial homogeneous differential equation, and additional terms that are

utilized to obtain a better numerical accuracy. This accuracy is limited by the number of terms that will not initiate divergence of the numerical results:

$$(1.9) \quad F = A + \varepsilon F_1 + \varepsilon^2 F_2 + \varepsilon^3 F_3 + \dots$$

$$(1.10) \quad \Theta = \varepsilon \theta_1 + \varepsilon^2 \theta_2 + \varepsilon^3 \theta_3 + \dots$$

which are subject to the boundary conditions which become:

$$(1.11) \quad \begin{aligned} \eta = 0, & \quad F_1 = F_w, & F_2 = F_3 = 0, & F'_1 = 1, \\ F'_2 = F'_3 = 0, & \theta_1 = 1, & \theta_2 = \theta_3 = 0, & \eta \rightarrow \infty, \\ F'_n = 0, & \theta_n = 0, & n = 1, 2, 3. \end{aligned}$$

Equation (1.10), the temperature representation, along with Eq. (1.9) and the associated boundary conditions (1.11), contain an undetermined parameter ε which helps in the collection of terms for each set of the resulting linear differential equations. In some problems, it will have a physical meaning which results in a power series of that parameter. Substitution of the series representation into the differential equations and collection of terms with the same powers of ε result in a set of linear differential equations, and the first three sets are:

$$(1.12) \quad F_1''' + AF_1'' - (M + D^{-1}) F_1' = 0,$$

$$(1.13) \quad \theta_1'' + P_r A \theta_1' + P_r \gamma_X \theta_1 = 0,$$

$$(1.14) \quad F_2''' + AF_2'' - (M + D^{-1}) F_2' = \alpha_X F_1'^2 - F_1 F_1'',$$

$$(1.15) \quad \theta_2'' + P_r A \theta_2' + P_r \gamma_X \theta_2 = -P_r F_1 \theta_1',$$

$$(1.16) \quad F_3''' + AF_3'' - (M + D^{-1}) F_3' = 2\alpha_X F_1' F_2' - F_1 F_2'' - F_2 F_1'',$$

$$(1.17) \quad \theta_3'' + P_r K \theta_3' + P_r \gamma_X \theta_3 = -P_r F_1 \theta_2' - P_r F_2 \theta_1'.$$

The solutions to the first three sets, Eqs. (1.18)–(1.23), when substituted into Eqs. (1.9) and (1.10), provide the required representations for F and Θ . The constant A is determined by satisfying the boundary conditions $F(0)$ and is a function of P_r and M .

$$(1.18) \quad \theta_1 = e^{-a_2 \eta},$$

$$(1.19) \quad F_1 = (f_w + a_1^{-1}) - a_1^{-1} e^{-a_1 \eta},$$

$$(1.20) \quad \theta_2 = (-a_8 + a_7 \eta) e^{-a_2 \eta} + a_8 e^{-(a_1 + a_2) \eta},$$

$$(1.21) \quad F_2 = a_6 + (a_5 + a_4\eta) e^{-a_1\eta} + a_3 e^{-2a_1\eta},$$

$$(1.22) \quad \theta_3 = (a_{18}\eta + a_{19}\eta^2 - a_{21} - a_{22}) e^{-a_2\eta} + (a_{21} + a_{20}\eta) e^{-(a_1+a_2)\eta} \\ + a_{22} e^{-(2a_1+a_2)\eta},$$

$$(1.23) \quad F_3 = -(a_{13} + a_{14} + a_{17}) + (a_{17} + a_{15}\eta + a_{16}\eta^2) e^{-a_1\eta} \\ + (a_{13} + a_{12}\eta) e^{-2a_1\eta} + a_{14} e^{-3a_1\eta}.$$

The constants a_i , $i = 1, 2, 3, \dots, 22$ are given in the Appendix.

The series for Θ , its first derivative $\Theta'(0)$ – the wall temperature gradient, F' – the velocity profile, and $F''(0)$ – the wall velocity gradient. Knowing the velocity, we can calculate the skin friction and from the temperature field, the rate of heat transfer in terms of the Nusselt number; thus, the skin friction coefficient $C_f R_e^{0.5} = -F''(0)$, and the Nusselt number $Nu = -R_e^{0.5} \Theta'(0)$, where $R_e = \frac{UX}{2\xi}$ is the Reynolds number, $\mu = \frac{\xi}{\rho}$ is the dynamic viscosity.

2. RESULTS AND DISCUSSION

In order to verify the accuracy of our present method, a comparison is made of non-dimensional wall temperature gradient $\Theta'(0)$ with those reported by JACOBI [30], TSOU *et al.* [31], ALI [32] and CHAMKHA [33] for various values of the Prandtl number Pr . Either, a comparison of non-dimensional wall velocity gradient $F''(0)$ with those reported by CHANDRAN *et al.* [22] and CHAMKHA [33], for various values of the suction/blowing coefficient F_w . The result of this comparison is given in Tables 1 and 2. The comparisons of all the above cases are found to be in excellent agreement. Sets of representative numerical results are illustrated graphically.

Figures 2 and 3 illustrate variations of different values of magnetic field pa-

Table 1. Comparison of non-dimensional wall temperature gradient ($-\Theta'(0)$) for various values of the Prandtl number.

	$Pr = 0.7$	$Pr = 1.0$	$Pr = 10.0$
JACOBI A.M. [30]	0.3492	0.4438	1.6790
TSOU <i>et al.</i> [31]	0.3492	0.4438	1.6804
ALI M. [32]	0.3476	0.4416	1.6713
CHAMKHA A.J. [33]	0.3524	0.4453	1.6830
Present work	0.35145	0.4468	1.6845

Table 2. Comparison of non dimensional wall velocity gradient ($-F''(0)$) for various values of F_w .

	$F_w = -0.2$	$F_w = -0.1$	$F_w = 0.0$	$F_w = 0.1$	$F_w = 0.2$
CHANDRAN <i>et al.</i> [22]	0.5155	0.5700	0.6275	0.6881	0.7515
CHAMKHA [33]	0.5174	0.5714	0.6288	0.6894	0.753
Present work	0.5168	0.5725	0.62834	0.68864	0.75264

parameter (M) for non-dimensional velocity and non-dimensional distributions of temperature, respectively. Flows were subjected to transverse magnetic fields and wall temperatures that were constant or varied as a fractional power of the distance in the flow direction. General results of these investigations are that the imposed magnetic field decreases the velocity field, wall shear, flow rate and wall heat transfer; also the onset of free convection was retarded while the fluid temperature and the time required for the flow to reach steady state were increased. In addition, considerable influences on the flow and thermal fields can be produced under moderate magnetic field strengths only for liquid metal flows, while the effects of induced magnetic fields and Joule heating are very small. This is illustrated by the reduction of $F'(\eta)$ and growth of $\Theta(\eta)$ as M increases in Figs. 2 and 3, respectively.

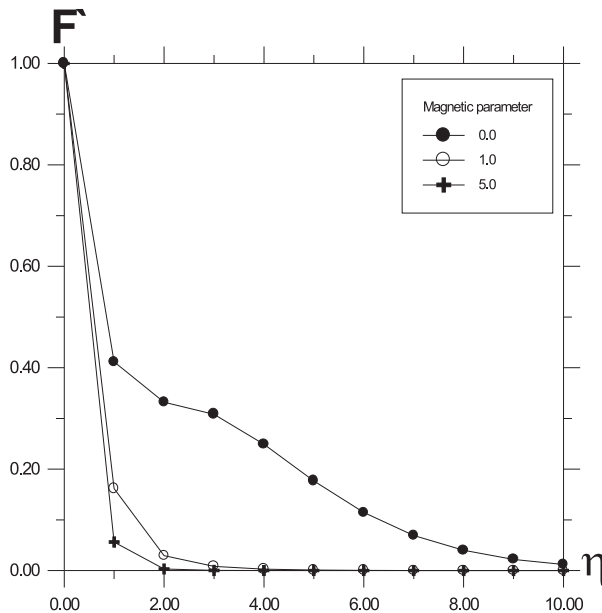


FIG. 2. Variation of velocity profiles F' with η , for $M = 0, 1, 5$, $D^{-1} = .1$, $Re = 400$, $\alpha_X = .1$, $A = .725$.

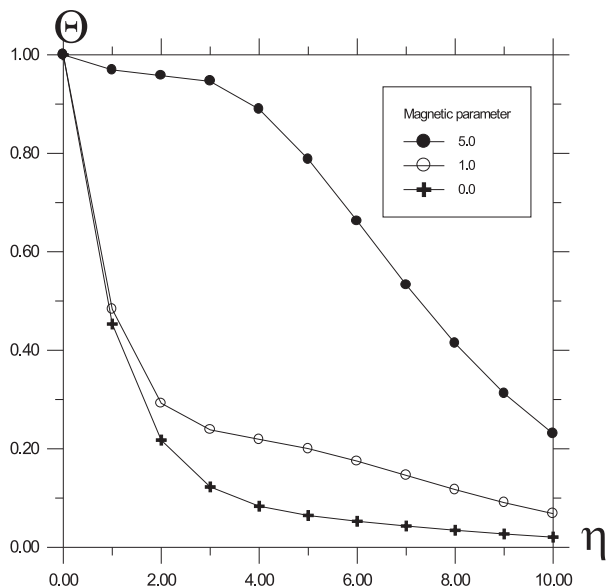


FIG. 3. Variations of temperature profiles Θ with η , for $M = 0, 1, 5$, $D^{-1} = .1$, $R_e = 400$, $\alpha_x = .1$, $A = .725$.

The effect of surface mass transfer F_w on the dimensionless velocity and temperature distributions is displayed in Figs. 4 and 5. The effect of suction consists in making the velocity and temperature distribution more uniform within the boundary layer. Imposition of fluid suction at the surface has a tendency to reduce both the hydrodynamic and thermal thickness of the boundary layer, where viscous effects dominate. This has the effect of reducing both the fluid velocity and temperature above the plate. This follows from the decreases in non-dimensional temperature $\Theta(\eta)$ as the suction/injection parameter F_w increases, as shown in Figs. 4 and 5.

Figures 6 and 7 show the changes in the fluid tangential and normal non-dimensional velocity and non-dimensional temperature, as the inverse Darcy number (D^{-1}) and the non-dimensional porous medium inertia coefficient are altered, respectively. The parameter (D^{-1}) represent resistance to the flow since they restrict the motion of the fluid along the plate. Therefore they have the same effect as the magnetic parameter M , they are decreasing the fluid velocity and increasing its temperature as shown in the figures. Figures 8 and 9 show the effect of non-dimensional porous medium inertia coefficient (α_x) on the non-dimensional velocity and non-dimensional temperature profiles. The parameter α_x represents resistance to flow since it reduces the motion of the fluid along the plate. Therefore they have the same effect as the magnetic parameter M , they are decreasing the fluid velocity and increasing its temperature, as shown in the figures.

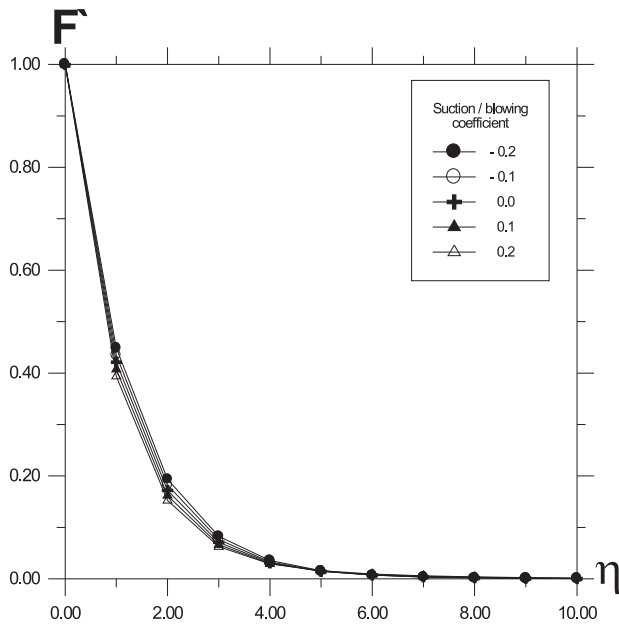


FIG. 4. Variation of velocity profiles F' with η , for $f_w = -.2, -.1, 0, .1, .2$, $D^{-1} = .1$, $R_e = 400$, $\alpha_X = .1$, $A = .725$.

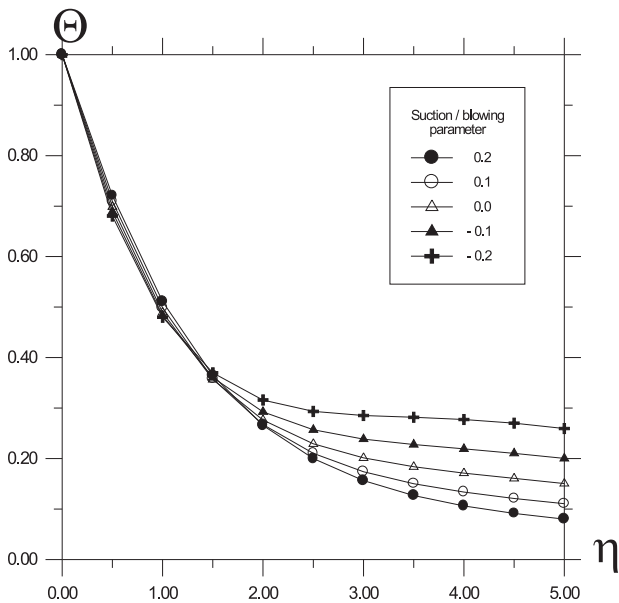


FIG. 5. Variations of temperature profiles Θ with η , for $f_w = -.2, -.1, 0, .1, .2$, $D^{-1} = .1$, $R_e = 400$, $\alpha_X = .1$, $A = .725$.

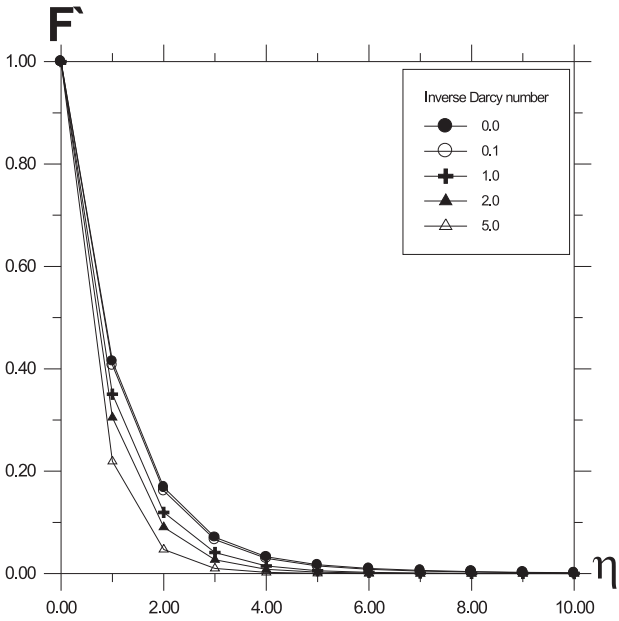


FIG. 6. Variation of velocity profiles F' with η , for $D^{-1} = 0, .1, 1, 2, 5$, $R_e = 400$, $\alpha_X = .1$, $M = 1$, $A = .725$.

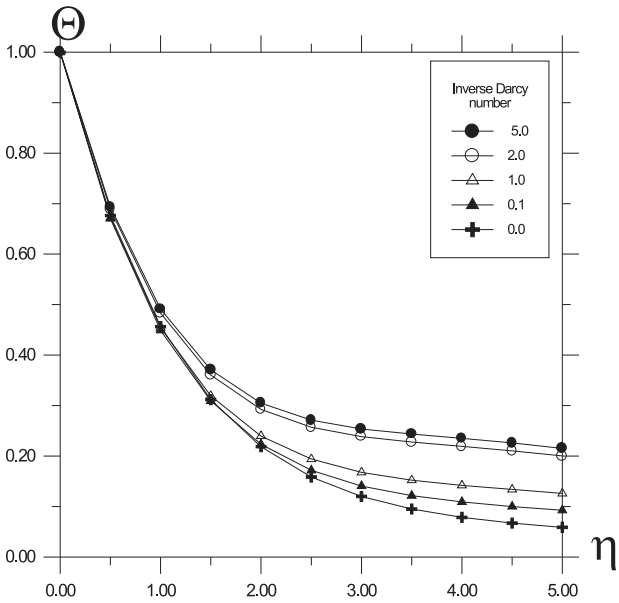


FIG. 7. Variations of temperature profiles Θ with η , for $D^{-1} = 0, .1, 1, 2, 5$, $R_e = 400$, $\alpha_X = .1$, $M = 1$, $A = .725$.

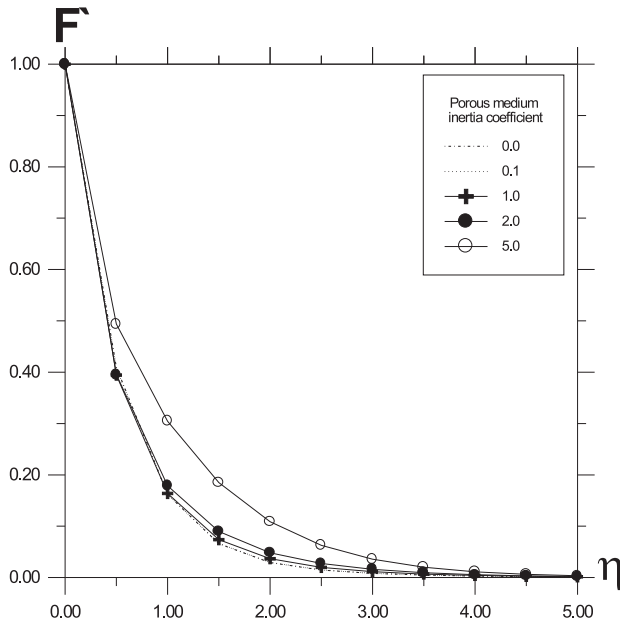


FIG. 8. Variation of velocity profiles F' with η , for $\alpha_X = 0, .1, 1, 2, 5$, $M = 1$, $D^{-1} = .1$, $\gamma_X = 0$, $f_w = .1$.

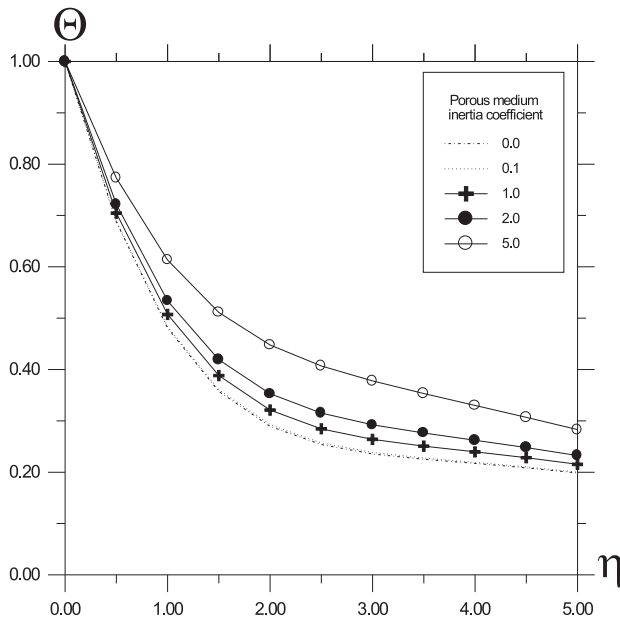


FIG. 9. Variations of temperature profiles Θ with η , for $\alpha_X = 0, .1, 1, 2, 5$, $M = 1$, $D^{-1} = .1$, $\gamma_X = 0$, $f_w = .1$.

Figure 10 presents the influence of various values of Prandtl number on the non-dimensional temperature profile. Increasing the Prandtl number reduces the thermal boundary layer along the plate. This yields a reduction in the fluid temperature. The reason of this effect is that higher Prandtl number implies more viscous fluid which increases the boundary layer thickness, and this causes reduction in the shear stress. The effects of inverse Darcy number D^{-1} on the non-dimensional surface velocity gradient is shown in Fig. 11. The presence of a porous medium in the flow presents resistance to flow, thus, slowing the flow and increasing the pressure reduction across it. Therefore, as the inverse Darcy number D^{-1} increases, the resistance due to the porous medium increases and the surface velocity gradient increases. It is seen from the figure that the skin friction increases monotonically with increasing parameter M . Figure 12 illustrates the change in the value of non-dimensional surface temperature $(-\Theta'(0))$ as a result of changing both the Hartmann parameter M and inverse Darcy number D^{-1} . It is seen from the figure that the non-dimensional surface temperature $(-\Theta'(0))$ decreases monotonically with increasing parameter M and decreases with increasing D^{-1} . The reason for this is that the presence of a porous medium D^{-1} causes higher restriction to the fluid flow, which in turn slows its motion. As a result of this, the Nusselt number at the plate surface decreases. The variations of various values of the dimensionless suction/blowing coefficient on the

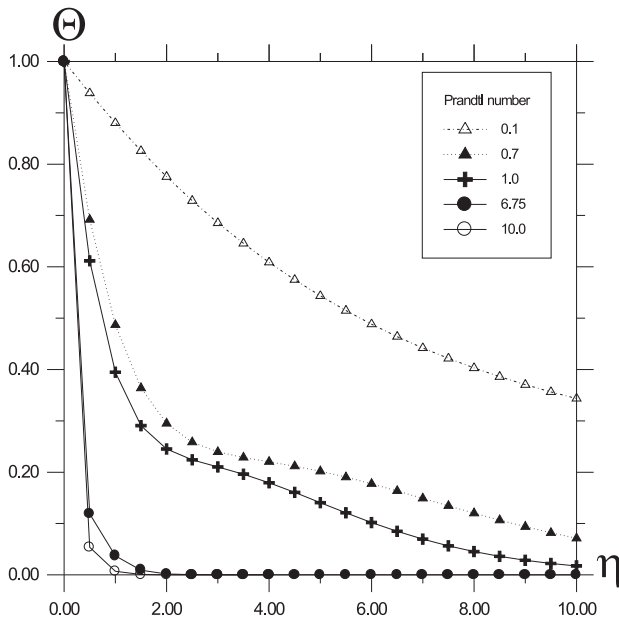


FIG. 10. Variation of temperature profiles Θ with η , for $P_r = -.1, -.7, 1, 6.75, 10$, $\gamma_X = 0$, $f_w = .1$, $Re = 400$, $A = .725$, $M = 1$, $D^{-1} = .1$.

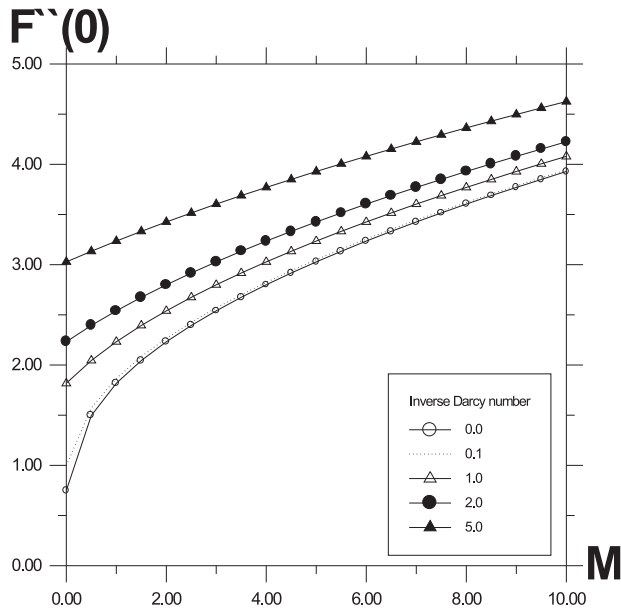


FIG. 11. Variation of wall velocity gradient profiles F'' with M , for $D^{-1} = 0, .1, 1, 2, 5$, $Re = 400$, $A = 1.25$, $\eta = 1$, $\alpha_X = .1$, $\gamma_X = 0$, $f_w = .1$.

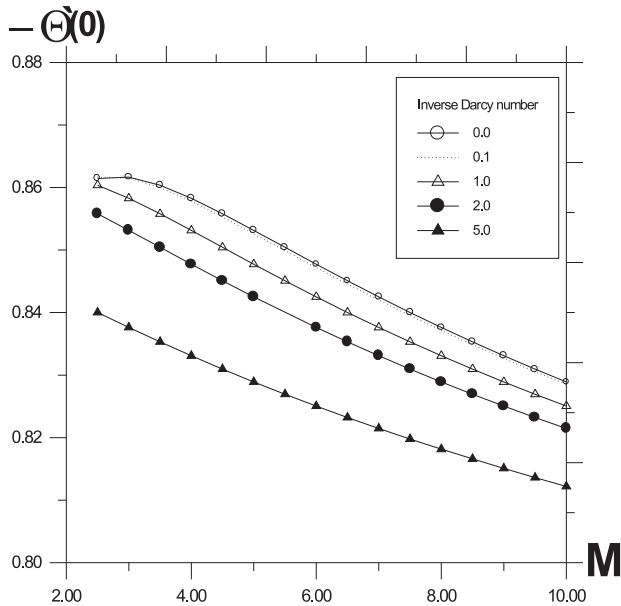


FIG. 12. Variation of wall temperature gradient profiles Θ' with M , for $D^{-1} = 0, .1, 1, 2, 5$, $Re = 400$, $A = .875$, $\eta = 1$, $\alpha_X = .1$, $\gamma_X = 0$, $f_w = .1$.

non-dimensional surface velocity gradient profiles F'' is shown in Fig. 13. It is seen from the figure that, as expected, the non-dimensional surface velocity gradient profiles F'' increase monotonically with increasing magnetic parameter M . Blowing decreases the wall shear stress both in free and forced convection flows. Suction decreases the wall shear stress in the free convection flow but increases it in forced convection flow. This is clear from the figure. LIEN *et al.* [34] reported a similar result for the isothermal wall temperature condition for free convection flows.

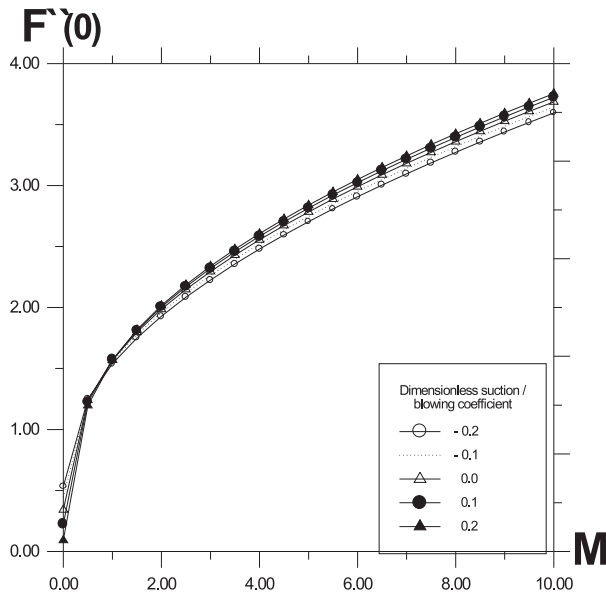


FIG. 13. Variation of wall velocity gradient profiles with M , for $f_w = -.2, -.1, 0, .1, .2$, $Re = 400$, $A = .875$, $\eta = 1$, $\alpha_X = .1$, $\gamma_X = 0$, $Pr = .7$, $D^{-1} = .1$.

The effects of suction/blowing coefficient F_w on the non-dimensional wall temperature gradient is presented in Fig. 14. The suction makes the temperature distribution more uniform within the boundary layer and decreases the thermal boundary layer thickness. The non-dimensional wall temperature gradient increases as the suction/blowing parameter F_w increases. It is seen from the figure that the non-dimensional wall temperature gradient profiles increase monotonically with increasing parameter M . Figure 15 illustrates the change in the values of non-dimensional wall temperature gradient with various values of the dimensionless heat generation/absorption coefficient Q and Prandtl number Pr . Increasing the value of Pr reduces the thermal boundary layer along the plate. This reduces the fluid temperature at every point above the plate surface and increases the dimensional wall temperature gradient. The non-dimensional wall temperature gradient increases as the Prandtl number Pr increases. The reason for this

trend is that higher Prandtl number implies more viscous fluid which increases the boundary layer thickness and this causes reduction in the shear stress.

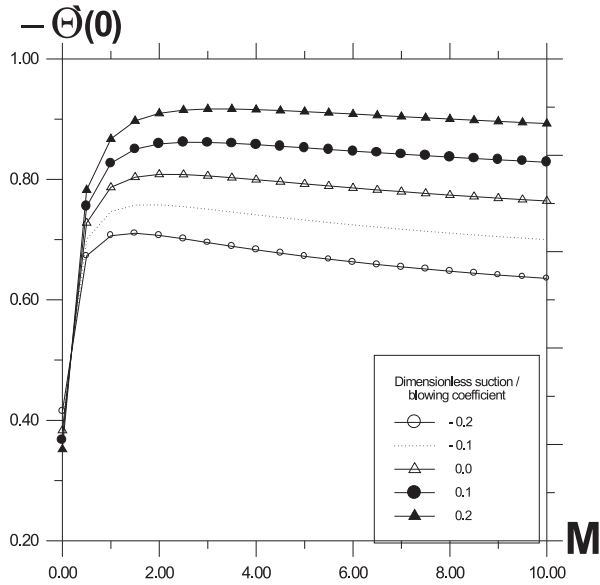


FIG. 14. Variation of wall temperature gradient profiles Θ' with M , for $f_w = -.2, -.1, 0, .1, .2$, $Re = 400$, $A = .875$, $\eta = 1$, $\alpha_X = .1$, $\gamma_X = 0$, $Pr = .7$, $D^{-1} = .1$.

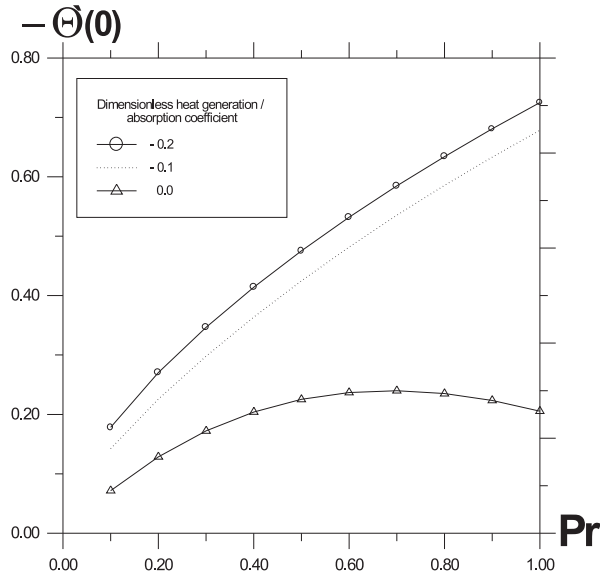


FIG. 15. Variation of wall temperature gradient profiles Θ' with Pr , for $Q = -.2, -.1, 0$, $Re = 400$, $A = 1.75$, $\eta = 1$, $\alpha_X = .1$, $\gamma_X = 0$, $M = 1$, $D^{-1} = .1$.

3. CONCLUSIONS

The problem of steady, laminar, simultaneous heat and mass transfer by natural convection boundary layer flow of an electrically-conducting and heat-generating fluid, driven by a continuously moving porous plate immersed in a fluid saturated porous medium in the presence of a transverse magnetic field was considered. The resulting transformed governing equations are solved numerically by a perturbation technique. The results are presented for the major parameters including the magnetic parameter, the Prandtl number, Darcy number, the dimensionless heat generation/absorption coefficient and the dimensionless suction/blowing coefficient. A systematic study on the effects of the various parameters on flow, heat and mass transfer characteristics is carried out. The particular conclusions drawn from this study can be listed as follows:

1. In the presence of a magnetic field, the velocity is found to be decreased, associated with a reduction in the velocity gradient at the wall, and thus the local skin-friction coefficient decreases. Also, the applied magnetic field tends to decrease the wall temperature gradient which yields a decrease in the local Nusselt number.
2. The effect of energy generation, varying in space and with local temperature, is to heat the fluid and increase the velocities inside the boundary layer and consequently, to decrease the heat transfer rates and increase the skin friction. On the contrary, the effect of energy absorption terms either space or temperature-dependent, is to cool the fluid and consequently, to increase the heat transfer rates. The mean skin friction increases with increasing of the suction parameter and decreases as the Prandtl number increases. The mean rate of heat transfer increases as the suction parameter or the Prandtl number increase, but decreases as the space or temperature-dependent heat generation term increases.
3. To increase the buoyancy ratio is to increase the local skin friction. On the other hand, increasing the buoyancy may increase or decrease the local Nusselt number, depending upon the competition between the impacts of viscous dissipation and the buoyancy ratio.
4. The local Nusselt number can be increased by increasing the values of the Prandtl number and the wall temperature. Heat is found to be transferred from the fluid to the plate (which is indicated by a negative Nusselt number) at a negative value.
5. As compared to an impermeable surface, the local skin-friction, the local Nusselt number will increase when suction is present at the permeable wall, where as the opposite trend is true for the case when the wall is subjected to injection of fluid.

APPENDIX

$$a_1 = \frac{A + \sqrt{A^2 + 4(M + D^{-1})}}{2},$$

$$a_2 = \frac{P_r A + \sqrt{P_r^2 A^2 - 4P_r \gamma_X}}{2},$$

$$a_3 = \frac{(\alpha_X - 1)}{-2a_1 (4a_1^2 - 2a_1 A - (M + D^{-1}))},$$

$$a_4 = \frac{-a_1 (F_w + a_1^{-1})}{[-3a_1^2 + 2Aa_1 + (M + D^{-1})]},$$

$$a_5 = \frac{-2a_1 a_3 + a_4}{a_1},$$

$$a_6 = -a_5 - a_3,$$

$$a_7 = \frac{(F_w + a_1^{-1}) a_2 P_r}{P_r A - 2a_2},$$

$$a_8 = \frac{-a_2 P_r}{a_1 ((a_1 + a_2) ((a_1 + a_2) - P_r A) + P_r \gamma_X)},$$

$$a_9 = ((F_w + a_1^{-1}) (a_1^2 a_5 - 2a_1 a_4)),$$

$$a_{10} = ((F_w + a_1^{-1}) 4a_1^2 a_3 - a_1 a_5 + 2a_4),$$

$$a_{11} = (F_w + a_1^{-1}) a_1^2 a_4,$$

$$a_{12} = \frac{2a_1 a_4 (1 - \alpha_X)}{-2a_1 (4a_1^2 - 2Aa_1 - (M + D^{-1}))},$$

$$a_{13} = \frac{(2\alpha_X (-a_1 a_5 + a_4) - a_{10} + a_1 a_5) - a_{12} (12a_1^2 - 4Aa_1 - (M + D^{-1}))}{-2a_1 (4a_1^2 - 2Aa_1 - (M + D^{-1}))},$$

$$a_{14} = \frac{a_1 a_3 (5 - 4\alpha_X)}{-3a_1 (9a_1^2 - 3a_1 A - (M + D^{-1}))},$$

$$\begin{aligned}
a_{15} &= \frac{(a_1 a_6 - a_9)(6a_1^2 - 4Aa_1 - 2(M+D^{-1})) + a_{11}(2A - 6a_1)}{(3a_1^2 - 2Aa_1 - (M+D^{-1}))(6a_1^2 - 4Aa_1 - 2(M+D^{-1})) - a_1(2A - 6a_1)(-a_1^2 + Aa_1 - (M+D^{-1}))}, \\
a_{16} &= \frac{-a_{11}(3a_1^2 - 2Aa_1 - (M+D^{-1})) - a_1(-a_1^2 + Aa_1 + (M+D^{-1}))(a_1 a_6 - a_9)}{(3a_1^2 - 2Aa_1 - (M+D^{-1}))(6a_1^2 - 4Aa_1 - 2(M+D^{-1})) - a_1(2A - 6a_1)(-a_1^2 + Aa_1 - (M+D^{-1}))}, \\
a_{17} &= a_1^{-1}(a_{12} - 2a_1 a_{13} - 3a_1 a_{14} + a_{15}), \\
a_{18} &= \frac{(-P_r(F_w + a_1^{-1})(a_7 + a_2 a_8) + a_2 a_6 P_r)(2P_r A - 4a_2) - 2P_r a_2 a_7(F_w + a_1^{-1})}{(P_r A - 2a_2)(2P_r A - 4a_2) - 2(a_2^2 - P_r A a_2 + P_r \gamma_X)}, \\
a_{19} &= \frac{(P_r A - 2a_2)(P_r(F_w + a_1^{-1})a_2 a_7) - (a_2^2 - P_r A a_2 + P_r \gamma_X)(-P_r(F_w + a_1^{-1})(a_2 a_8 + a_7) + a_2 a_6 P_r)}{(P_r A - 2a_2)(2P_r A - 4a_2) - 2(a_2^2 - P_r A a_2 + P_r \gamma_X)}, \\
a_{20} &= \frac{-a_2 a_7 P_r}{a_1((a_1 + a_2)((a_1 + a_2) - P_r A) + P_r \gamma_X)}, \\
a_{21} &= \frac{(P_r(F + a_1^{-1})a_8(a_1 + a_2) + P_r a_1^{-1}(a_7 + a_2 a_8) - a_{20}(P_r A - 2(a_1 + a_2)))}{((a_1 + a_2)((a_1 + a_2) - P_r A) + P_r \gamma_X)}, \\
a_{22} &= \frac{-a_8 P_r(a_1 + a_2)}{a_1((2a_1 + a_2)((2a_1 + a_2) - P_r A) + P_r \gamma_X)}.
\end{aligned}$$

Reynolds number = Inertia force/Viscous force = $Re = \rho \nu L / \mu$; the higher is the Reynolds number, the greater will be the relative contribution of the inertia effect. The smaller is the Reynolds number, the greater will be the relative magnitude of the viscous stress.

The Hartmann number $R_h = (Re R_H R_\sigma)^{0.5}$ is the ratio of the magnetic force to the viscous force and it was introduced by Hartmann in order to describe his experiments with viscous magnetohydrodynamic channel flow; the magnetic number $R_m = (R_H R_\sigma)^{0.5}$ is the ratio of the magnetic force to the inertial force, and when R_σ is very small, R_m is also used to measure the electromagnetic effects on the flow.

Prandtl number $Pr = \mu C_P / K = \nu / \alpha$ it is the ratio of kinematic viscosity to thermal diffusivity. It takes into account three physical properties of the fluid at a time. It is the ratio of two constants in molecular transportation. Symbol ν denotes the impulse transport through molecular friction, where α is the heat energy transport by conduction. It physically represents the relative speed at which momentum and energy are propagated through a fluid.

Nusselt number $Nu = hL/K$, it is a dimensionless heat transfer coefficient, which equals the ratio of the heat transfer rate q to the rate at which heat would be conducted within the fluid under a temperature gradient $\Delta\theta/L$. It can also be defined as the ratio of heat flow rate by convection under unit temperature gradient through a stationary thickness of L meter.

Darcy's model. During the last century, the researchers have derived generalized forms of the Darcy equation using either deterministic or statistical models. The well-known original form of the equation has been rewritten as: $u = -\frac{K}{\mu} \cdot \nabla P$ for an isotropic medium, where K is the so-called intrinsic permeability, and ∇P is the pressure gradient. Although Darcy's law can describe the flow through many naturally occurring porous media, it is not valid for all types of situations. In fact, defined for a porous medium, the Reynolds number is based on permeability of the porous medium as $Re_K \geq 1$. The Darcy number was based on the permeability of the porous medium (K).

ACKNOWLEDGMENTS

Appreciation is extended to the Referees for their constructive and helpful comments and suggestions. These led to improvements in the revised paper.

REFERENCES

1. E. M. SPARROW and R. D. CESS, *Int. J. Heat Mass Transfer*, **3**, 267, 1961.
2. N. RILEY, *J. Fluid Mech.*, **18**, 577, 1964.
3. A. RAPTIS and A. K. SINGH, *Int. Comm. Heat Mass Transfer*, **10**, 313, 1983.
4. N. C. SACHETI, P. CHAMDRAN and A. K. SINGH, *Int. Comm. Heat Mass Transfer*, **21**, 131, 1994.
5. M. A. HOSSAIN, *Int. J. Heat Mass Transfer*, **35**, 3485, 1992.
6. N. G. KAFOUSSIAS, *Mech. Res. Commun.*, **19**, 89, 1992.
7. R. GULAB and R. MISHRA, *Indian J. Pure Appl. Math.*, **8**, 637, 1977.
8. A. RAPTIS and N. KAFOUSSIAS, *Energy Research*, **6**, 241, 1982.
9. A. A. RAPTIS, *Energy Research*, **10**, 97, 1986.
10. H. S. TAKHAR and P. C. RAM, *Int. Comm. Heat Mass Transfer*, **21**, 371, 1994.
11. M. M. ABDELKHALEK, *International Communications in Heat and Mass Transfer*, **33**, 249, 2006.
12. M. M. ABDELKHALEK, *Arab J. of Nucl. Sci. and Applications*, **36**, 2, 189, 2003.
13. M. M. ABDELKHALEK, *Indian J. Phys.*, **80**, 6, 625–635, 2006.

14. M. M. ABDELKHALEK, Arab J. of Nucl. Sci. and Applications, **36**, 3, 243, 2003.
15. M. M. ABDELKHALEK, CAMES, **14**, 3, 471–485, 2007.
16. M. M. ABDELKHALEK, Egyptian J. of Physics, **34**, 3, 2003.
17. D. MOALEM, Int. J. Heat Mass Transfer, **19**, 529, 1976.
18. A. CHAKRABARTI and A. S. GUPTA, Q. Appl. Math., **37**, 73, 1979.
19. K. VAJRVELU and J. NAYFEH, Int. Commun. Heat Mass Transfer, **19**, 701, 1992.
20. T. C. CHIAM, Int. J. Engng. Sci., **33**, 429, 1995.
21. A. J. CHAMKHA, Int. Commun. Heat Mass Transfer, **23**, 875, 1996.
22. P. CHANDRAN, N. C. SACHETI and A. K. SINGH, Int. Commun. Heat Mass Transfer, **23**, 889, 1996.
23. K. VAJRVELU and A. HADJINICALAOU, Int. J. Engrg. Sci., **35**, 1237, 1997.
24. A. J. CHAMKHA, Int. J. of Heat and Fluid Flow, **20**, 84, 1999.
25. ALI AL-MUDHAF and ALI J. CHAMKHA, Heat Mass Transfer, **42**, 112, 2005.
26. O. A. RAMIREZ-IRAHETA, H. M. SOLIMAN and S. J. ORMISTON, Heat Mass Transfer, **42**, 398, 2006.
27. MD. ANWAR HUSSAIN and D. A. S. REES, Heat Mass Transfer, **41**, 367, 2005.
28. A. AZIZ, T. Y. NA, *Perturbation Methods in Heat Transfer*, Springer-Verlag, Berlin, 1–184, 1984.
29. R. KENNETH CRAMER, SHIH-I PAI, *Magnetofluid Dynamics for Engineers and Applied Physicists*, McGraw-Hill Book Company, New York, 164–171, 1973.
30. A. M. JACOBI, J. Heat Transfer, **115**, 1058, 1993.
31. F. K. TSOU, E. M. SPARROW and R. J. GOLDSTEIN, Int. J. Heat Mass Transfer, **10**, 219, 1967.
32. M. ALI, Int. J. Heat and Fluid Flow, **16**, 280, 1995.
33. A. J. CHAMKHA, Int. Comm. Heat Mass Transfer, **24**, 6, 815, 1997.
34. F. S. LIEN and C. K. CHEN, Trans. ASME, **108**, 398, 1986.

Received October 04, 2007; revised version January 24, 2008.

AN INVESTIGATION OF METAL TRANSFER PROCESS IN GMAW

M. S. Węglowski¹⁾, Y. Huang²⁾, Y. M. Zhang²⁾

¹⁾ **Institute of Welding**

Testing of Materials Weldability and Welded Constructions Department

Bl. Czesława 16/18, 44-100 Gliwice, Poland

²⁾ **University of Kentucky**

Center for Manufacturing

Lexington, KY 40506, USA

This paper presents the studies of the metal transfer process in gas metal arc welding with mild steel electrode. It aims at mathematic description of the droplet flight trajectory, droplet velocity and acceleration. To this end, the droplet flight trajectory was first fitted using the 3rd order polynomial regression and it was found that the model can be reduced to the 2nd order. The average diameter of a droplet, transfer rate of droplets, average velocity and acceleration of a droplet were calculated. The geometric shape factor was estimated. A new metal transfer monitoring method which is based on narrow band filter and does not require He-Ne laser, has been used in this study to observe the metal transfer process.

1. INTRODUCTION

The GMAW (Gas Metal Arc Welding) process employs a continuous consumable solid wire electrode and an externally supplied active shielding gas. A scheme of the process is shown in Fig. 1. The consumable wire electrode produces an arc with the workpiece making part of the electric circuit and providing a filler to the weld joint. The wire is fed to the arc by an automatic wire feeder, of which both push and pull-types are employed, depending on the wire composition, diameter, and welding application. The externally supplied shielding gas plays dual roles in the GMAW. First, it protects the arc and the molten or hot, cooling weld metal from the contamination of the air. Second, it provides the desired arc characteristics through its effect on ionization. A variety of gases can be used, depending on the reactivity of the metal being welded, the design of the joint and the specific arc characteristics that are desired.

Metal transfer is the process of the molten metal's movement from the electrode tip to the workpiece, which includes droplet formation, detachment and transfer in the arc gap. The transport of droplets into the weld pool is largely responsible for the finger penetration commonly observed in the fusion zone [1, 2].

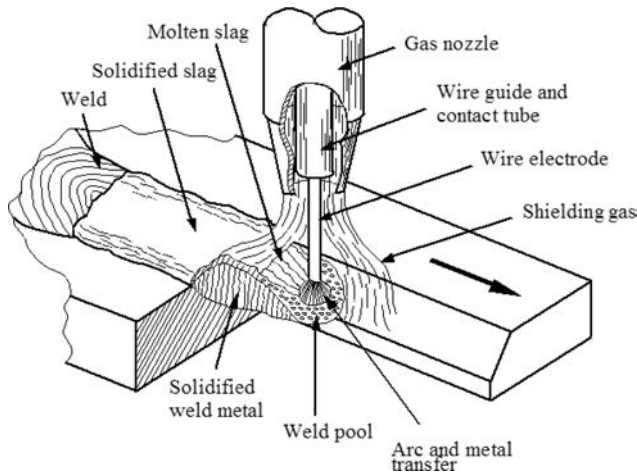


FIG. 1. Illustration of GMAW.

There are a few modes of metal transfer in GMAW such as short circuiting, globular and spray transfer. In the short circuiting transfer the end of the electrode actually touches the molten pool, creating a momentary short circuit. This condition triggers an increase in current sufficient to melt the tip of the electrode and then reestablish the arc between the electrode and the workpiece. The cycle repeats itself about 50 to 250 times per second. This type of transfer is good for welding thin metals in all positions, incomplete fusion may occur in base metal in excess of 3.2 mm. The globular transfer occurs at a current range above short circuiting transfer. The melted droplets that transfer into the molten pool are about two to four times the diameter of the electrode, and they fall in an irregular pattern and with an irregular frequency. This type of transfer typically produces spatters, and in most instances, it is the type of transfer when CO_2 is the only shielding gas. Spray transfer occurs at high welding currents with argon-rich ($> 90\%$) shielding gas mixtures. The molten droplets are small, and they are forced across the arc in an axial pattern. The arc column is constricted. This type of transfer produces minimal spatter and is conducive to high deposition rates. The rotational spray transfer occurs when a solid wire is used with a long electrode extension of 20 to 40 mm and the shielding gas is a mixture of $\text{Ar} + \text{CO}_2$ or $\text{Ar} + \text{O}_2$. The long electrode extension creates resistance heating of the electrode that causes its end to become molten. Electromechanical forces make the molten end of the electrode rotate in a helical pattern. The shielding gas mixture affects the surface tension of the molten end assisting in the rotational transfer. Deposition rates of 10 to 15 kg/h are attained with this transfer mode [3].

Metal transfer has been a subject matter of many investigations. A better understanding of the metal transfer process is important for improvements in the quality and productivity of welding. The welding voltage, current, arc length,

shielding gas and wire feed rate can all affect the metal transfer process. Among them, current is most often studied for its influence on the droplet size, frequency and acceleration in the arc.

Many papers described the methodology of mathematical analysis for the formation of droplets and analysed and calculated the effects of individual forces acting on metal droplets at the tip of the wire in GMAW [4]. In order to determine the dominant factors, which affect the metal transfer mode, a dimensional analysis has been conducted in previous studies [5]. Several dimensionless numbers which are derived on the basis of the surface-tension force are the Weber (We), Bond (Bo), N_{SE} , N_{SV} . Here the subscripts S and V denote the surface tension and viscosity. These numbers represent the relative effects of electrode melting, gravitational, electromagnetic and viscous forces with respect to the surface-tension force, respectively. The N_{SE} number was found to be the most important dimensionless number influencing the characteristics of metal transfer [5]. Through the arc sensing methods are also widely used to study metal transfer. By recording and analysing fluctuations of the welding voltage and/or current, it is possible to predict the metal transfer mode [6]. Due to its simplicity and nonintrusive nature, through the arc sensing can also be used to study the GMAW process, but can also be used in welding process control. Most of recent investigations focused on studying the effect of waveform parameters on the mode of metal transfer in pulsed gas metal arc welding (GMAW-P) [7–11]. The metal transfer mode is also an interesting subject matter in newly developed welding methods such as double electrode gas metal arc welding (DE-GMAW) developed at the University of Kentucky [12, 13]. Some studies focused on detailed analysis of droplet velocity and developed a model based only on the electromagnetic pinch force [14]. Many efforts have been made to optimize welding parameters to achieve one droplet per pulse (ODPP-GMAW) [15]. Further, a non-isothermal numerical model has been developed to simulate the metal transfer process in GMAW. Experiments with high-speed photography and laser-shadow imaging show that the simulation results were in broad agreement with the actual welding process [16]. The newest investigations about metal transfer even allow to create a new classification of mode of metal transfer modes [17]. The melting of the wire, which is fundamental and influences the process stability and productivity, has also been a main topic of some investigations [18]. Recently, hybrid laser-MIG welding methods have also been studied [19].

Droplet acceleration in the arc has been calculated by many authors [20–25] using the empirical formulation presented by LANCASTER [26]. To calculate the plasma drag force exerted on the droplet using this formulation, the droplet was assumed to have a spherical shape and accelerate to the workpiece with a constant acceleration [27]. The acceleration of the droplet is found to be near constant by JONES *et al.* [28] and assumed to be constant by many authors in their

calculations [20–24]. With many factors influencing metal transfer, theoretical models such as the static force balance theory [29–30] and the pinch instability theory [31–32] have been proposed to explain the metal transfer phenomena, but the success is limited. The authors [33] investigated the relative magnitudes of the detaching forces in static force balance theory and showed good agreement with experimental results within the range of globular transfer; however, in the spray transfer mode, the theory deviates significantly from the experiment.

Despite a significant progress, the existing investigations that have been carried out up to date have not covered the subject matter of mathematic description of droplet flight trajectory, changes of droplet velocity and droplet acceleration, although this subject matter can further our understanding of the metal transfer process. Hence, the droplet size, droplet transfer rate, mathematic descriptions of droplet flight trajectory and droplet velocity and droplet acceleration, are analyzed in this paper. In previous investigations the back-lighting technique has been used to image the metal transfer process using a He-Ne laser [34]. The problem with this method is that the laser and imaging plane must be placed on two opposite sides of the torch. A high-speed camera with a narrowband pass filter is used to directly view the metal transfer process. This technique is easier to use because of the elimination of the need for back-lighting.

2. THEORETICAL BACKGROUND

The static force balance theory postulates that the drop detaches from the electrode when the static detaching forces on the drop exceeds the static retaining forces. Four different forces have been considered [33]:

- the gravitational force,
- electromagnetic force,
- plasma drag force,
- surface tension force.

The gravitational force is due to the mass of the drop and acts as a detaching force when welding in flat position:

$$(2.1) \quad F_g = \frac{4}{3}\pi R^3 \rho_D g,$$

where R – radius of droplet, ρ_D – density of droplet.

The electromagnetic force on the drop results from divergence or convergence of current flow within the electrode. The electromagnetic force is given by Lorentz's law:

$$(2.2) \quad F_{em} = \bar{J} \times \bar{B},$$

where J – current density, B – magnetic flux.

By assuming that the current density on the drop is uniform, the total electromagnetic force on a drop can be obtained by integrating Eq. (2.2) over the current conducting surface of the drop [14]:

$$(2.3) \quad F_m = \frac{\mu_0 I^2}{4\pi} f(s),$$

where I – welding current, μ_0 – the magnetic permeability of the free space, $f(s)$ – a geometric shape factor depending on the droplet radius and neck diameter during droplet growth and detachment.

The plasma drag force on the liquid drop can be estimated by considering the drag force on a sphere immersed in a fluid of uniform velocity field [33]:

$$(2.4) \quad F_d = C_D A_P \left(\frac{\rho_f v_f^2}{2} \right),$$

where C_D – drag coefficient, A_P – projected area on the plane perpendicular to the fluid flow, ρ_f – density of the fluid, v_f – velocity of the gas.

Surface tension force, which acts to retain the liquid drop on the electrode is given as follows:

$$(2.5) \quad F_S = 2\pi\alpha\gamma,$$

where α – radius of the electrode, γ – surface tension of the liquid.

From the static force balance theory, the droplet size can be calculated under the assumption that the drop is not detached from electrode if the sum of detaching forces equals the retaining force [33]:

$$(2.6) \quad F_\gamma = F_{em} + F_g + F_d.$$

Hence, Eq. (2.6) holds during the process of droplet formation. After the droplet is detached, it travels in the arc gap subjecting the sum of the following forces:

$$(2.7) \quad F_{em} + F_g + F_{arc},$$

where F_{arc} accounts all other possible forces except for the electromagnetic and gravitational forces. To calculate the geometric shape factor $f(s)$ defined in (2.3), the other forces are omitted. Hence,

$$(2.8) \quad \frac{4}{3}\pi R^3 \rho_D a = \frac{\mu_0 I^2}{4\pi} f(s) + \frac{4}{3}\pi R^3 \rho_D g,$$

where a is the acceleration of the droplet in the air gap. As a result, the geometric shape factor can be calculated as:

$$(2.9) \quad f(s) = \frac{\frac{16}{3}\pi^2 R^3 \rho_D (a - g)}{\mu_0 I^2}.$$

3. EXPERIMENTAL SETUP AND PROCEDURE

Mild steel Quantum ARC 6 carbon steel wire (AWS A5.18, ER70S-6) equivalent to SG2 was used in the experiments. The electrode’s diameter is 1.2 mm (0.045 inch). The chemical composition of the wire is given in Table 1. The shielding gas used was pure argon.

Table 1. Chemical composition of wire.

C	Mn	Si	P	S	Cu
0.06–0.15	1.40–1.85	0.8–1.15	<0.025	<0.025	<0.05

Experiments were carried out on an automated GMAW platform. A simple scheme of the experimental setup with data flow is shown in Fig. 2. The torch was moved while the work-piece was in a fixed position such that the camera was stationary in relation to the work-piece. All welds were made with a standard water cooled welding gun Miller Roughneck C 4015. The wire feeder was a Miller R-115. The torch was moved at the travel speed of 25 cm/min (10 inch/min) to make bead-on-plate welds. Direct current levels between 206 and 262 A were examined, all at an operating voltage 32 V. All experiments were carried out with a tip-to-work distance of 15 mm. The current and, therefore, the metal transfer mode were changed by changing the wire feed rates in the range from 4.57 m/min to 6.85 m/min (180 to 270 inch/min). The conventional three-phase welding machine Hobart EXCEL – ARC 8065 CC/CV was used.

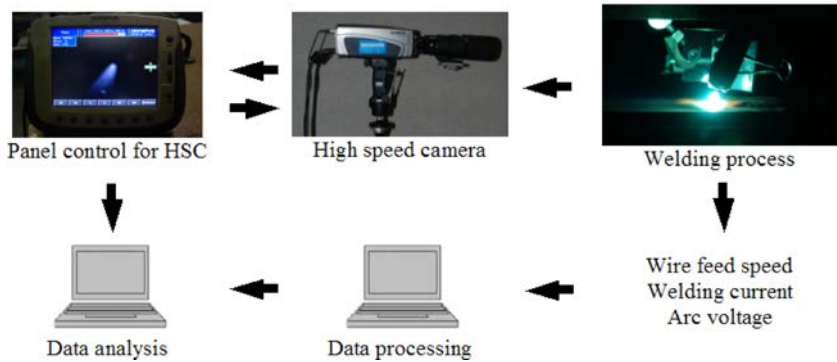


FIG. 2. Experimental setup with flow of data.

During welding the arc voltage, welding current and wire feed speed were continuously measured. Electrical current was measured by Hall effect current sensor Model CLN-500. The voltage was measured by a resistance bridge directly in the output of power supply. Signals from the welding circuit were recorded on the PC through the data acquisition card NI DAQ 6036E. Analysis of the metal

transfer process was performed using high speed camera Olympus i-SPEED at 3000 frame per second (fps). The camera direction was perpendicular to the welding direction. In addition to an aperture of 11 and a shutter of 1, a narrow-band filter (central wavelength 685 nm, bandwidth 20 nm) was used to reduce the arc brightness in order to image the metal transfer.

4. RESULTS AND DISCUSSION

The recorded images of metal transfer from the high speed camera are analyzed by i-SPEED viewer and IrfanViewer software. An image sequence of droplet track in GMAW for wire feed speed 270 inch/min – welding current 262 A and arc voltage 32 V at 3000 frames per second, is shown in Fig. 3; and for wire feed speed 180 inch/min – welding current 206 A in Fig. 4. The arrow marks the same droplet being tracked. Experiments were performed on clean plates. The macroscopic examination of padding welds with welding parameters are given in Table 2.

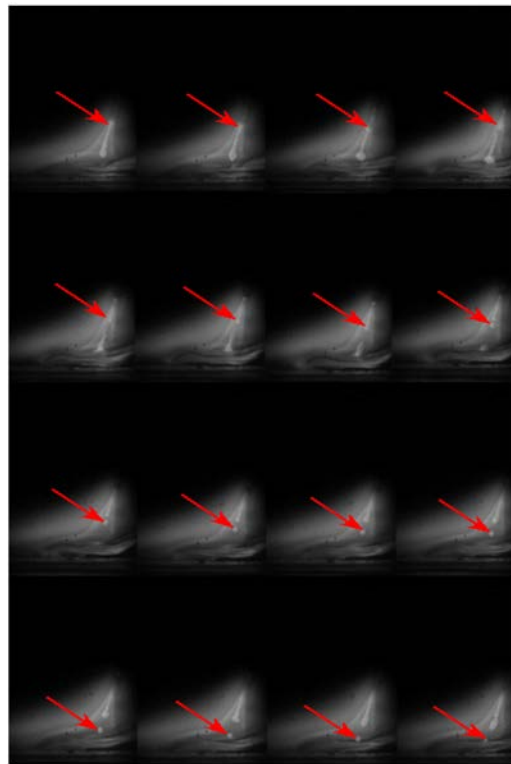


FIG. 3. Image sequence of droplet track in GMAW. Wire speed 270 inch/min (6.85 m/min) – welding current 262 A, arc voltage 32 V, 100% Ar. Sampling speed is 3000 frames per second. The arrow marks the same droplet.

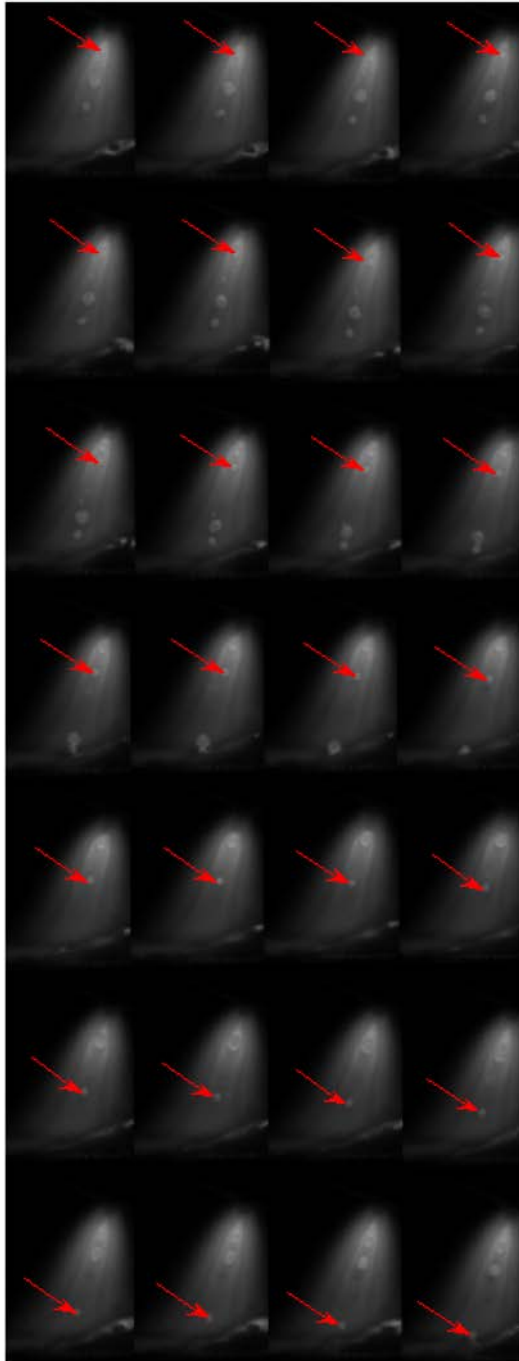

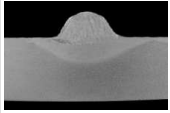

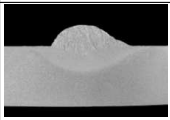

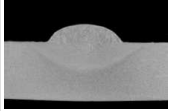

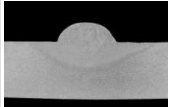

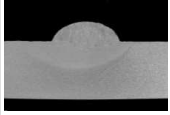

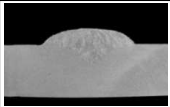



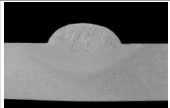

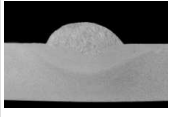

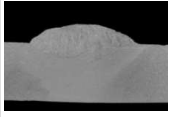


FIG. 4. Image sequence of droplet track in GMAW. Wire speed 180 inch/min (4.57 m/min)
– welding current 206 A, arc voltage 32 V, 100% Ar. Sampling speed is 3000 frames per
second. The arrow marks the same droplet.

Table 2. Macroscopic examination of padding welds.

No	Wire feed speed [inch/min]/[m/min] welding current [A] and standard deviation $I \pm S_{dI}$	Appearance	Macroscopic Section 1:1
1	180/4.57 206 ± 19		
2	190/4.83 211 ± 33		
3	200/5.08 216 ± 12		
4	210/5.33 225 ± 7		
5	220/5.59 229 ± 5		
6	230/5.84 232 ± 4		
7	240/6.10 247 ± 7		
8	250/6.35 250 ± 3		
9	260/6.60 256 ± 8		
10	270/6.85 262 ± 5		

4.1. Droplet diameter and number of droplets per second

The first goal of this study was to calculate the diameter of the droplet. To this end, it was necessary to measure droplet diameter in two directions (horizontal d_h and vertical d_v diameter), as shown in Fig. 5. When the droplet to be analyzed reaches a particular location in the image, the diameter D of the droplet is calculated as:

$$(4.1) \quad D = \frac{(d_h + d_v)}{2}.$$

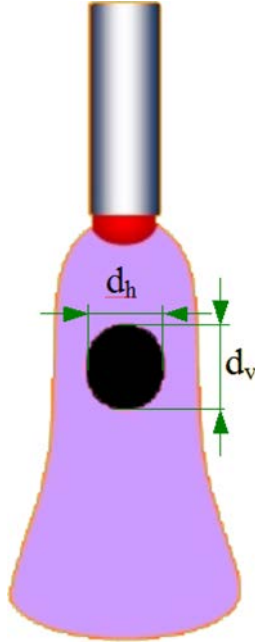


FIG. 5. Methodology for calculating the diameter of a single droplet in GMAW; d_h – horizontal diameter, d_v – vertical diameter.

The average diameter was calculated for each set of welding parameters using seven image sequences. The minimal and maximal values were not used in the calculation. Next sequence was used if the difference between horizontal and vertical diameter was higher than 20%. The standard error of droplet diameter was calculated based on the following formula:

$$(4.2) \quad S_D = \sqrt{S_d^2 + S_i^2},$$

where S_D – standard error of droplet diameter, S_d – standard deviation, S_i – measurement resolution.

The measurement resolution was $S_i = 0.1$ mm. The results of calculation are given in Table 3. To calculate the transfer rate, the following assumptions were made:

- the difference between horizontal and vertical diameter is less than 20%, and the droplet can be assumed to be spherical approximately,
- the welding process is stable and transfer rate is constant vs. time,
- spatters are negligible.

Table 3. Relationship between wire feed speed and droplet diameter.

No	Wire feed [inch/min]	Mean value of d_v/d_h [%]	Standard deviation S_d [mm]	Real value with standard error $D \pm S_D$ [mm]
1	180	101.86	0.12	0.99 ± 0.16
2	190	110.08	0.12	0.90 ± 0.16
3	200	105.07	0.06	0.82 ± 0.12
4	210	93.36	0.07	0.68 ± 0.12
5	220	100.41	0.08	0.65 ± 0.13
6	230	101.23	0.12	0.52 ± 0.15
7	240	96.54	0.12	0.51 ± 0.15
8	250	103.08	0.06	0.48 ± 0.12
9	260	102.16	0.02	0.46 ± 0.10
10	270	99.81	0.03	0.43 ± 0.10

The second goal was to calculate the droplet transfer rate (the number of droplets detached per second). In a unit time, the total volume of the transferred droplets is equal to the molten metal:

$$(4.3) \quad n \frac{4}{3} \pi \left(\frac{D}{2} \right)^3 = \frac{1}{4} \pi d^2 v_{el},$$

where n – number of droplets per second, D – average diameter of droplet [m], V_{el} – wire feed [m/s].

The number of droplets can thus be calculated as:

$$(4.4) \quad n = \frac{3}{8} \cdot \frac{d^2}{D^3} \cdot v_{el}.$$

The results of the transfer rate calculation are shown in Fig. 6 for wire feed rate in the range from 180 inch/min to 270 inch/min with volume of droplet.

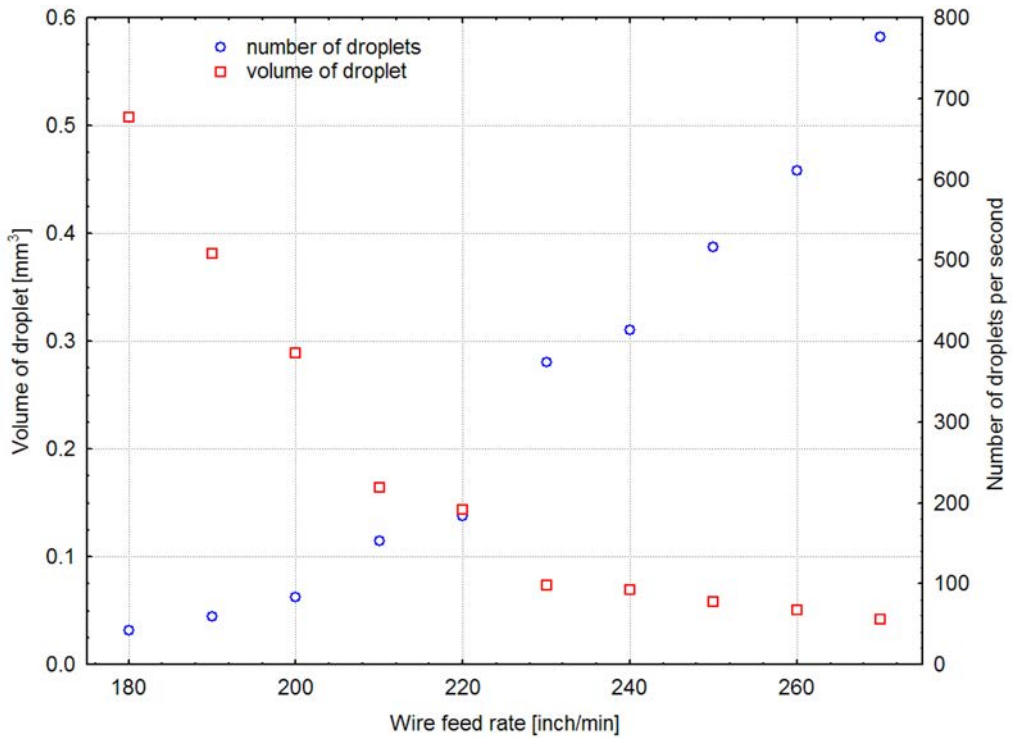


FIG. 6. Influence of wire speed rate (welding current) on droplet volume and transfer rate.

4.2. Droplet velocity and acceleration

The authors first used a 3rd degree polynomial to fit the travel of the droplet:

$$(4.5) \quad y(t) = A + B_1 \cdot t + B_2 \cdot t^2 + B_3 \cdot t^3,$$

where t – time [ms], y – distance traveled along the arc axis after detachment [mm], A , B_i – coefficients.

The resultant coefficients fitted with the residual are given in Table 4.

Since the residual in all cases is relatively small, a reduced model of 2nd degree is considered:

$$(4.6) \quad y(t) = A + B_1 \cdot t + B_2 \cdot t^2.$$

The resultant coefficients and residuals are given in Table 5 for wire feed rate in the range from 180 inch/min to 270 inch/min. As it can be seen, the residuals are still small and are in the range of acceptable error. Hence, the 2nd

Table 4. Calculated coefficients in formula 4.5 in relation to wire feed rate.

No	Wire feed rate [inch/min]	A	B_1	B_2	B_3	ε [mm]
1	180	0.01114	0.24233	0.07043	-0.00021	0.1141
2	190	0.00672	0.15328	0.07731	-0.00117	0.0556
3	200	-0.00651	0.20726	0.06304	-0.00115	0.0473
4	210	0.10272	0.19594	0.06292	-0.00014	0.0615
5	220	-0.02921	0.12451	0.07911	-0.00139	0.1726
6	230	-0.05401	0.54832	-0.11971	0.01942	0.0592
7	240	0.10203	0.38482	0.02997	-0.00049	0.0428
8	250	0.03580	0.17848	0.10762	-0.00688	0.0410
9	260	-0.03676	0.48401	0.13222	-0.01175	0.0418
10	270	-0.10866	0.85462	-0.03029	0.009	0.0566

Table 5. Calculated coefficients in formula 4.6 in relation to wire feed rate.

No	Wire feed rate [inch/min]	A	B_1	B_2	ε [mm]
1	180	0.00363	0.25293	0.06754	0.1138
2	190	-0.02305	0.20089	0.06274	0.1489
3	200	-0.03243	0.25064	0.04921	0.0495
4	210	0.10624	0.19032	0.06462	0.0457
5	220	-0.06465	0.18118	0.06176	0.2230
6	230	0.19185	0.04307	0.07449	0.1132
7	240	0.09091	0.40344	0.02403	0.0444
8	250	-0.08189	0.39559	0.03193	0.0639
9	260	-0.09613	0.65459	0.04412	0.0448
10	270	-0.04073	0.68622	0.04618	0.0639

degree polynomial model can be accepted. The resultant models of 2nd degree are graphically shown in Fig. 7.

To calculate the changes in velocity v_i for wire feed speed in the range of 180 inch/min to 270 inch/min, the derivative of movement equation (4.6) can be calculated. To achieve droplet velocity in unit of mm/s formula (4.6) was multiplication by 1000 times. The results of the calculation are shown in Fig. 8.

To calculate the average droplet velocity, the following formula was used:

$$(4.7) \quad \bar{v}_i = \frac{1}{T} \int_0^T v_i(t) dt,$$

where T is the time the droplet reaches the weld pool. To calculate the droplet acceleration, the 2nd derivative of movement equation was calculated:

$$(4.8) \quad \ddot{y}(t) = 2 \cdot B_2.$$

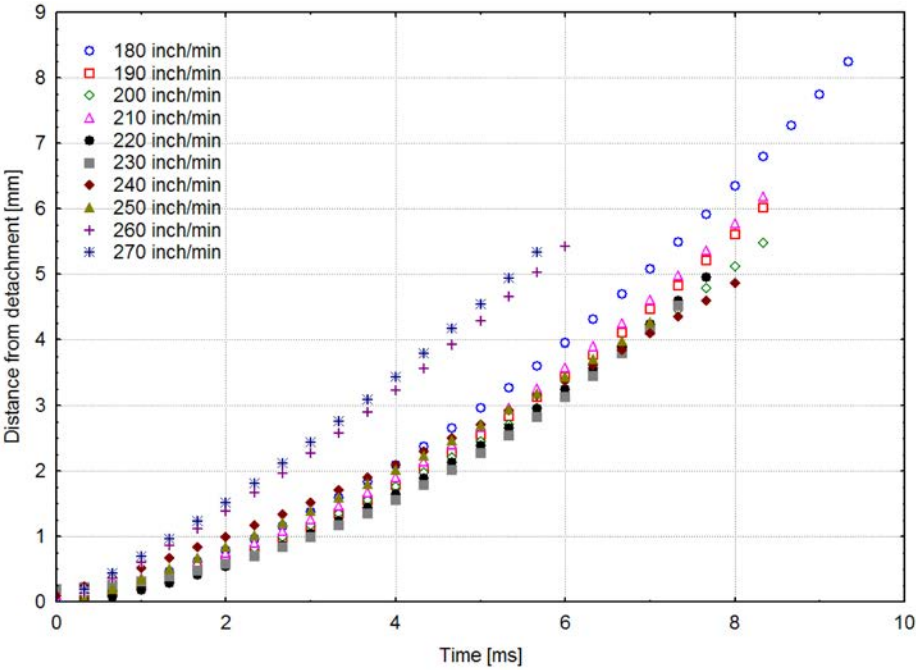


FIG. 7. Influence of wire speed rate (welding current) on droplet flight trajectory.

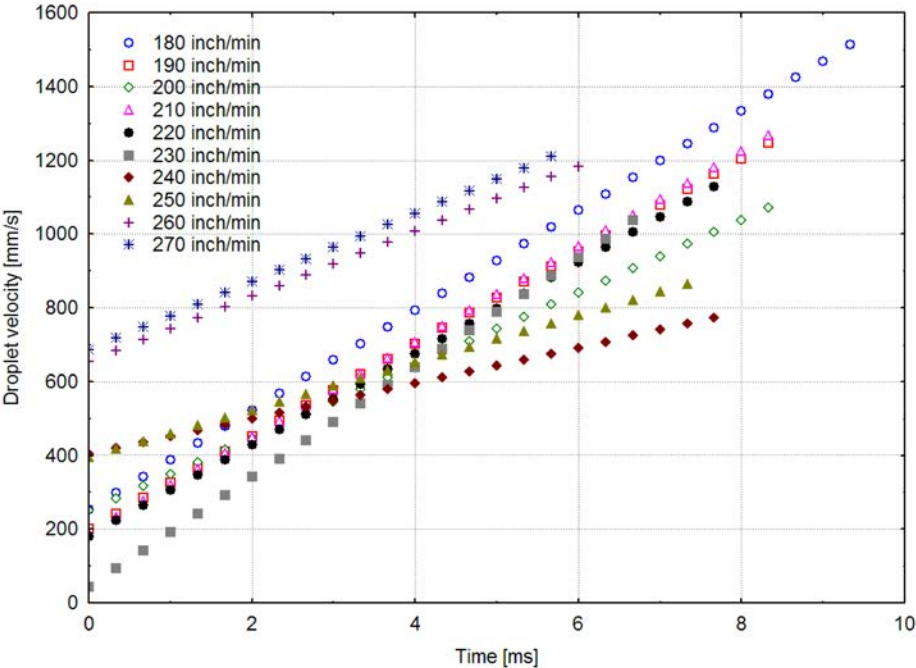


FIG. 8. Influence of wire speed rate (welding current) on droplet velocity vs. time.

The results of average droplet velocity and acceleration are given in Table 6.

Table 6. The average droplet velocity and droplet acceleration.

No	Wire feed rate [inch/min]	Average velocity [mm/s]	Average acceleration [m/s^2]
1	180	883.30	135.08
2	190	723.72	125.48
3	200	660.64	98.40
4	210	728.82	129.24
5	220	645.67	123.52
6	230	539.67	148.98
7	240	587.67	48.06
8	250	629.74	63.86
9	260	919.31	88.24
10	270	947.90	92.36

4.3. Geometric shape factor

Based on formula (2.9), results of droplet diameter in Table 3, and droplet acceleration in Table 6, the geometric shape factor has been calculated. The relationship between droplet diameter and geometric shape factor is shown in Fig. 9.

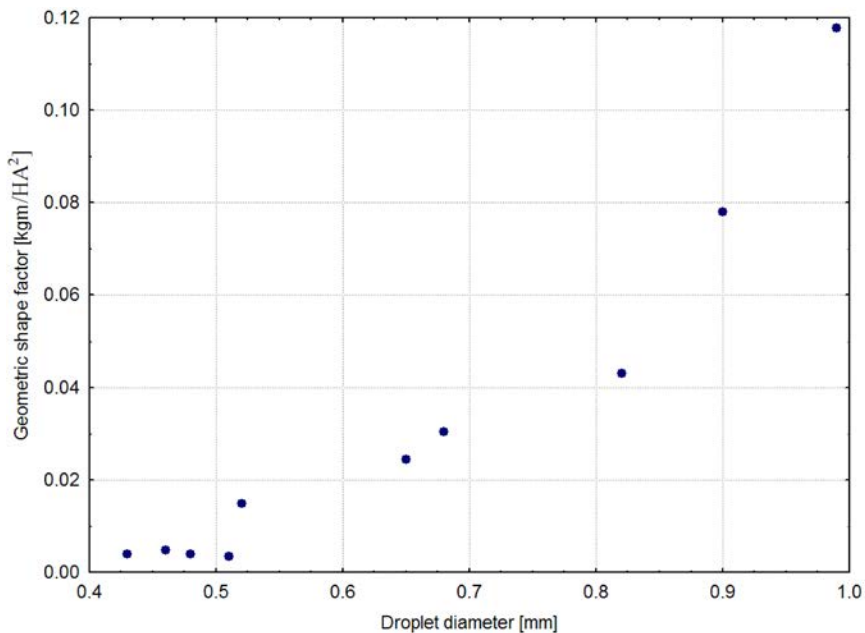


FIG. 9. Influence of droplet diameter (determined by the wire speed rate or welding current) on geometric shape factor $f(s)$.

As can be seen in Fig. 8, the geometric shape factor of a droplet strongly depends on the droplet diameter and increases as the droplet diameter increases.

5. CONCLUSION

In this paper, measurement data of metal transfer has been obtained from the GMAW process in the range of welding wire speed from 180 inch/min to 270 inch/min. The authors can conclude:

1. Measurement of the droplet diameter has shown that average diameter of droplet in the range of wire feed rate from 180 to 270 inch/min changes in the range from 0.99 ± 0.16 mm to 0.43 ± 0.10 mm.
2. The results of calculated the drop frequency (droplet transfer rate) is in the range from 42 to 776 droplets per second.
3. To fit the droplet flight trajectory, a 2nd degree polynomial is adequate.
4. To calculate drop velocity, the first order derivative of the fitted quadratic curves of drop trajectory was calculated. The average drop velocity in the range of wire feed rate from 180 to 270 inch/min varies from 883.30 to 947.90 mm/s.
5. To calculate the drop acceleration, the second order derivative of the fitted quadratic curves of drop trajectory was calculated. The acceleration is constant for each wire feed speed and in the range of 48.06 to 148.98 m/s².
6. The geometric shape factor of the droplet was calculated. This coefficient depends on the droplet radius and varies from 0.0039 to 0.1178 for the droplet diameter in the range from 0.43 to 0.99 mm.

The experience gained would allow the authors to determine further directions on metal transfer research and use the simple method proposed in this study to on-line monitor the welding process in automated GMAW.

ACKNOWLEDGEMENTS

The authors would like to thank the Fulbright Commission for financing this research, which was done within the framework of the research project Young Advanced Research Grant – University of Kentucky Centre for Manufacturing, Welding Research and Development Laboratory and the Applied Machine Vision Laboratory 2007–2008. This research is also supported in part by the National Science Foundation under grant CMMI-0726123.

REFERENCES

1. R. W. MESSLER, *Principles of Welding, Processes, Physics, Chemistry, and Metallurgy*, Ch. 3, John Wiley & Sons, New York 1999.
2. R. L. O'BREIN, *Welding Handbook, vol. 2 Welding processes*, American Welding Society, Miami 1991.
3. Welding Workbook: *Gas Metal Arc Welding, Transfer Modes*, Datasheet No 202a, Welding Journal, **76**, 2, 57–58, 1997.
4. J. HAIDAR, *An analysis of the formation of metal droplets in arc welding*, Journal of Physics D: Applied Physics, **31**, 10, 1233–1244, 1998.
5. S. K. CHOI, Y. S. KIM, C. D. YOO, *Dimensional analysis of metal transfer in GMA welding*, Journal of Physics D: Applied Physics, **32**, 3, 326–334, 1999.
6. J. A. JOHNSON, N. M. CARLSON, H. B. SMARTT, D. E. CLARK, *Process control of GMAW: sensing of metal transfer mode*, Welding Journal, **70**, 4, 91–99, 1991.
7. C. S. WU, M. A. CHEN, Y. F. LU, *Effect of current waveforms on metal transfer in pulsed gas metal arc welding*, Measurement Science and Technology, **16**, 12, 2459–2465, 2005.
8. G. WANG, G. HUANG, Y. M. ZHANG, *Numerical analysis of metal transfer in gas metal arc welding under modified pulsed current conditions*, Metallurgical and Materials Transactions B, **35B**, 5, 857–866, 2004.
9. N. JACOBSEN, *Monopulse investigation of drop detachment in pulsed gas metal arc welding*, Journal of Physics D: Applied Physics, **25**, 5, 783–797, 1992.
10. P. K. GHOSH, L. DORN, M. HÜBNER, V. K. GOYAL, *Arc characteristics and behaviour of metal transfer in pulsed current GMA welding of aluminium alloy*, Journal of Materials Processing Technology, **194**, 1–3, 163–175, 2007.
11. S. K. CHOI, C. D. YOO, Y. S. KIM, *The dynamic analysis of metal transfer in pulsed current gas metal arc welding*, Journal of Physics D: Applied Physics, **31**, 2, 207–215, 1998.
12. K. LI, Y. M. ZHANG, *Metal Transfer in Double-Electrode Gas Metal Arc Welding*, Journal of Manufacturing Science and Engineering-Transactions of the ASME, in print.
13. Z. Z. WANG, Y. M. ZHANG, *Image processing algorithm for automated monitoring of metal transfer in double-electrode GMAW*, Measurement Science and Technology, **18**, 7, 2048–2058, 2007.
14. Q. LIN, X. LI, S. W. SIMPSON, *Metal transfer measurements in gas metal arc welding*, Journal of Physics D: Applied Physics, **34**, 3, 347–353, 2001.
15. P. K. PALANI, N. MURUGAN, *Selection of parameters of pulsed current gas metal arc welding*, Journal of Materials Processing Technology, **172**, 1, 1–10, 2006.
16. F. WANG, W. K. HOU, S. J. HU, *Modelling and analysis of metal transfer in gas metal arc welding*, Journal of Physics D: Applied Physics, **36**, 9, 1143–1152, 2003.
17. D. IORDACHESCU, L. QUINTINO, *Steps toward a New Classification of Metal Transfer in Gas Metal Arc Welding*, Journal of Materials Processing Technology, in press.
18. P. J. MODENESI, R. I. REIS, *A model for melting rate phenomena in GMA welding*, Journal of Materials Processing Technology, **189**, 1–3, 199–205, 2007.

19. G. CAMPANA, A. FORTUNATO, A. ASCARI, G. TANI, L. TOMESANI, *The influence of arc transfer mode in hybrid laser-MIG welding*, Journal of Materials Processing Technology, **191**, 1–3, 111–113, 2007.
20. C. H. KIM, W. ZHANG, T. DEBROY, *Modeling of Temperature Field and Solidified Surface Profile During Gas-Metal Arc Fillet Welding*, Journal of Applied Physics, **94**, 4, 2667–2679, 2003.
21. H. G. FAN, R. KOVACEVIC, *Droplet Formation, Detachment, and Impingement on the Molten Pool in Gas Metal Arc Welding*, Metall. Mater. Trans. B, **30B**, 4, 791–801, 1999.
22. H. G. FAN, R. KOVACEVIC, *A Unified Model of Transport Phenomena in Gas Metal Arc Welding including Electrode, Arc Plasma and Molten Pool*, Journal of Physics D: Applied Physics, **37**, 18, 2531–2544, 2004.
23. S. SUBRAMANIAM, D. R. WHITE, D. J. SCHOLL, W. H. WEBER, *In Situ Optical Measurement of Liquid Drop Surface Tension in Gas Metal Arc Welding*, Journal of Physics D: Applied Physics, **31**, 16, 1963–1967, 1998.
24. Y. WANG, H. L. TSAI, *Impingement of Filler Droplets and Weld Pool Dynamics During Gas Metal Arc Welding Process*, International Journal of Heat and Mass Transfer, **44**, 11, 2067–2080, 2001.
25. Y. WANG, H. L. TSAI, *Effects of Surface Active Elements on Weld Pool Fluid Flow and Weld Penetration in Gas Metal Arc Welding*, Metallurgical and Materials Transactions B, **32B**, 3, 501–515, 2001.
26. J. F. LANCASTER, *The Physics of Welding*, 2nd ed., Pergamon, Oxford 1986.
27. J. HU, H. L. TSAI, *Metal Transfer and Arc Plasma in Gas Metal Arc Welding*, Journal of Heat Transfer, **129**, 8, 1025–1035, 2007.
28. L. A. JONES, T. W. EAGAR, J. H. LANG, *A Dynamic Model of Drops Detaching from a Gas Metal Arc Welding Electrode*, Journal of Physics D: Applied Physics, **31**, 107–123, 1998.
29. J. C. AMSON, *An analysis of the gas shielded consumable metal arc welding system*, British Welding Journal, **41**, 4, 232–249, 1962.
30. J. H. WASZNIK, L. H. J. GRAAT, *Experimental investigation of the forces acting on a drop of weld metal*, Welding Journal, **62**, 4, 109–116, 1983.
31. C. J. ALLUM, *Metal transfer in arc welding as a varicose instability: Part 1 – varicose instability in a current-carrying liquid cylinder with surface charge*, Journal of Physics D: Applied Physics, **18**, 7, 1431–1446, 1985.
32. C. J. ALLUM, *Metal transfer in arc welding as a varicose instability: Part 2 – development of model for arc welding*, Journal of Physics D: Applied Physics, **18**, 7, 1447–1468, 1985.
33. Y. S. KIM, T. W. EAGER, *Analysis of Metal Transfer in Gas Metal Arc Welding*, Welding Journal, **72**, 6, 296–278, 1993.
34. C. D. ALLEMAND, R. SCHOEDER, D. E. RIES, T. W. EAGER, *A method of filming metal transfer in welding arcs*, Welding Journal, **64**, 1, 45–47, 1985.

Received February 12, 2008; revised version June 2, 2008.

CONSTITUTIVE MODELLING AND NUMERICAL SIMULATION OF DYNAMIC BEHAVIOUR OF ASPHALT-CONCRETE PAVEMENT

A. Z b i c i a k

Warsaw University of Technology
Faculty of Civil Engineering, Institute of Structural Mechanics
Armii Ludowej 16, 00–637 Warszawa, Poland

The main objective of the paper is to present a simple constitutive model suited for dynamic simulation of asphalt-concrete mixtures. ABAQUS/Explicit FE software is used for this purpose. The model belongs to the class of overstress hypoelastic-viscoplastic materials, taking into account the effect of pressure-dependence on yielding. The implementation of constitutive relations formulated in the paper is done through user subroutine module VUMAT. The results of numerical simulation of dynamic behaviour of multilayer pavement structure, illustrating the applicability of the algorithm, is also discussed.

Key words: dynamic plasticity, asphalt concrete pavement, FEM.

1. INTRODUCTION

Rheological properties of engineering materials are characterized by elastic, plastic and viscous phenomena. The plastic behaviour is always associated with large deformations, whereas the viscosity is observed during fast loading. The loads acting on asphalt-concrete pavement structure are dynamic in nature. Thus, the crucial problem in analysis of such pavements is a formulation of constitutive model of the material, taking into account the rate-dependence phenomenon. Our objective is to present a simple class of constitutive equations describing the behaviour of pressure-sensitive materials such as asphalt concrete, suited for dynamic simulation. During our investigation we will not consider any creep effects because the analysis is limited to fast loading processes [2, 19].

Within the framework of the theory of viscoplasticity [16] it is possible to consider the influence of load intensity as well as its velocity on the process of formation of permanent deformations. The theory states that there is a limit state of stress defining the range of elastic behaviour. We assume that the limit state may be defined by the yield function depending on two invariants – the norm of deviatoric stress and the trace of the stress tensor. After reaching the limit state, viscoplastic effects may be observed. In order to describe the viscosity phenomenon, additional parameters should be taken into consideration.

The model presented herein introduces only one viscous parameter related to the total stress space. Thus, the relations to be obtained belongs to the class of Duvaut-Lions overstress materials [6] in which the rate-independent plastic part of the stress tensor may be calculated as a projection of the total stress on the static yield surface.

We will start with large strain formulation. After some simplifying assumptions, a hypoelastic-viscoplastic model will be introduced. The form of constitutive relationships to be obtained herein allows a user-defined implementation within the Finite Element (FE) commercial codes. The numerical integration algorithm was coded in ABAQUS software [1]. The implementation was done through user subroutine module VUMAT in order to study the behaviour of multilayer pavement structure.

2. KINEMATICS

Analysing large elasto-viscoplastic deformations we should start with an assumption stating that the total deformation gradient \mathbf{F} is decomposed multiplicatively into elastic and viscoplastic parts [11, 12]

$$(2.1) \quad \mathbf{F} = \mathbf{F}^e \mathbf{F}^{vp}, \quad \text{if} \quad d\mathbf{x} = \mathbf{F} d\mathbf{X},$$

where \mathbf{F} maps a line element $d\mathbf{X}$ in the reference configuration to the $d\mathbf{x}$ in the deformed configuration.

In Eq. (2.1), both tensors \mathbf{F}^e as well as \mathbf{F}^{vp} contain stretches and rigid body rotations. For simplification we will assume that all rigid rotations are associated with viscoplastic deformation gradient. Thus, using the polar decomposition theorem we obtain

$$(2.2) \quad \mathbf{F}^e = \mathbf{V}^e \quad \text{and} \quad \mathbf{F}^{vp} = \mathbf{V}^{vp} \mathbf{R},$$

where \mathbf{R} describes total rotations. Moreover, \mathbf{V}^e and \mathbf{V}^{vp} are left stretch tensors in elastic and viscoplastic part respectively.

Differentiating Eq. (2.1)₂ and making use of Eq. (2.1)₁, we obtain the following expression defining velocity gradient \mathbf{L} as well as its elastic and viscoplastic parts given by \mathbf{L}^e and \mathbf{L}^{vp} :

$$(2.3) \quad \mathbf{L} = \frac{d\mathbf{v}}{d\mathbf{x}} = \dot{\mathbf{F}} \mathbf{F}^{-1} = \mathbf{L}^e + \mathbf{V}^e \mathbf{L}^{vp} (\mathbf{V}^e)^{-1}$$

$$\text{if} \quad \mathbf{L}^e = \dot{\mathbf{V}}^e (\mathbf{V}^e)^{-1} \quad \text{and} \quad \mathbf{L}^{vp} = \dot{\mathbf{F}}^{vp} (\mathbf{F}^{vp})^{-1}.$$

The velocity gradient can be decomposed into a symmetric part denoted by \mathbf{D} and a skew-symmetric part denoted by \mathbf{W}

$$(2.4) \quad \mathbf{L} = \mathbf{D} + \mathbf{W} \quad \text{where} \quad \mathbf{D} = \frac{1}{2} (\mathbf{L} + \mathbf{L}^T) \quad \text{and} \quad \mathbf{W} = \frac{1}{2} (\mathbf{L} - \mathbf{L}^T).$$

Of course, the same decomposition scheme holds for its elastic part $\mathbf{L}^e = \mathbf{D}^e + \mathbf{W}^e$ and viscoplastic part $\mathbf{L}^{vp} = \mathbf{D}^{vp} + \mathbf{W}^{vp}$. Thus, based on Eq. (2.3)₁ we obtain

$$(2.5) \quad \mathbf{L} = \mathbf{D}^e + \mathbf{W}^e + \mathbf{V}^e \mathbf{D}^{vp} (\mathbf{V}^e)^{-1} + \mathbf{V}^e \mathbf{W}^{vp} (\mathbf{V}^e)^{-1}.$$

Eventually, taking the symmetric part in Eq. (2.5) we obtain

$$(2.6) \quad \mathbf{D} = \text{sym}(\mathbf{L}) = \mathbf{D}^e + \text{sym} \left[\mathbf{V}^e \mathbf{D}^{vp} (\mathbf{V}^e)^{-1} \right] + \text{sym} \left[\mathbf{V}^e \mathbf{W}^{vp} (\mathbf{V}^e)^{-1} \right].$$

Assuming that elastic stretches are small, i.e. $\mathbf{V}^e = (\mathbf{V}^e)^{-1} = \mathbf{I}$, we obtain from (2.6) the well-known decomposition rule for the rate of deformation tensor

$$(2.7) \quad \mathbf{D} = \mathbf{D}^e + \mathbf{D}^{vp}.$$

The decomposition scheme expressed by Eq. (2.7), along with assumption stating that $\mathbf{W}^{vp} = \mathbf{0}$, is widely used in FEM programmes [3, 18].

3. CONSTITUTIVE RELATIONSHIPS

We assume that the elastic part is described by hypoelastic law relating any objective rate of Kirchhoff stress $\boldsymbol{\tau}^\nabla$ to the elastic rate of deformation

$$(3.1) \quad \boldsymbol{\tau}^\nabla = \mathbf{C} \cdot \mathbf{D}^e,$$

where the \mathbf{C} denotes the 4th rank tensor of elastic coefficients.

Combining Eq. (2.7) with Eq. (3.1) we obtain

$$(3.2) \quad \boldsymbol{\tau}^\nabla = \mathbf{C} \cdot (\mathbf{D} - \mathbf{D}^{vp}).$$

In the case of isotropy, the above equation is replaced by

$$(3.3) \quad \boldsymbol{\tau}^\nabla = K \text{tr}(\mathbf{D} - \mathbf{D}^{vp}) \mathbf{I} + 2G \text{dev}(\mathbf{D} - \mathbf{D}^{vp}),$$

where the elastic constants K and G denote the bulk modulus and shear modulus respectively.

The operators $\text{tr}(\cdot)$ and $\text{dev}(\cdot) := (\cdot) - \frac{1}{3} \text{tr}(\cdot) \mathbf{I}$ used in Eq. (3.3) denote the trace and deviator.

The objective rate of the tensor $\boldsymbol{\tau}$ in the above expressions is given by

$$(3.4) \quad \boldsymbol{\tau}^\nabla = \dot{\boldsymbol{\tau}} + \boldsymbol{\tau} \boldsymbol{\Omega} - \boldsymbol{\Omega} \boldsymbol{\tau},$$

where $\dot{\boldsymbol{\tau}}$ is the material rate with respect to the basis of $\boldsymbol{\tau}$. The $\boldsymbol{\Omega}$ is a skew-symmetric spin tensor. Various forms of $\boldsymbol{\Omega}$ can be taken into account. For example setting $\boldsymbol{\Omega} = \mathbf{W}$ in Eq. (3.4), gives the Jaumann rate. Another objective stress

rate, the Green–Naghdi rate, is obtained by taking $\mathbf{\Omega} = \dot{\mathbf{R}}\mathbf{R}^T$. For numerical simulations, the Green–Naghdi rate will be used because of needs of the user material subroutine implemented in FE code.

The additive decomposition of the rate of deformation tensor introduced in Eq. (2.7), may be interpreted via rheological model to be shown in Fig. 1. Such a model, firstly defined by Bingham in the case of 1D stress-strain state, represents a family of elasto-viscoplastic materials called over-stress type models [12]. For such materials, before reaching a plastic limit state, the material behaves like a perfectly elastic one. After that, a rate-dependent yielding is observed.

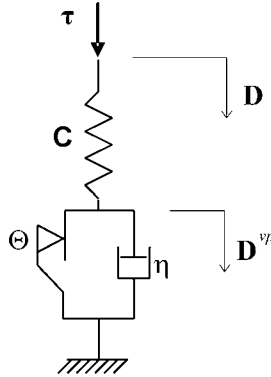


FIG. 1. Rheological model of the material.

Based on the Fig. 1, it can be proved that the total stress $\boldsymbol{\tau}$ is equal to elastic stress $\boldsymbol{\tau}^e$ and may be decomposed into the stress acting in plastic network $\boldsymbol{\tau}^p$ and viscous network $\boldsymbol{\tau}^v$. Thus, we have the relation

$$(3.5) \quad \boldsymbol{\tau} = \boldsymbol{\tau}^e = \boldsymbol{\tau}^p + \eta \mathbf{D}^{vp},$$

in which scalar η denotes the viscosity parameter. This is the only rate-dependent material coefficient to be taken into consideration. In general case, one should consider a tensor of viscous parameters being similar to the elastic operator \mathbf{C} or assume two coefficients related to volumetric and deviatoric subspaces like in Eq. (3.3). Because of the complexity of laboratory tests for asphalt, we assume only the single-rate-parameter model.

Now we need to describe the plastic properties of our model. The system of constitutive relations of a perfectly plastic material is defined by the set of admissible stresses Θ as well as by the maximum dissipation rule [15]:

$$(3.6) \quad \boldsymbol{\tau}^p \in \Theta,$$

$$(3.7) \quad \mathbf{D}^{vp} \in \mathcal{K}(\boldsymbol{\tau}^p, \Theta) := \{\boldsymbol{\tau}^p : \mathbf{D}^{vp} \cdot (\boldsymbol{\tau}^p - \tilde{\boldsymbol{\tau}}) \geq 0 \quad \forall \tilde{\boldsymbol{\tau}} \in \Theta\}.$$

It should be assumed that the Θ -set is convex, closed, limited and contains zero. The mapping \mathcal{K} used in Eq. (3.7), determines the set of viscoelastic rates assigned to $\boldsymbol{\tau}^p$. This set has the form of an external normal cone to the Θ -set at $\boldsymbol{\tau}^p$.

Alternatively, the system of Eqs. (3.5), (3.6) and (3.7), may be replaced by the following minimization problem:

$$(3.8) \quad \mathbf{D}^{vp} = \arg \min_{\tilde{\mathbf{D}}} \left[\frac{1}{2} \eta \left\| \tilde{\mathbf{D}} \right\|^2 + \Pi_{\Theta}(\tilde{\mathbf{D}}) - \boldsymbol{\tau} \cdot \tilde{\mathbf{D}} \right]$$

$$\text{if} \quad \Pi_{\Theta}(\tilde{\mathbf{D}}) := \sup_{\boldsymbol{\tau}^p \in \Theta} \tilde{\mathbf{D}} \cdot \boldsymbol{\tau}^p,$$

where Π_{Θ} denotes the support functional of the Θ -set [15].

The system of constitutive relations given by Eqs. (3.3), (3.5), (3.6) and (3.7) or by Eqs. (3.3) and (3.8) is valid for any isotropic elasto-viscoplastic material in which the plasticity constraints are described by appropriate definition of the Θ -set. Let us assume that this set is described by smooth yield function Φ as follows:

$$(3.9) \quad \Theta := \{ \boldsymbol{\tau}^p : \Phi(\boldsymbol{\tau}^p) \leq 0 \}.$$

Thus, we can replace the Eqs. (3.6) and (3.7) by the following set [8]:

$$(3.10) \quad \mathbf{D}^{vp} = \lambda \frac{\partial \Phi(\boldsymbol{\tau}^p)}{\partial \boldsymbol{\tau}^p}, \quad \Phi(\boldsymbol{\tau}^p) \leq 0, \quad \lambda \geq 0, \quad \lambda \Phi(\boldsymbol{\tau}^p) = 0,$$

where the scalar λ is called the Lagrange multiplier. Equation (3.10)₁ is called the associated flow rule while Eqs. (3.10)₂, (3.10)₃ and (3.10)₄ are the loading/unloading conditions or Kuhn–Tucker conditions.

Obtaining of the detailed form of Eqs. (3.10) needs the appropriate yield condition to be taken into consideration. In the paper we will analyse a pressure-sensitive Mises–Schleicher (MS) yield condition [5]. The yield function associated with this condition has a form

$$(3.11) \quad \Phi(\boldsymbol{\tau}^p) = \|\text{dev } \boldsymbol{\tau}^p\|^n + \alpha R^{n-1} \text{tr } \boldsymbol{\tau}^p - R^n \quad \text{where} \quad R = \sqrt{2} k.$$

Three additional material parameters were introduced via Eq. (3.11). Symbol k denotes the yield limit stress based on pure shear test. Dimensionless parameters $\alpha \geq 0$ and $n \geq 1$ determine the shape of the yield function in the meridian cross-section visualized in Fig. 2a.

Taking $\alpha = 0$ and $n = 2$ in Eq. (3.11) we obtain the pressure-insensitive Huber–Mises–Hencky (HMH) yield condition. If we substitute $n = 1$ in Eq. (3.11), we will obtain the Drucker–Prager (DP) yield function. Let us note that the DP

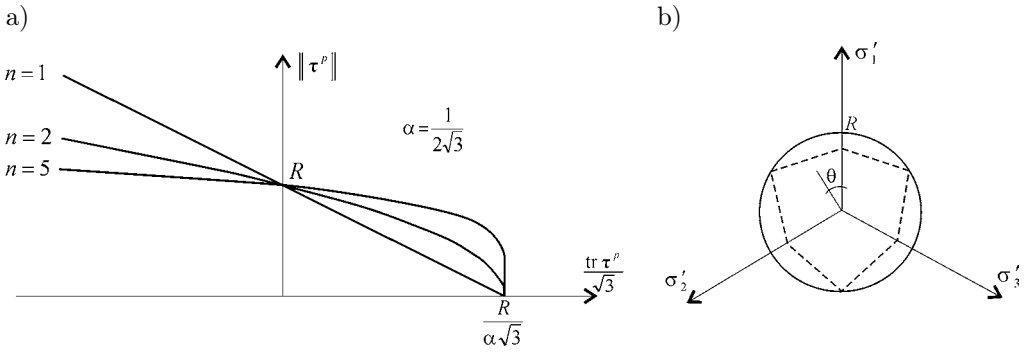


FIG. 2. Meridian (a) and deviatoric (b) sections of the Mises-Schleicher yield surface.

function is non-differentiable for $\text{tr } \boldsymbol{\tau}^p = R/\alpha$. In this point the Eqs. (3.10) are not valid. The analysis of non-smooth yield surfaces is still an open problem in the theory of plasticity. This is not our objective to deal with this problem, so our formulation will be limited to this specific point.

Deviatoric section of MS yield function is of circular shape as it is shown in Fig. 2b (continuous line). In this figure we visualized also, by a dashed line, the locus of Coulomb–Mohr (CM) yield function to be widely used in geomechanics [5]. The CM yield condition may be defined by the following equation:

$$(3.12) \quad \frac{\text{tr } \boldsymbol{\tau}^p}{3} \sin \phi + \frac{1}{\sqrt{2}} \|\boldsymbol{\tau}^p\| \left[\sin\left(\theta + \frac{\pi}{3}\right) + \frac{1}{\sqrt{3}} \cos\left(\theta + \frac{\pi}{3}\right) \sin \phi \right] - c \cos \phi = 0,$$

$$\text{for } \theta \in (0, \pi/3) \quad \text{where} \quad \theta = \frac{1}{3} \arccos \frac{\sqrt{6} \text{tr}(\boldsymbol{\tau}^p)^3}{\|\boldsymbol{\tau}^p\|^3}.$$

The CM yield condition defines a yield function having the shape of a pyramid with non-regular hexagonal base. The material parameters k and α describing the MS function, can be evaluated based on the CM coefficients: ϕ – friction angle and c – cohesion parameter. Assuming that the CM surface is inscribed in the DP surface and that their apexes coincide, the following relations between the material coefficients of both conditions are valid:

$$(3.13) \quad k = \frac{6 \cos \phi}{\sqrt{3} (3 - \sin \phi)} c, \quad \alpha = \frac{2\sqrt{2} \sin \phi}{\sqrt{3} (3 - \sin \phi)}.$$

Having assumed the MS yield condition, we can specify the relation (3.10)₁

$$(3.14) \quad \mathbf{D}^{vp} = \lambda n \|\text{dev } \boldsymbol{\tau}^p\|^{n-2} \text{dev } \boldsymbol{\tau}^p + \lambda \alpha R^{n-1} \mathbf{I}.$$

The system of relationships defining our material model is composed of Eqs. (3.3), (3.5), (3.11) and (3.14) completed by conditions (3.10)₂, (3.10)₃

and (3.10)₄. Using these relations we need to have the λ multiplier calculated. After this we can calculate the rate of viscoplastic deformation from Eq. (3.14) and substitute it into Eq. (3.3) in order to obtain the objective stress rate $\boldsymbol{\tau}^\nabla$. Finally, using Eq. (3.4) the material stress rate $\dot{\boldsymbol{\tau}}$ may be calculated.

Numerical simulations of the pavement structure will be carried out using the explicit integration algorithm implemented in ABAQUS software (the equations of motion will be solved explicitly). The incremental steps needed for dynamic explicit codes are very small. Thus, we can use the following simple explicit integration scheme in order to update the stress tensor:

$$(3.15) \quad \boldsymbol{\tau}_{t+\Delta t} = \boldsymbol{\tau}_t + \dot{\boldsymbol{\tau}} \Delta t.$$

In order to obtain the Lagrange multiplier, we have to analyse two cases. If $\Phi(\boldsymbol{\tau}) \leq 0$, then $\lambda = 0$ and $\mathbf{D}^{vp} = \mathbf{0}$ and $\boldsymbol{\tau}^p = \boldsymbol{\tau}^e = \boldsymbol{\tau}$ (elastic case). If $\Phi(\boldsymbol{\tau}) > 0$, then $\Phi(\boldsymbol{\tau}^p) = 0$ and $\lambda > 0$. In this case the value of λ can be obtained based on Eqs. (3.5), (3.11) and (3.14). We may rewrite these equations eliminating \mathbf{D}^{vp} , what gives the following two relations:

$$(3.16) \quad \boldsymbol{\tau} = \boldsymbol{\tau}^p + \lambda \eta n \|\text{dev } \boldsymbol{\tau}^p\|^{n-2} \text{dev } \boldsymbol{\tau}^p + \lambda \eta \alpha R^{n-1} \mathbf{I},$$

$$(3.17) \quad \|\text{dev } \boldsymbol{\tau}^p\|^n + \alpha R^{n-1} \text{tr } \boldsymbol{\tau}^p - R^n = 0.$$

After some algebra, these equations may be written as follows:

$$(3.18) \quad \lambda = \frac{\|\text{dev } \boldsymbol{\tau}\| - \|\text{dev } \boldsymbol{\tau}^p\|}{n \eta \|\text{dev } \boldsymbol{\tau}^p\|^{n-1}},$$

$$(3.19) \quad \|\text{dev } \boldsymbol{\tau}^p\|^n + \alpha R^{n-1} (\text{tr } \boldsymbol{\tau} - 3 \lambda \eta \alpha R^{n-1}) - R^n = 0.$$

In the above scalar equations, the unknowns are λ and $\|\text{dev } \boldsymbol{\tau}^p\|$. It is obvious that for any $n > 1$ and $\alpha \neq 0$, we cannot give any explicit formula for the λ multiplier. In such a case we have to solve the nonlinear algebraic Eq. (3.19). For numerical simulations to be shown in the next chapter, the implicit Newton method was used.

Let us take into consideration two special cases in which the multiplier λ can be expressed in explicit form. For the DP yield function we take $n = 1$. Thus, it can be proved that

$$(3.20) \quad \lambda = \frac{\|\text{dev } \boldsymbol{\tau}\| + \alpha \text{tr } \boldsymbol{\tau} - R}{\eta (1 + 3\alpha^2)} \quad \text{and} \quad \mathbf{D}^{vp} = \lambda \left(\frac{\text{dev } \boldsymbol{\tau}}{\|\text{dev } \boldsymbol{\tau}\|} + \alpha \mathbf{I} \right).$$

In the case of the HMH yield condition, substituting $\alpha = 0$ into Eq. (3.20) we obtain a well-known formula (see [4])

$$(3.21) \quad \mathbf{D}^{vp} = \frac{\text{dev } \boldsymbol{\tau}}{\eta} \left(1 - \frac{R}{\|\text{dev } \boldsymbol{\tau}\|} \right).$$

It is obvious that for the HMH yield criterion, the plastic deformation does not cause any volume changes. Thus, the Eq. (3.21) may be rewritten replacing the Kirchhoff stress tensor $\boldsymbol{\tau}$ by the Cauchy stress tensor $\boldsymbol{\sigma}$.

4. APPLICATION

The aim of formulation of constitutive equations is to predict the behaviour of pavement structure under dynamic load. The problem we should solve is a coupled system composed of initial-boundary-value problem, given by the momentum equilibrium and the constitutive equations. Since the boundary-value problem is usually solved by the FEM, the constitutive model has to be implemented in an appropriate way.

The constitutive equations considered can be mathematically classified as a coupled system of non-linear ordinary differential equations, building an initial-value problem. The solution of such a system can be embedded in an incremental FEM formulation with displacement approach, leading to the well-known explicit FEM problem for non-linear material equations, which has to be solved iteratively [3]. The constitutive equations were programmed within the ABAQUS/Explicit system [1]. The system requires the incremental procedure to be defined in VUMAT subroutine coded in FORTRAN language.

In this section we will show the results of dynamic simulation of multilayer asphalt concrete pavement exposed to the impulse of pressure. Such a load may be a simplified model of the aircraft tire impact at the time of landing [13, 14]. We will assume the axisymmetric topology of the model. The schematic view of the model is visualized in Fig. 3. The load acts during 0.1 [s] with the intensity of $q = 1200$ [kPa]. The pressure is uniformly distributed over the circular area with the radius equal to 20 [cm]. The pavement layers were modelled using 2820 axisymmetric 4-node elements of the CAX4 type (see [1]). They rest on a discrete Kelvin–Voigt viscoelastic foundation have the elasticity parameter equal to $\bar{k} = 150$ [MN/m³] and the viscosity module $\bar{\eta} = 1$ [MNs/m³]. The FE mesh is built over the 1.4 [m] \times 4.0 [m] rectangular area.

We carried out three numerical calculations assuming various material properties of the pavement layers. The first simulation was executed for a perfectly-elastic material. The values of elastic parameters (see Table 1) are assumed to be partially based on [10, 19] and are of the same value like in [20]. The parameters presented in Table 1 were also used for next simulations.

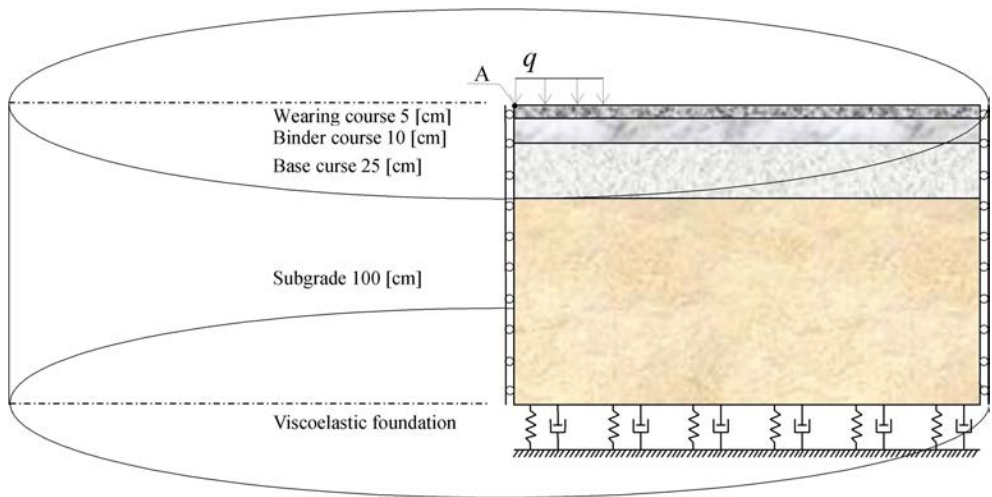


FIG. 3. Schematic view of the structure.

Table 1. Elastic parameters of pavement layers.

	K [MPa]	G [MPa]
Wearing course	160	74
Binder course	186	86
Base course	439	203
Subgrade	125	58

The second simulation was carried out for elasto-plastic rate-independent material with MS yield condition. The inelastic material constants for each layer have the following values: $n = 1.2$; $k = 160$ [kPa] and $\alpha = 0.2$.

The third simulation concerns the elastic-viscoplastic model presented in the previous section. The material constants are of the same value like in previous simulation with the additional viscosity parameter equal to $\eta = 500$ [kPa · s].

The contours of equivalent HMH stress are visualized in Figs. 4 and 5 (elasto-plastic pavement) and in Figs. 6 and 7 (elasto-viscoplastic pavement). The scale deformation factor to be used in these figures is equal to 20. The contour plots show differences in distributions of stresses at the moment of unloading for $t = 0.1$ [s], as well as at the end of analysis for $t = 1$ [s].

Additionally, Fig. 8 shows the displacement history curves at point A located in wearing course (see Fig. 3), constructed for three material models to be taken into consideration. The results allow to evaluate both the maximum deflection and the maximum permanent deflection in the structure. Thus, the maximum deflections to be obtained have the values between approx. 2 [mm] (elastic pavement) and approx. 4.5 [mm] (elasto-plastic pavement). When the load is

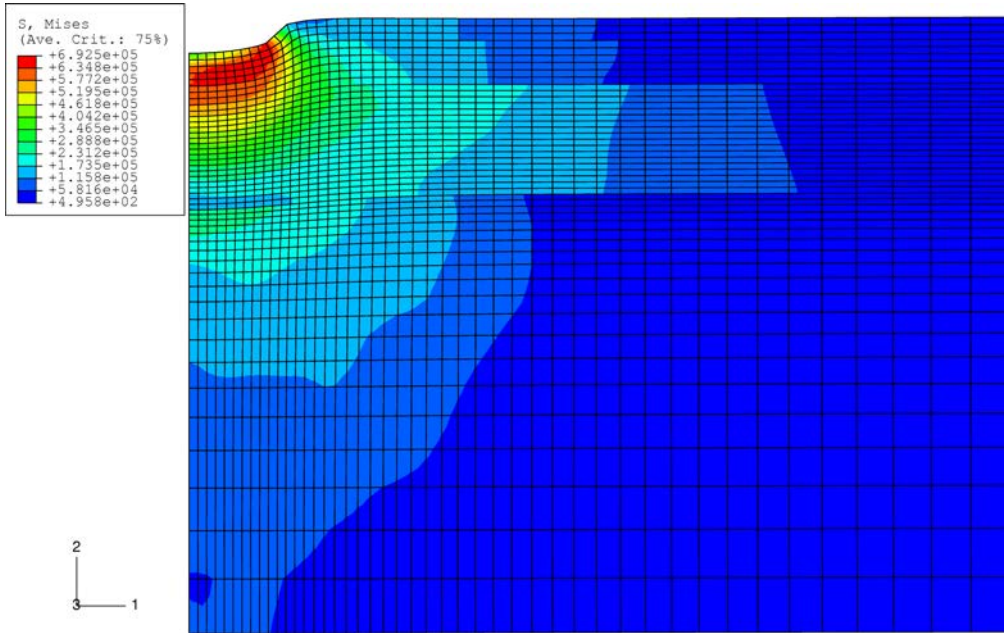


FIG. 4. Contours of equivalent HMM stress in elasto-plastic pavement for $t = 0.1$ [s].

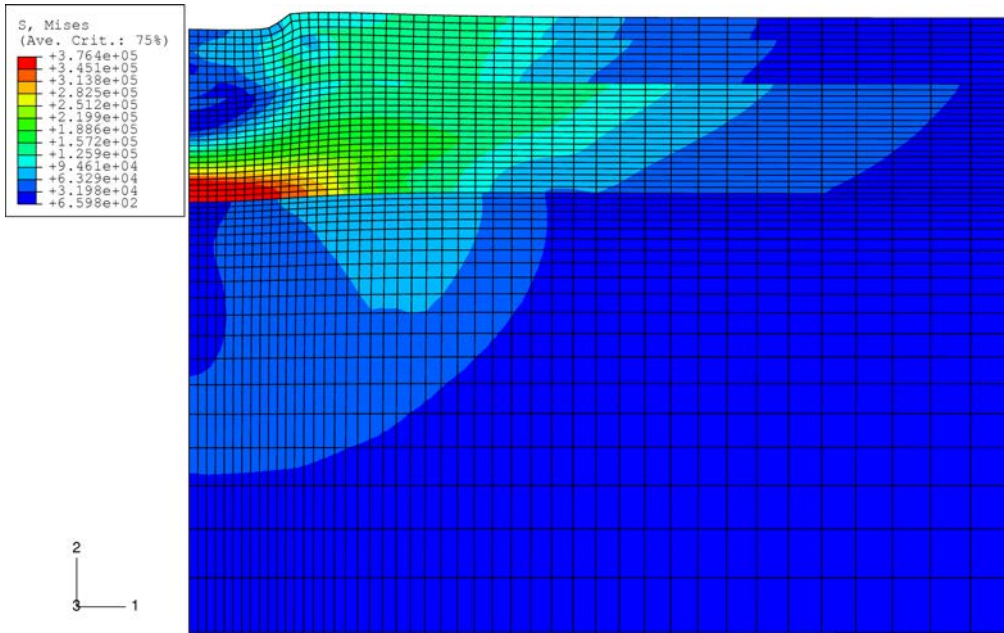


FIG. 5. Contours of equivalent HMM stress in elasto-plastic pavement for $t = 1$ [s].

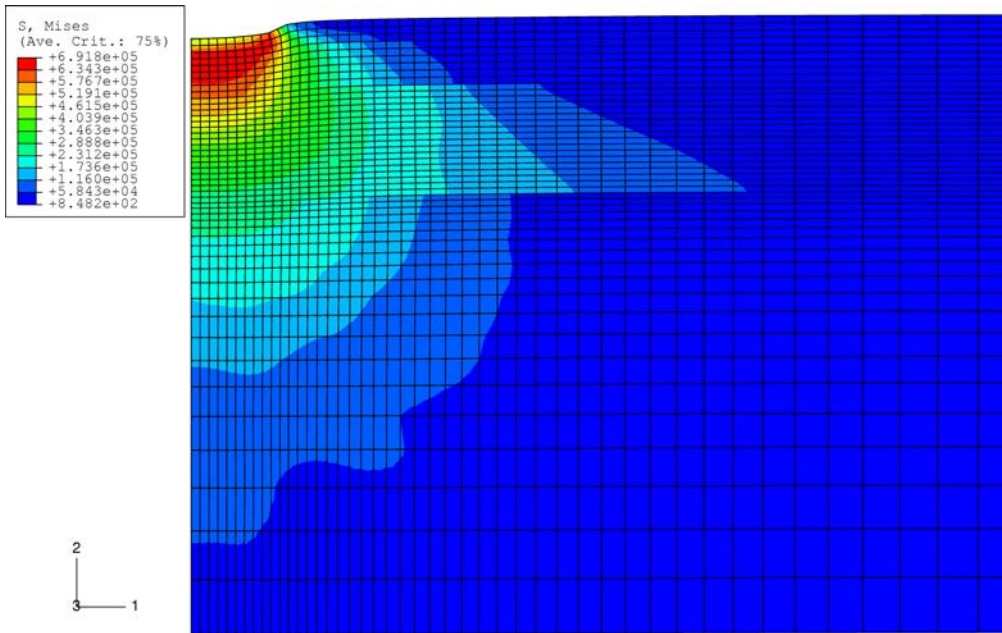


FIG. 6. Contours of equivalent HMH stress in elasto-viscoplastic pavement for $t = 0.1$ [s].

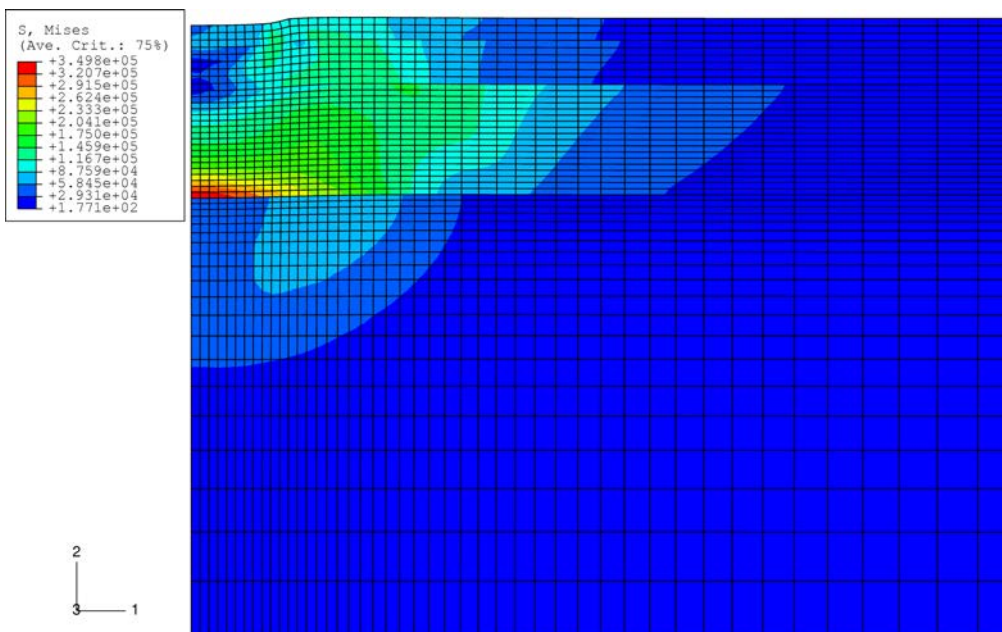


FIG. 7. Contours of equivalent HMH stress in elasto-viscoplastic pavement for $t = 1$ [s].

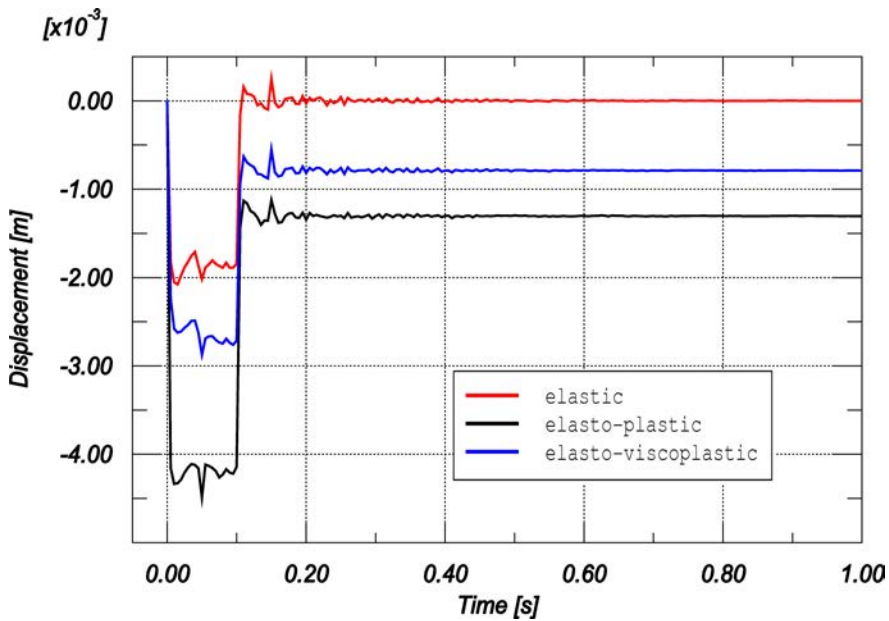


FIG. 8. Vertical displacement history curves for various materials of the pavement structure.

removed, the permanent vertical displacements are equal to approx. 1.3 [mm] (elasto-plastic pavement) and approx. 0.8 [mm] (elasto-viscoplastic pavement).

It should be strongly emphasized that these results must be viewed with some caution as they are based on insufficient laboratory tests.

Moreover, the results of the elasto-plastic rate-independent analysis may not be simply obtained basing on Eqs. (3.18) and (3.19) because if $\eta = 0$ (no viscosity) then the Eq. (3.18) is singular. The constitutive relationships for the rate-independent model can be formulated using the procedure described in [8].

5. CONCLUSIONS

The numerical studies which have been conducted demonstrate that the material model presented in the paper may be used in order to characterize asphalt pavement's dynamic behaviour in a wide range of material parameters. As it was emphasized in the previous section, the detailed analysis needs complex experimental tests to be conducted. The numerical example we presented herein shows only the applicability of the theory. Additional testing is required of the static and dynamic ranges of load rates, in order to evaluate plastic and viscous properties of the material. For example, a somewhat similar material model presented by GONZÁLES *et al.* [7] was calibrated basing on direct tensile test results carried out for various strain rates. In our case such an experiment should be completed

by testing the material in pure shear stress state because of the complexity of the yield surface.

There exist many possible enhancements to the current model. For instance, in the case of large pressure-stress states, the material obeying the Mises–Schleicher yield condition does not exhibit the plasticity phenomenon, what leads to inadequate prediction of inelastic volume changes. Thus, some modification of the yield function leading to so-called cap models should be also considered [12]. This problems is now being studied by the author.

REFERENCES

1. ABAQUS Analysis User's Manual, Ver. 6.5, 2004.
2. S. F. BROWN, *Achievements and challenges in asphalt pavement engineering*, Proc. of 8th Int. Conf. on Asphalt Pavements, Seattle 1997.
3. M. A. CRISFIELD, *Non-linear finite element analysis of solids and structures*, Essentials and Advanced Topics, **1–22**, Wiley, Chichester 1991.
4. N. D. CRISTESCU, *Dynamic Plasticity*, World Scientific Publ., New York 2007.
5. W. DERSKI, R. IZBICKI, I. KISIEL, Z. MRÓZ, *Rock and Soil Mechanics*, PWN, Warsaw 1988.
6. G. DUVAUT, J. L. LIONS, *Inequalities in Mechanics and Physics* [in French], DUNOD, Paris 1972.
7. J. M. GONZÁLES, J. MIQUEL, S. H. OLLER, R. MIRÓ, *A viscoplastic constitutive model with strain rate variables for asphalt mixtures' numerical simulation*, Comp. Materials Science, **38**, 543–560, 2007.
8. W. GRZESIKIEWICZ, W. WOJEWÓDZKI, A. ZBICIAK, *Non-smooth dynamic problem formulation for elastic-perfectly plastic solid*, Theoretical Foundations of Civil Engng., **11**, 339–350, 2003.
9. M. N. S. HADI, B. C. BODHINAYAKE, *Non-linear finite element of flexible pavements*, Advances in Engng. Software, **34**, 657–662, 2003.
10. J. JUDYCKI, *Rheological models of asphalt pavement* [in Polish], Trans. of Gdańsk Univ. of Technology, **368**, 123–145, Gdańsk 1984.
11. A. S. KHAN, S. HUANG, *Continuum Theory of Plasticity*, Wiley, New York 1995.
12. V. A. LUBARDA, *Elastoplasticity Theory*, CRC, Boca Raton 2002.
13. P. NITA, *Construction and maintenance of aircraft pavements* [in Polish], Publ. House on Transport and Telecommunications, Warsaw 1999.
14. P. NITA, *Concrete aircraft pavements. Theory and construction* [in Polish], Publ. House of the Air Force Technical Institute, Warsaw 2005.
15. P. D. PANAGIOTOPOULOS, *Inequality problems in mechanics and applications. Convex and nonconvex energy functions*, Birkhäuser, 1985.
16. P. PERZYNA, *Theory of Viscoplasticity* [in Polish], PWN, Warsaw 1966.

17. J. PILAT, P. RADZISZEWSKI, *Asphalt Pavements* [in Polish], Publ. House on Transport and Telecommunications, Warsaw 2003.
18. J. C. SIMO, T. J. R. HUGHES, *Computational Inelasticity*, Springer-Verlag, New York 1998.
19. A. SZYDŁO, P. MACKIEWICZ, *Asphalt mixes deformation sensitivity to change in rheological parameters*, J. of Materials in Civil Engng., 1–9, Jan/Feb 2005.
20. A. ZBICIAK, W. WOJEWÓDZKI, *Numerical simulation of creep behaviour of asphalt pavement*, Theoretical Foundations of Civil Engng., **14**, 459–46, Warsaw 2006.

Received February 27, 2008; revised version September 4, 2008.

WŁODZIMIERZ STANISŁAW TRZYWDAR BURZYŃSKI
(1900–1970)



Was born into the family of a secondary-school teacher of physics in Przemyśl on the 29th of April 1900. His father Marian Jan Tomasz Trzywdar Burzyński graduated in Kraków from the Cracow University in physics and astronomy and received the PhD degree in physics, his mother Wanda (her maiden name Rutkowska) passed away prematurely when Włodzimierz was only three years old. Przemyśl, a town near the border of the Austro-Hungarian Empire, was

converted into a “Przemyśl fortress”. It didn’t help much since in the Spring of 1915 the fortress was besieged by the Russian Army and the whole Austro-Hungarian garrison was taken into the Russian captivity. In November 1918, after 123 years of partition, Poland regained freedom. However this was not given for granted. The 18 years old Włodzimierz, still a student of the secondary school, was not accepted by a commission of the Austrian-Hungarian Army due to his weak health. However after a couple of months, already as a student of the Lwów Polytechnic, he joined the Polish Army as a volunteer and took part in the fights with Ukrainians (1st November – 16th December 1918). Next he studied at the Lwów Polytechnic, Faculty of Civil Engineering, and joined the Polish Army for the second time (4th – 22nd August 1920) to fight the bolsheviks. For the third time he joined the volunteers and took part in the Silesian Uprising (3rd May 1921 – 26th of July 1921 in Upper Silesia). For his courage and activity in fight Włodzimierz Burzyński was honoured with an “Upper Silesian Ribbon of Courage of the First Class”.



Włodzimierz Burzyński defended his civil engineering diploma with distinction on 12th of June 1925, in the next year he married Irena Wanda Walkowicz on 16th February 1926. The married couple had two sons. In 1922 student W. Burzyński became an instructor at the Lwów Polytechnic. In 1925 he became an assistant. Under the supervision of the famous professor M.T. Huber, who then held the chair of mechanics, he prepared his doctoral thesis on the strength hypotheses [1] and obtained the Ph.D. degree in February 1928. After years, we have arrived at the conclusion that the results of Burzyński’s thesis are of lasting value and should be translated into English and published in [2]. This is so since after eighty years, there appear some papers devoted to the same topic using W. Burzynski’s ideas.

A LA GLOIRE DE LA PATRIE



POUR LA GRANDEUR DE LA SCIENCE

EN VERTU DE LA LOI VOTÉE PAR LA DIÈTE DE LA RÉPUBLIQUE POLONAISE

LA HAUTE ÉCOLE POLYTECHNIQUE DE LÉOPOL

SOUS LE RECTORAT DE SA MAGNIFICENCE

MONSIEUR LE DOCTEUR JULIEN TOKARSKI

PROFESSEUR DE MINÉRALOGIE ET DE PÉTROGRAPHIE

ET SOUS LE DÉCANAT

DE MONSIEUR LE DOCTEUR ANTOINE WERESZCZYŃSKI

PROFESSEUR DE DROIT, DOYEN DE LA FACULTÉ DE GÉNIE CIVIL ET HYDRAULIQUE

CONFÈRE

à MONSIEUR L'INGÉNIEUR WLADIMIR STANISLAS BURZYŃSKI

NÉ À PRZEMYŚL PALATINAT DE LÉOPOL

LES GRADE, TITRE, DIGNITÉ ET PRIVILÈGES DE DOCTEUR ÈS SCIENCES TECHNIQUES

CERTIFIANT QU'IL A TEOIGNÉ CONFORMÉMENT AUX RÉGLEMENTS DE SA PRÉPARATION SCIENTIFIQUE PAR LA PRÉSENTATION D'UNE THÈSE INTITULÉE:

„ÉTUDE SUR LES HYPOTHÈSES DE LA TENSION“

ET SUBI LES EXAMENS DE RIGUEUR AVEC LA MENTION TRÈS BIEN, EN FOI DE QUOI LE PRÉSENT DIPLOME LUI EST DÉLIVRÉ.

FAIT À LÉOPOL CE 5-IÈME JOUR DE MAI DE L'AN 1928.

LE RECTEUR

Prof. Dr. Julien Tokarski



LE DOYEN

Prof. Dr. Antoine Wereszczyński

LE PROMOTEUR

Prof. Dr. Lucien Grabowski

A postdoctoral grant from the Polish Culture Fund enabled him to spend eight months in Göttingen and Zurich and to get acquainted with many distinguished scientists in the field of the solid body mechanics: L. Prandtl (Göttingen) and M. Roš (Zürich) as well as with Th. v. Kármán (Aachen), K. v. Sanden (Karlsruhe) and R. v. Mises (Berlin). His paper “Über die Anstrengungshypothesen” was published in Schweizerische Bauzeitung [3]. W. Burzyński obtained the D.Sc. degree for his habilitation thesis entitled “On an expansion of the elastic potential and its applications” [4] in 1932 and received the title of professor at the Lwów Polytechnic from the President of the Republic of Poland on the 29th September 1934. As a result of an open competition, W. Burzyński became the successor of Professor M.T. Huber at the chair of mechanics. In 1938 Professor W. Burzyński was elected a corresponding member of the Academy of Technological Sciences in Warsaw, and a member of the editorial board of the “Zentralblatt für Mechanik”. In the same year he was elected the dean of the mechanical faculty. When Poland was in 1939 partitioned again and Lwów was occupied by the Soviets, Burzyński kept his post of the dean, moreover he became, by a decision of Polish professors who trusted him, the main adviser to entire staff in the case when they didn't know what to do in new circumstances.

Inż. WŁODZIMIERZ TRZYWDAR BURZYŃSKI

STUDJUM NAD HIPOTEZAMI WYTEŻENIA

(Z 104 RYSUNKAMI W TEKŚCIE)

Praca niniejsza została przedstawiona, jako podstawa do uzyskania stopnia doktora nauk technicznych, Komisji Doktorskiej Politechniki lwowskiej w składzie następującym:

Przewodniczący: *Prof. Dr. Antoni Wereszczyński.*
Referenci: *Prof. Inż. Dr. Jan Bogucki,*
Prof. Inż. Dr. Maksymilian T. Huber,
Prof. Dr. Włodzimierz Stożek.

Data przedłożenia pracy: 7. I. 1928.

Data egzaminu ścisłego: 20. II. 1928.

NAKŁADEM AKADEMJI NAUK TECHNICZNYCH

After almost two years, the German troops and Gestapo overtook the town. All the universities were shut down together with secondary schools in Polish language. A number of professors from Lwów's academic schools, together with many family members, were shot. Another year has passed before the Germans decided to organise the Fachkursen. Professor W. Burzyński accepted the position of the deputy director of the Technische Fachkursen. The representative of the Polish Government on Exile advised to accept the decision. After mobilization of the Ukrainian students (1943) to SS division "Hałyczyna", the programs of the courses could resemble those of the polytechnic.

In July 1944 the town was overtaken by the Red Army (with the help of the Polish Home Army). The Polytechnics was reopened under a new name and new Soviet orders. W. Burzyński was appointed the deputy director of the school for scientific matters. On the fourth of January 1945 he was arrested with a number of the other distinguished professors and spent in prison over 7 months. After release from prison he spent another year in Lwów teaching students and doing the research. Professor W. Burzyński left Lwów in July 1946 and went to the Silesian Institute of Technology where he became the chairman of two chairs, namely that of the Technological Mechanics on the Faculty of the Mechanical Engineering and that of the Strength of Materials in Civil Engineering Faculty. In August of 1946 W. Burzyński was elected by an assembly of teachers and students, the new Rector of the school. Unfortunately the regulations have changed and for over thirty years there were no elections of the rectors, deans etc. any longer in all the academic schools in Poland.

Suddenly, in October 1949, his scientific career was abruptly terminated by an incurable disease. In spite of this he was elected a member of Cracow Polish Academy of Letters, a member of the Warsaw Scientific Society, and an honorary member of the Polish Society of Theoretical and Applied Mechanics. Professor W. Burzyński died in Gliwice on July 17, 1970. In 1982 the Polish Academy of Sciences published, in two volumes, his “Collected Papers” [5].

Zbigniew S. Olesiak
and the Editorial Committee

ACKNOWLEDGEMENT

We would like to express our gratitude to Dr. Eng. Maciej Burzyński for his kind help and making accessible the private documents of his father, as well as for the agreement to use them in this publication.

REFERENCES

1. W. BURZYŃSKI, *Study on Material Effort Hypotheses*, under the imprint of the Academy of Technical Sciences, Lwów, 1928, 1–192; reprinted in: Włodzimierz Burzyński: *Dzieła Wybrane*, tom I, Polska Akademia Nauk, PWN Warszawa, 1982, 67–257 (in Polish).
2. W. BURZYŃSKI, *Theoretical foundations of the hypotheses of material effort*, Czasopismo Techniczne, 1929, 47, 1–41, Lwów; reprinted in: Włodzimierz Burzyński: *Dzieła Wybrane*, tom I, Polska Akademia Nauk, PWN Warszawa, 1982, 265–303 (in Polish), English translation in: Engng. Trans., **56**, 3, 269–305, 2008.
3. W. v. BURZYŃSKI, *Ueber die Anstrengungshypothesen*, Schweizerische Bauzeitung, Vol. 94, Nr. 21, 23. November 1929, 259–262; reprinted in Włodzimierz Burzyński: *Dzieła Wybrane*, tom I, Polska Akademia Nauk, PWN Warszawa, 1982, 259–262.

4. W. BURZYŃSKI, *On an expansion of the elastic potential and its applications, under the imprint of the Academy of Technical Sciences*, Goebethner i Wolff, Warszawa, 1932 (in Polish); reprinted in Włodzimierz Burzyński: *Dzieła Wybrane*, tom II, Polska Akademia Nauk, PWN Warszawa, 1982, 7–140.
5. W. BURZYŃSKI, *Collected Papers (Dzieła Wybrane)*, Polska Akademia Nauk, PWN Warszawa, 1982 (in Polish).

Received November 24, 2008.

BURZYŃSKI YIELD CONDITION VIS-À-VIS THE RELATED STUDIES REPORTED IN THE LITERATURE

R. B. P e c h e r s k i

**Institute of Fundamental Technological Research
Polish Academy of Sciences**

Świętokrzyska 21, 00-049 Warszawa, Poland

The paper is written in accompaniment of the publication of English translation of W. BURZYŃSKI's paper [1], which deals with the yield criterion for materials revealing the sensitivity of yield strength to pressure derived by W. BURZYŃSKI during preparation of his doctor thesis in 1927 [2]. More recently the dependence of yield strength on pressure is related to the so-called strength differential (SD) effect, i.e. asymmetry of elastic range, cf. e.g. [3, 4]. Therefore, the original Burzyński's formulation of yield condition remains actual and acquires increasing significance. The position of Burzyński's energy-based approach in the literature is reported and his main achievement in this field concerning the recent studies is discussed.

Key words: Burzyński yield condition (criterion), strength differential effect, asymmetry of elastic range, hypotheses of material effort.

1. INTRODUCTION

The aim of the paper is to show that the original results of W. BURZYŃSKI presented in his doctoral thesis [2] are of fundamental significance and remain important also for recent studies related with modelling of yield and failure of solids characterized by asymmetry of elastic range and possessing, in general, anisotropic properties. It concerns, in particular, soils and rocks, e.g. applications in modelling of interaction of a cutting-tool with geological settings [5], as well as modern materials, e.g.: polymers [6], different kinds of composites and cellular or porous solids [7, 8], high-strength steels or, in general, ultra-fine grained alloys and nano-metals [9]. It is worthy to mention that the Burzyński criterion is cited in the aforementioned papers [5–9]. Therefore, we have decided to publish English translation of the paper of BURZYŃSKI [1] that contains not only the main results of his doctoral thesis [2], which appeared on January 1928 as a comprehensive monograph, but presents also his matured view on the state of the art of yield conditions and failure criteria at that time, which ripened during the nine months long post-doctoral study travel to Germany and Switzerland, connected with seminars and discussions with leading specialists in the field, cf.

the biographical note [10]. From December 1928 until March 1929, W. Burzyński visited the University of Göttingen, and from April until August 1929 he visited the Confederate Material Testing Laboratory (*Eidgenössische Materialprüfung Anstalt – EMPA*) at the Zurich Polytechnic (*ETH – Eidgenössische Technische Hochschule*) in Zürich, where, among others, on the 1st of June 1929 he took part in the 26th Conference of the Swiss Association of Material Testing for Technology (*26. Diskussionstag des Schweizerischen Verbandes für die Materialprüfungen der Technik*) and delivered the lecture, published in [11]. Unfortunately, W. Burzyński was unable to disseminate his knowledge and defend his views since 1949, when serious illness terminated his scientific carrier. Therefore, we would like to share his scientific legacy with the research community, in particular now, when his concepts concerning the yield conditions have been confirmed and rediscovered many times independently by many researchers.

2. BURZYŃSKI YIELD CONDITION REPORTED IN THE LITERATURE

The concept of Burzyński yield condition was presented in detail and compared with several later independent propositions by M. ŻYCZKOWSKI [12, 13], J.J. SKRZYPEK [14] and M. JIRÁSEK and Z.P. BAŽANT [15], as well as by G.S. PISARENKO and A.A. LEBEDEV [16] and V.V. BOZHIDARNIK, G.T. SULYM [17]. It has been also discussed in recent works on strength theory [18] and plasticity [19]. The first foreign references can be found in the papers of G.D. SANDEL (1930) [20], H. GEIRINGER and W. PRAGER (1934) [21], M. ROŠ and A. EICHINGER (1949) [22], cf. also the comprehensive discussion on the impact of the Burzyński's results on the development of yield criteria by A. BECCHI [23], in his historical essay concerning the hundred years of studies on the yield criteria. The strong critics of the previous proposition of G.D. SANDEL in [24] by W. BURZYŃSKI in [11], as well as in papers in Polish [1, 2], awoke the vivid polemics and exchange of letters of the both authors with the editor [25, 26] and [27].

At that time, the yield criterion proposed by M.T. HUBER (1904), R. v. MISES (1913) and H. HENCKY (1924) [28–30], for isotropic solids characterized by equal magnitude of yield stress in tension and compression, was well established and confirmed experimentally, cf. e.g. [1]. The open question remained, however, in the subject of yield criteria for isotropic materials revealing different magnitudes of the yield stress in tension and compression, the so-called strength differential (SD) effect leading to the asymmetry of elastic range. Also the formulation of yield criteria for anisotropic solids was an open question at that time; as said in [2], p. 127: “*it's still a thing of a distant future*”. Nevertheless, the first work on anisotropic yield criteria was published by R. v. MISES in 1928 [31]. Quite independently, an energy-based approach to the description

of yield criterion of orthotropic and transversally isotropic materials was presented in depth by W. BURZYŃSKI in [2], as a consistent development of the energy-based Huber's approach to isotropic solids [28], cf. also the discussion in [1], p. 291–292, and the concise remark in [11], p. 261. The contribution of W. Burzyński was discussed in [12], p. 111: *“The generalization of Huber-Mises-Hencky yield condition in the case of anisotropic bodies may also be achieved by using energy considerations ... In the most general case of anisotropy, the elastic energy cannot be decomposed into the energy of volume change and energy of shape change. This problem was first investigated by W. BURZYŃSKI [2], who proved that the existence of such a decomposition results in five relations between the elastic moduli, and thus only 16 moduli remain independent”*. (In [12], p. 69, the reference to the known since the publication of *Origins of Clerk Maxwell's Electric Ideas*, Cambridge, 1937, the first proposition of elastic energy of distortion as a measure of material effort by J.C. Maxwell in 1856 is also mentioned). The Burzyński yield criterion for orthotropic solids and its relation with the condition proposed twenty years later by R. HILL [32] for materials with symmetric elastic range, as well as for orthotropic solids revealing the SD effect studied by P.S. THEOCARIS [33–35] will be discussed independently in the forthcoming paper [36].

According to the comprehensive analysis of existing criteria in [1] and [2], the first problem was undertaken already in the Coulomb criterion, which can be expressed by the following equivalent relations, cf. [2]:

$$(2.1) \quad \frac{\sigma_1 - \sigma_3}{2} + \frac{k_c - k_t}{k_c + k_t} \frac{\sigma_1 + \sigma_3}{2} = k_s, \quad k_c \sigma_1 - k_t \sigma_3 = k_c k_t$$

$$\text{or} \quad \pm \tau + \frac{k_c - k_t}{2\sqrt{k_c k_t}} \sigma - \frac{1}{2} \sqrt{k_c k_t} = 0,$$

where k_c and k_t are the magnitudes of the yield stress at compression and tension, respectively, while k_s is the yield strength in shear, given by the relation $k_s \frac{k_t k_c}{k_t + k_c}$, and τ, σ are the shear and normal stresses acting in the plane of shear. Another approach was related to the Duguet–Mohr hypothesis, which reads [2]:

$$(2.2) \quad (\sigma_1 - \sigma_3)^2 + (k_c - k_t)(\sigma_1 + \sigma_3) = k_c k_t,$$

$$\tau^2 + \frac{k_c - k_t}{2} \sigma - \frac{(k_c + k_t)^2}{16} = 0.$$

These conditions have been, however, completely rejected by the researches at that time because of the just detected large discrepancies with experimental results, which were related, *inter alia*, with the lack of influence of the intermediate principal stress, [1, 2, 11]. This problem was also studied by G.D. SANDEL [24],

who assumed that the measure of material effort is the shear strain that depends linearly on volumetric change of strain, which led to the following equivalent relations:

$$(2.3) \quad (n+1)\sigma_1 + n\sigma_2 + (n-1)\sigma_3 \leq 2k_s, \quad k_c\sigma_1 + \frac{k_ck_t}{2}\sigma_2 - k_t\sigma_3 = k_ck_t,$$

where $n = \frac{k_c - k_t}{k_c + k_t}$, $k_s = \frac{k_t k_c}{k_t + k_c}$.

Then the problem was undertaken, within the framework of energy-based approach, by F. SCHLEICHER (1900–1957), cf. the short biographical note in [38], who presented his results during the application lecture delivered on the 8th of May 1925 at the Technische Hochschule Karlsruhe, in the summary of the presentation at the autumn 1925 GAMM conference in Danzig (Gdańsk) [39] and published as a full paper in [40]. Also R. v. Mises mentioned the possibility of accounting for the SD effect assuming that the yield strength depends on pressure, in the editorial note to the paper of F. SCHLEICHER [40], p. 199: *“Eine mit der hier entwickelten wesentlich gleichlautende Plastizitätsbedingung ist von mir in einem Vortrage im Ausschuß für Technische Mechanik des Berliner Bezirksvereines deutscher Ingenieure am 17. Juli 1925 mitgeteilt worden. Ich habe dabei namentlich gezeigt, wie die neue Hypothese, die eine konsequente Erweiterung der von mir im Jahre 1913 eingeführten darstellt, durch die neuen Versuche von Lode notwendig gemacht und durch sie voll bestätigt wird. Die Bezeichnung “Energiekriterium” lehne ich ab, da der in Frage kommende Ausdruck für den plastischen Körper kein Mass der Energie bildet. R. v. Mises”*.

(One of developed here, essentially similar yield condition has been announced by myself in a lecture delivered during the meeting of the Commission of Technical Mechanics of the Berlin Branch of the German Association of Engineers on the 17th of July 1925. I have particularly shown by that how the new hypothesis, which is a consistent extension of that one introduced by myself in the year 1913, appeared necessary due to the new experimental investigations by Lode and also gained full confirmation by these experiments. I am rejecting the notion “energy-based criterion” because the pertinent relation for the case of plastic bodies gives no measure of energy).

F. SCHLEICHER proposed in [40] an energy-based hypothesis, in which the equivalent stress reads:

$$(2.4) \quad \sigma_{vf} = \sqrt{2E\Phi} = f(p),$$

where E is the Young modulus, Φ is the total elastic energy density and p is the pressure $p = \frac{\sigma_1 + \sigma_2 + \sigma_3}{3}$ and f is a certain function which, according to the assumption of F. Schleicher, can be linear or parabolic with respect to pressure p . In particular, the following relation can be obtained in the space of principal stresses:

$$(2.5) \quad \sigma_1^2 + \sigma_2^2 + \sigma_3^2 - 2\mu(\sigma_1\sigma_2 + \sigma_2\sigma_3 + \sigma_3\sigma_1) + (k_c - k_t)(\sigma_2 + \sigma_2 + \sigma_3) = k_c k_t,$$

where μ is the Poisson ratio. The Schleicher's application of the total elastic energy density as a measure of material effort was strongly criticized by W. BURZYŃSKI in his paper published in German [11], as well as in his earlier doctoral thesis [2] and the later paper written in Polish [1]. The discrepancy with the experimental data discussed in [40], the unrealistic transition to the Beltrami criterion for $k_t = k_c$ and the presence in the yield condition (2.5) of the Poisson ratio μ , were mostly criticized. In contrast to G.D. Sandel, F. Schleicher neither answered to the Burzyński's critics nor referred to any of his papers. Nevertheless, he changed his view on the measure of material effort and in the next paper, published on the 13th April 1928 in [41], he replaced in (2.4) the total elastic energy Φ by the density of elastic energy of distortion Φ_f :

$$(2.6) \quad \sigma_g = \sqrt{6G\Phi_f} = f(p).$$

Discussing the possible applications of the general form (2.6), F. Schleicher suggested the application of linear dependence of the equivalent stress on pressure to certain brittle materials. In such a way, he is arriving at the cone in the coordinates (σ_g, p) , what corresponds also with a certain special linear form of Burzyński criterion, cf. [1], p. 289, and to the similar condition derived later by DRUCKER and PRAGER [3]. Considering (2.6) in an equivalent form

$$(2.7) \quad \frac{1}{3}\sqrt{(\sigma_1 - \sigma_2)^2 + (\sigma_2 - \sigma_3)^2 + (\sigma_2 - \sigma_3)^2} = F(p),$$

one obtains the relation proposed in [2], p. 183, as a certain generalization of Mohr's criterion. Similar generalization was considered later by some authors, e.g. A. NADAI [42], p. 225–228.

3. CONCLUSIONS

The more careful study of the discussed above problem leads to the conclusion that as a matter of fact there is not the dependency of the yield strength on pressure that is essential for the adequate formulation of yield condition, but it is rather the proper relation between the densities of energy of distortion Φ_f and volumetric change Φ_v for different materials under varying states of stress. The physically justified interplay of the both parts of elastic energy at the elastic limit, which defines in a proper way the material effort at a given state of stress, is a key point of the formulation of an adequate yield function and yield condition. This problem was underlined and discussed in recent papers

of R.M. CHRISTENSEN [43, 44]. One of main achievements of W. BURZYŃSKI was, according to our opinion, that he had solved this crucial question in an original way proposing the following formulation for the hypothesis of variable-volumetric-distortional limit energy, cf. [1], p. 288:

$$(3.1) \quad \Phi_f + \eta(p)\Phi_v = K,$$

where a particular form of the pressure dependency of the function $\eta(p)$ is assumed, $\eta = \omega + \frac{\delta}{p}$. The core of Burzyński's idea is the exchange of three material parameters: ω , δ , K , appearing in (3.1) with the triplet of material constants, k_t , k_c , k_s known from experiments of tension, compression and simple shear. The other form of the function $\eta(p)$ could be also considered in order to account for the ductile-brittle transition under the tri-axial states of stress in a considered material. The Eq. (3.1) leads to one of possible formulations of the W. Burzyński yield condition

$$(3.2) \quad \sigma_1^2 + \sigma_2^2 + \sigma_3^2 - 2\lambda(\sigma_1\sigma_2 + \sigma_2\sigma_3 + \sigma_3\sigma_1) + (k_c - k_t)(\sigma_2 + \sigma_2 + \sigma_3) = k_c k_t,$$

where $\lambda = \frac{k_c k_t}{2k_s^2} - 1$ and, depending on the sign of λ and the relation between material constants k_c , k_t and k_s , the Eq. (3.2) can represent in the axes of principal stresses a paraboloid, ellipsoid or a cone of revolution, cf. the discussion in [1], p. 289. Similar formulations were repeated independently during the last eighty years over and over by many researches, often without the clarity of the in-depth analysis and physical foundations of Burzyński's work.

ACKNOWLEDGEMENT

The paper was prepared under the auspices of the Commission of Applied Mechanics of the Kraków Branch of the Polish Academy of Sciences.

REFERENCES

1. W. BURZYŃSKI, *Teoretyczne podstawy hipotez wyężenia*, Czasopismo Techniczne, 1929, **47**, 1–41, Lwów [in Polish]; reprinted in: Włodzimierz BURZYŃSKI: *Dzieła Wybrane*, tom I, Polska Akademia Nauk, PWN Warszawa, 1982, 264–303 [in Polish]; English translation: *Theoretical foundations of the hypotheses of material effort*, Engng. Trans., **56**, 3, 269–305, 2008.
2. W. BURZYŃSKI, *Studjum nad Hipotezami Wyężenia*, (Study on Material Effort Hypotheses), Nakładem Akademji Nauk Technicznych (issued by the Academy of Technical Sciences), Lwów, January 7, 1928, 1–192 [in Polish]; reprinted in: Włodzimierz BURZYŃSKI: *Dzieła Wybrane*, tom I, Polska Akademia Nauk, PWN Warszawa, 1982, 67–258 [in Polish].

3. D. C. DRUCKER, *Plasticity theory, strength-differential (SD) phenomenon, and volume expansion in metals and plastics*, Met. Trans., **4**, 667–673, 1973.
4. C. D. WILSON, *A critical re-examination of classical metal plasticity*, J. Appl. Mech., **69**, 63–68, 2002.
5. A. NARDIN, G. ZAVARISE, B. A. SCHREFLER, *Modelling of cutting tool – soil interaction – Part I: contact behaviour*, Computational Mechanics, **31**, 327–339, 2003.
6. V. A. KOLUPAEV, S. KOLLING, A. BOLCHOUN, M. MONEKE, *A limit surface formulation for plastically compressible polymers*, Mechanics of Composite Materials, **43**, 245–258, 2007.
7. P. KORDZIKOWSKI, M. JANUS-MICHALSKA, R. B. PEŁCHERSKI, *Specification of energy-based criterion of elastic limit states for cellular materials*, Archives of Metallurgy and Materials, **50**, 621–634, 2005.
8. V. A. KOLUPAEV, A. KRAATZ, M. MONEKE, A. BOLCHOUN, *Beschreibung der mehraxialen Kriechphänomene bei Hartschaumstoffen*, KGK. Kautschuk, Gummi, Kunststoffe, **59**, 17–26, 2006.
9. R. B. PEŁCHERSKI, P. KORDZIKOWSKI, *Phenomenological description of mechanical properties and modelling of inelastic deformation of nano-structured materials*, Archives of Metallurgy and Materials, 2009 – submitted for publication.
10. Z. S. OLESIAK, *Włodzimierz Stanisław Trzywdar Burzyński*, Engng. Trans., **56**, 4, 377–382, 2008.
11. W. BURZYŃSKI, *Ueber die Anstrengungshypothesen*, Schweizerische Bauzeitung, **94**, Nr. 21, 23. November 1929, 259–262; reprinted in Włodzimierz BURZYŃSKI: *Dzieła Wybrane*, tom I, Polska Akademia Nauk, PWN Warszawa, 1982, 259–262.
12. M. ŻYCZKOWSKI, *Combined Loadings in the Theory of Plasticity*, PWN-Polish Scientific Publishers, Warszawa, 1981.
13. M. ŻYCZKOWSKI, *Discontinuous bifurcations in the case of the Burzyński-Torre yield condition*, Acta Mechanica, **132**, 19–35, 1999.
14. J. J. SKRZYPEK, *Plasticity and Creep. Theory, Examples, and Problems*, R. B. Hetnarski (English Edition Editor), CRC Press, Boca Raton, 1993.
15. M. JIRÁSEK, Z. P. BAŽANT, *Inelastic Analysis of Structures*, J. Wiley, Chichester, 2002.
16. G. S. PISARENKO, A. A. LEBEDEV, *The Deformation and Strength of Materials under Complex State of Stress* [in Russian], Naukova Dumka, Kiev, 1973.
17. V. V. BOZHIDARNIK, G. T. SULYM, *Elements of the Theory of Plasticity and Fracture* [in Ukrainian], CWIT, Lviv, 1999.
18. M.-H. YU, *Unified Strength Theory and its Applications*, Springer-Verlag, Berlin, Heidelberg, 2004.
19. M.-H. YU, G.-W. MA, H.-F. QIANG, Y.-Q. ZHANG, *Generalized Plasticity*, Springer-Verlag, Berlin, Heidelberg, 2006.
20. G. D. SANDEL, *Die Anstrengungsfrage*, Schweizerische Bauzeitung, **95**, Nr. 26, 28. Juni 1930, 335–338.
21. H. GEIRINGER, W. PRAGER, *Mechanik isotroper Körper im plastischen Zustand*, Ergebnisse der exakten Naturwissenschaften, **13**, 314–363, 1934.

22. M. ROŠ, A. EICHINGER, *Die Bruchgefahr fester Körper bei ruhender – statischer – Beanspruchung. Ergebnisse der an der Eidg. Materialprüfungs- und Versuchsanstalt für Industrie, Bauwesen und Gewerbe von 1925–1949 durchgeführten Untersuchungen*, Bericht Nr. 172, Zürich, September 1949.
23. A. BECCHI, *I Criteri di Plasticità: Cento Anni di Dibattito (1864–1964)*, Doctor Thesis, Firenze, 1994.
24. G. D. SANDEL, *Ueber die Festigkeitsbedingungen*, Dissertation, T.H. Stuttgart, 1919; Jä-necke Verlagsbuchhandlung, Leipzig, 1925.
25. G. D. SANDEL, Letter to the editor, *Schweizerische Bauzeitung*, **95**, 15. Februar, Nr. 7, 87, 1930.
26. W. BURZYŃSKI, Letter to the editor, *Schweizerische Bauzeitung*, **95**, 15. Februar, Nr. 7, 87, 1930.
27. G. D. SANDEL, Letter to the editor, *Schweizerische Bauzeitung*, **95**, 1 März, Nr. 9, 123, 1930.
28. M. T. HUBER, *Właściwa praca odkształcenia jako miara wyężenia materiału*, *Czasopismo Techniczne*, Lwów, 1904 (see also the English translation: *Specific work of strain as a measure of material effort*, *Arch. Mech.*, **56**, 173–190, 2004).
29. R. v. MISES, *Mechanik der festen Körper im plastisch-deformablen Zustand*, Göttingen Nachrichten, Math.-Phys. Klasse, Z. 4 (1), 582–592, 1913.
30. H. HENCKY, *Zur Theorie plastischer Deformationen und der hierdurch im Material hervorgerufenen Nachspannungen*, *ZAMM*, **4**, 323–334, 1924.
31. R. v. MISES, *Mechanik der plastischen Formänderung von Kristallen*, *ZAMM*, **8**, 161–185, 1928.
32. R. HILL, *A theory of the yielding and plastic flow of anisotropic metals*, *Proc. Roy. Soc. London*, **A193**, 281–297, 1948; also *The Mathematical Theory of Plasticity*, Oxford, Clarendon Press, 1950, p. 318–340.
33. P. S. THEOCARIS, T. P. PHILIPPIDIS, *The paraboloidal failure surface of initially anisotropic elastic solids*, *J. Reinf. Plastics Compos.*, **6**, 378–395, 1987.
34. P. S. THEOCARIS, *The paraboloid failure surface for the general orthotropic material*, *Acta Mech.*, **79**, 53–79, 1989.
35. P. S. THEOCARIS, *Variances in failure tensor polynomials for anisotropic bodies*, *Eng. Fracture Mech.*, **51**, 707–733, 1995.
36. R. B. PEŁCHERSKI, T. FRAŚ, *Study of the yield condition for anisotropic solids revealing asymmetry of elastic range with comparison of the criteria proposed by Burzyński, Hill and Theocaris* – forthcoming paper.
37. G. D. SANDEL, *Über die Festigkeitsbedingungen*, Dissertation, T.H. Stuttgart, 1919.
38. KARL-EUGEN KURRER, *The History of The Theory of Structures: From Arch Analysis to Computational Mechanis*, J. Wiley, 2008; *Geschichte von Baustatik*, Ernst and Sohn Verlag, Berlin, 2002.
39. F. SCHLEICHER, *Die Energiegrenze der Elastizität (Plastizitätsbedingung)*, *Vorträge der Danziger Tagung*, *ZAMM*, **5**, 478–479, 1925.

40. F. SCHLEICHER, *Der Spannungszustand an der Fließgrenze (Plastizitätsbedingung)*, ZAMM, **6**, 199–216, 1926.
41. F. SCHLEICHER, *Über die Sicherheit gegen Überschreiten der Fliessgrenze bei statischer Beanspruchung*, Der Bauingenieur, **9**, Heft 15, 253–261, 13 April 1928.
42. A. NADAI, *Theory of Flow and Fracture of Solids*, Vol. I, second edition, McGraw Hill, New York, 1950.
43. R. M. CHRISTENSEN, *A two-property yield, failure (fracture) criterion for homogeneous, isotropic materials*, J. Eng. Mater. Technol., **126**, 45–52, 2004.
44. R. M. CHRISTENSEN, *A comparative evaluation of three isotropic, two property failure theories*, J. Appl. Mech., **73**, 852–859, September 2006.

Received December 17, 2008.

DIRECTIONS FOR THE AUTHORS

The periodical *ENGINEERING TRANSACTIONS (ROZPRAWY INŻYNIERSKIE)* presents original papers which should not be published elsewhere.

As a rule, the volume of a paper should not exceed 40 000 typographic signs, that is about 20 type-written pages, format: 210×297 mm, leaded. The papers should be submitted in two copies and follow the norms outlined by the Editorial Office. The following directions are particularly important:

1. The paper submitted for publication should be written in English.
2. The title of the paper should be as short as possible. The text should be preceded by a brief introduction; it is also desirable that a list of notations used in the paper should be given.
3. Short papers should be divided into section and subsection, long papers into sections, subsections and points. Each section, subsection or point must bear a title.
4. The formula number consists of two figures: the first represents the section number and the other the formula number in that section. Thus the division into subsections does not influence the numbering of formulae. Only such formulae should be numbered to which the author refers throughout the paper. This also applies to the resulting formulae. The formula number should be written on the left-hand side of the formula; round brackets are necessary to avoid any misunderstanding. For instance, if the author refers to the third formula of the set (2.1), a subscript should be added to denote the formula, viz. (2.1)₃.
5. All the notations should be written very distinctly. Special care must be taken to distinguish between small and capital letters as precisely as possible. Semi-bold type must be underlined in black pencil. Explanations should be given on the margin of the manuscript in case of special type face.
6. Vectors are to be denoted by semi-bold type, transforms of the corresponding functions by tildes symbols. Trigonometric functions are denoted by sin, cos, tg and ctg, inverse functions – by arc sin, arc cos, arc tg and arc ctg; hyperbolic functions are denoted by sh, ch, th and cth, inverse functions – by Arsh, Arch, Arth and Arcth.
7. The figures in square brackets denote reference titles. Items appearing in the reference list should include the initials of the first name of the author and his surname, also the full of the paper (in the language of the original paper); moreover;
 - a) In the case of books, the publisher's name, the place and year of publication should be given, e.g., 5. S. ZIEMBA, *Vibration analysis*, PWN, Warszawa 1970;
 - b) In the case of a periodical, the full title of the periodical, consecutive volume number, current issue number, pp. from ... to ..., year of publication should be mentioned; the annual volume number must be marked in semi-bold type as to distinguish it from the current issue number, e.g., 6. M. SOKOŁOWSKI, *A thermoelastic problem for a strip with discontinuous boundary conditions*, Arch. Mech., **13**, 3, 337–354, 1961.
8. The authors should enclose a summary of the paper. The volume of the summary is to be about 100 words.
9. The authors are kindly requested to enclose the figures prepared on diskettes (format WMF, EMF, GIF, PCX, BitMaP, EPS or PostScript).

Upon receipt of the paper, the Editorial Office forwards it to the reviewer. His opinion is the basis for the Editorial Committee to determine whether the paper can be accepted for publication or not.

Once the paper is printed, 25 copies of reprints free of charge are sent to the author.

The papers submitted for publication in the journal should be written in English. No royalty is paid to the authors.

Please send us, in addition to the typescript, the same text prepared on a diskette (floppy disk) 3 1/2" as an ASCII file, preferably in the **T_EX** or **L^AT_EX**.

Editorial Committee
ENGINEERING TRANSACTIONS
(ROZPRAWY INŻYNIERSKIE)

Aims and Scope

ENGINEERING TRANSACTIONS promotes research and practise in engineering science and provides a forum for interdisciplinary publications combining mechanics with material science, electronics (mechanotronics), medical science and biotechnologies (biomechanics), environmental science, photonics, information technologies and other engineering applications. The Journal publishes original papers covering a broad area of research activities including experimental and hybrid techniques as well as analytical and numerical approaches. Engineering Transactions is a quarterly issued journal for researchers in academic and industrial communities.

INTERNATIONAL COMMITTEE

S. A. ASTAPCIK (*Byelorussia*)

G. DOBMANN (*Germany*)

JI-HUAN HE (*China*)

M. N. ICHCHOU (*France*)

W. JÜPTNER (*Germany*)

A. N. KOUNADIS (*Greece*)

P. KUJALA (*Finland*)

J. LIN (*U. K.*)

G. PLUVINAGE (*France*)

V. V. SKOROKHOD (*Ukraine*)

P. C. B. TSAY (*Taiwan*)

Z. WESOŁOWSKI (*Poland*)

EDITORIAL COMMITTEE

L. DIETRICH – **Editor**

B. GAMBIN

K. KOWALCZYK-GAJEWSKA

Z. KOWALEWSKI

B. LEMPKOWSKI – secretary

J. HOLNICKI-SZULC

R. PEŁCHERSKI

Address of the Editorial Office:
Engineering Transactions
Institute of Fundamental Technological Research
Świętokrzyska 21,
PL 00-049 Warsaw, Poland

Phone: (48-22) 826 60 22, Fax: (48-22) 826 98 15, E-mail: publikac@ippt.gov.pl

Abstracted/indexed in:

Applied Mechanics Reviews, Current Mathematical Publications, Inspec, Mathematical Reviews, MathSci, Zentralblatt für Mathematik.

<http://et.ippt.gov.pl/>

SUBSCRIPTIONS

Address of the Editorial Office: Engineering Transactions

Institute of Fundamental Technological Research, Świątokrzyska 21

PL 00-049 Warsaw, Poland

Tel.: (48-22) 826 60 22, Fax: (48-22) 826 98 15, E-mail: publikac@ippt.gov.pl

Subscription orders for all journals edited by IFTR may be sent directly to the Editorial Office of the Institute of Fundamental Technological Research

Subscription rates

Annual subscription rate (2009) including postage is US \$ 176.

Please transfer the subscription fee to our bank account: Payee: IPPT PAN,

Bank: PKO SA. IV O/Warszawa,

Account no. 05124010531111000004426875.

All journals edited by IFTR are available also through:

- Foreign Trade Enterprise ARS POLONA ul. Obrońców 25, 03-933 Warszawa, Poland, Tel. 4822 509 86 38, 509 86 37
- RUCH S.A. ul. Jana Kazimierza 31/33, 01-248 Warszawa, Poland, Tel. 4822 532 89 00, Fax 4822 532 87 45
- International Publishing Service Sp. z o.o ul. Noakowskiego 10 lok. 38 00-664 Warszawa, Poland tel./fax: (48-22) 625 16 53, 625 49 55

Warunki prenumeraty

Prenumeratę na wszystkie czasopisma wydawane przez IPPT PAN prowadzi Biblioteka. Bieżące numery można nabyć a także zaprenumerować roczne wydanie Engineering Transactions bezpośrednio w Bibliotece IPPT PAN, Świątokrzyska 21, 00-049 Warszawa, Tel.: (48-22) 826 60 22; Fax: (48-22) 826 98 15.

Cena rocznej prenumeraty z bonifikatą (na rok 2009) dla krajowego odbiorcy wynosi 176 PLN. Również można je nabyć, a także zamówić (przesyłka za zaliczeniem pocztowym) we Wzorcowni Ośrodka Rozpowszechniania Wydawnictw Naukowych PAN, 00-818 Warszawa, ul. Twarda 51/55, tel. (48-22) 697 88 35.

Wpłaty na prenumeratę przyjmują także jednostki kolportażowe RUCH S.A. Oddział Krajowej Dystrybucji Prasy, 01-248 Warszawa, ul. Jana Kazimierza 31/33, Konto: PBK.S.A. XIII Oddział Warszawa nr 68124010531111000004430494. Dostawa odbywa się pocztą zwykłą w ramach opłaconej prenumeraty z wyjątkiem zlecenia dostawy pocztą lotniczą, której koszt w pełni pokrywa zleceniodawca. Tel.: (48-22) 620 10 39, fax: (48-22) 620 17 62.

Arkuszy wydawniczych 6.5; Arkuszy drukarskich 5.25

Papier offset. kl. III 70 g. B1

Oddano do druku w grudniu 2008 r. Druk ukończono w grudniu 2008 r.

Skład w systemie L^AT_EX K. Jezierska

Druk i oprawa: Drukarnia Braci Grodzickich, Piaseczno ul. Geodetów 47A

FROM THE EDITORIAL BOARD

The Editorial Committee wishes to express many thanks and appreciation to all the referees, listed below, for their valuable opinions concerning papers submitted to the Engineering Transactions in 2008.

B. Gambin (Warszawa), J. Holnicki-Szulc (Warszawa), Sz. Imiełowski (Warszawa), Z. Nowak (Warszawa), W. Sosnowski (Warszawa), S. Stupkiewicz (Warszawa), W. Szczśniak (Warszawa), Z. Szymański (Warszawa), T. Wierzbicki (Massachusetts, USA), K. Wiśniewski (Warszawa), T. Zieliński (Warszawa)